

12-93 JS @  
7-6

**PNL-8636**  
**UC-814**

---

**MSTS**  
**Multiphase Subsurface**  
**Transport Simulator**  
**Theory Manual**

**M. D. White**  
**W. E. Nichols**

---

**May 1993**

**Prepared for the U.S. Department of Energy**  
**Office of Civilian Radioactive Waste Management**  
**under Contract DE-AC06-76RLO 1830**

**Pacific Northwest Laboratory**  
**Operated for the U.S. Department of Energy**  
**by Battelle Memorial Institute.**



**PNL-8636**

## DISCLAIMER

This report was prepared as an account of work sponsored by an agency of the United States Government. Neither the United States Government nor any agency thereof, nor Battelle Memorial Institute, nor any of their employees, makes **any warranty, expressed or implied, or assumes any legal liability or responsibility for the accuracy, completeness, or usefulness of any information, apparatus, product, or process disclosed, or represents that its use would not infringe privately owned rights.** Reference herein to any specific commercial product, process, or service by trade name, trademark, manufacturer, or otherwise does not necessarily constitute or imply its endorsement, recommendation, or favoring by the United States Government or any agency thereof, or Battelle Memorial Institute. The views and opinions of authors expressed herein do not necessarily state or reflect those of the United States Government or any agency thereof.

PACIFIC NORTHWEST LABORATORY  
*operated by*  
BATTELLE MEMORIAL INSTITUTE  
*for the*  
UNITED STATES DEPARTMENT OF ENERGY  
*under Contract DE-AC06-76RLO 1830*

Printed in the United States of America

Available to DOE and DOE contractors from the  
Office of Scientific and Technical Information, P.O. Box 62, Oak Ridge, TN 37831;  
prices available from (615) 576-8401. FTS 626-8401.

Available to the public from the National Technical Information Service,  
U.S. Department of Commerce, 5285 Port Royal Rd., Springfield, VA 22161.

# MSTS

## MULTIPHASE SUBSURFACE TRANSPORT SIMULATOR THEORY MANUAL

M. D. White  
W. E. Nichols

May 1993

Prepared for  
the U.S. Department of Energy,  
Office of Civilian Radioactive Waste Management  
under Contract DE-AC06-76RLO 1830

Pacific Northwest Laboratory  
Richland, Washington 99352

MASTER

## Executive Summary

The U.S. Department of Energy, through the Yucca Mountain Site Characterization Project Office, has designated the Yucca Mountain site in Nevada for detailed study as the candidate U.S. geologic repository for spent nuclear fuel and high-level radioactive waste. Site characterization will determine the suitability of the Yucca Mountain site for the potential waste repository. If the site is determined suitable, subsequent studies and characterization will be conducted to obtain authorization from the Nuclear Regulatory Commission to construct the potential waste repository. A principal component of the characterization and licensing processes involves numerically predicting the thermal and hydrologic response of the subsurface environment of the Yucca Mountain site to the potential repository over a 10,000-year period. The thermal and hydrologic response of the subsurface environment to the repository is anticipated to include complex processes of countercurrent vapor and liquid migration, multiple-phase heat transfer, multiple-phase transport, and geochemical reactions. Numerical simulators based on mathematical descriptions of these subsurface phenomena are required to make numerical predictions of the thermal and hydrologic response of the Yucca Mountain subsurface environment. The engineering simulator called the Multiphase Subsurface Transport Simulator (MSTS) was developed at the request of the Yucca Mountain Site Characterization Project Office to produce numerical predictions of subsurface flow and transport phenomena at the potential Yucca Mountain site. This document delineates the design architecture and describes the specific computational algorithms that compose MSTS. Details for using MSTS and sample problems are given in the "User's Guide and Reference" companion document.

The fundamental purpose of MSTS is to produce numerical predictions of thermal and hydrologic flow and transport phenomena in variably saturated subsurface environments, which are composed of unfractured or highly fractured porous media. The simulator is designed to numerically model the flow of liquid water, water vapor, air, and heat through fractured porous media. Additionally, MSTS is capable of modeling the two-phase transport of radionuclides, heavy metals, or other contaminants through porous media. Quantitative predictions from MSTS are generated through the numerical solution of partial differential equations that describe subsurface environment transport phenomena. The description of the contaminated subsurface environment formulated in MSTS is founded on governing and constitutive equations. Governing equations are partial differential equations for the conservation of water mass, air mass, thermal energy, and species mass. Constitutive equations relate independent variables to coefficients of the governing conservation equations. Solution of the governing partial differential equations is by the integral volume finite-difference method. The governing equations that describe thermal and hydrogeological processes are solved simultaneously using Newton-Raphson iteration to resolve the nonlinearities in the governing equations. Species mass conservation governing equations are solved sequentially, by a direct application of the integral volume finite-difference method, once the coupled thermal and hydrological equations have been solved for the current time step.

Modeled transport processes within the subsurface environment at Yucca Mountain are described by the governing conservation equations and associated constitutive functions. Component mass transport through the subsurface environment occurs in response to gradients in phase pressures, gravitational body forces, and gas-phase vapor concentration differentials. Mass advective fluxes from pressure gradients and gravitational body forces follow Darcy's flow equations for the aqueous and gas phases. Diffusion of components through the gas phase occurs according to Fick's law modified for porous media with soil tortuosity parameters. Interphase mass transfer of water between the liquid and gas phases depends on an assumption of thermodynamic equilibrium. Solubilities of air within the aqueous phase follow Henry's law for chemical equilibrium. Heat transport within the subsurface environment occurs by thermal diffusion and

advection. Solid- and liquid-phase pathways for thermal diffusion are considered; thermal diffusion through the gas phase is neglected. Both sensible and latent advection of thermal energy are considered. Species transport through the subsurface environment occurs by diffusion, dispersion, and advection. Species diffusion, dispersion, and advection transport contributions are combined into a single transport coefficient with a power-law approximation to the exact solution.

Constitutive equation calculations represent a major portion of the total computational effort. Parameters computed through the constitutive equations include thermodynamic equilibrium parameters, physical properties, transport properties, rock or soil saturations, relative permeabilities, interphase mass transfer parameters, species partition functions, and thermal properties. Liquid water and water-vapor properties are computed from the International Formulation Committee's steam table functions. Air properties are computed from empirical functions. Rock or soil saturation, relative permeability, and capillary pressure functions were derived from several theoretical models for air-water porous media systems subject to arbitrary saturation paths. These theoretical models do not consider hysteretic saturation paths, nor do they include the effects of air occlusion or entrapment during imbibition.

The source code for MSTS is written in FORTRAN 77, following the American National Standards Institute (ANSI) standards, and includes calls to machine-dependent time and data subroutines for numerous computing platforms. Verification of MSTS has been performed through comparisons against analytical solutions, other numerical simulators, and experimental data. The source code is controlled and maintained under a quality assurance program that requires change documentation, new version testing, and systematic backups. Input files for MSTS can be generated with either an interactive graphical user interface or a conventional text editor. The graphical user interface, a Macintosh system program, allows the user to specify simulation parameters through a controlled interactive environment. Output generated by MSTS is completely controlled by the user through input specifications and includes thermal and hydrologic field states and fluxes (e.g., temperatures, pressures, saturations, component mass fractions, Darcy velocities, and heat transfer rates). Species transport output also includes field states and fluxes. Special screen outputs can be requested by the user to trace histories of field and flux variables interactively during the simulation. Both spatial and temporal output of field and flux variables can be generated for subsequent graphical analysis.

## Glossary of Symbols

### Roman Symbols

$a$	Jacobian coefficient matrix (banded matrix solver)
$A$	area, m <sup>2</sup>
$A$	Jacobian coefficient matrix
$a_{ij}, A_{ij}$	water-vapor constant
$a_{\ell,\gamma}, a_{g,\gamma}$	species transport coefficients (aqueous, gas), m/s
$a_{\ell,\gamma}^*, a_{g,\gamma}^*$	conjugate species transport coefficients (aqueous, gas), m/s
$a_{\gamma}$	species transport coefficients, m/s
$b_{ij}, B_{ij}$	liquid water constant
$b_p$	species transport solution vector coefficient, mol/s m <sup>2</sup>
$C$	Jacobian coefficient matrix (conjugate gradient solver)
$c_p^a$	specific heat @ constant volume (air), J/kg K
$C, C_{\ell}, C_g, C_s$	species concentration (per total volume, per aqueous volume, per gas volume, per solid volume), mol/m <sup>3</sup>
$D_{e,\gamma}$	thermal diffusive flux term, W/m <sup>2</sup>
$D_{\ell,\gamma}, D_{g,\gamma}$	combined species diffusive and dispersive flux term, m/s
$D_{d\ell}, D_{dg}$	species diffusion coefficient (aqueous, gas), m <sup>2</sup> /s
$\tilde{D}_{h\ell}$	species hydraulic dispersion coefficient (aqueous), m <sup>2</sup> /s
$D_{h\ell}^x, D_{h\ell}^y, D_{h\ell}^z$	hydraulic dispersion coefficient (east-west, north-south, top-bottom), m <sup>2</sup> /s
$D_g^{AB}$	gas-phase diffusivity (nonpolar gas pair), m <sup>2</sup> /s
$D_g^{aw}$	air/water-vapor binary diffusivity, m <sup>2</sup> /s
$D_g^{aw*}$	reference air/water-vapor binary diffusivity, m <sup>2</sup> /s
$E$	energy accumulation term, J/m <sup>3</sup>
$f(x)$	continuous function

## Roman Symbols (contd)

$F_{c,\gamma}$	species surface flux, mol/m <sup>2</sup> s
$F_{e,\gamma}$	thermal advective flux term, W/m <sup>2</sup>
$F_g^w, F_g^a$	gas-phase advective flux vector (water, air), kg/m <sup>2</sup> s
$F_\ell^w, F_\ell^a$	aqueous-phase advective flux vector (water, air), kg/m <sup>2</sup> s
$g$	acceleration of gravity, m/s <sup>2</sup>
$h_g^w, h_g^a$	gas-phase component enthalpy (water, air), J/kg
$h_\ell, h_g$	enthalpy (aqueous, gas), J/kg
$h^w, h^a$	enthalpy (water, air), J/kg
$H_{g\ell}^a$	Henry's constant, gas-aqueous phase (air), Pa
<b>J</b>	Jacobian index matrix (conjugate gradient solver)
$J_g^w, J_g^a$	gas-phase diffusive flux vector (water, air), kg/m <sup>2</sup> s
$\tilde{k}$	intrinsic permeability tensor, m <sup>2</sup>
$k^x, k^y, k^z$	intrinsic permeability (east-west, north-south, top-bottom), m <sup>2</sup>
$\tilde{k}_f, \tilde{k}_m$	intrinsic permeability tensor (fracture, matrix), m <sup>2</sup>
$\tilde{k}_e$	equivalent thermal conductivity tensor, W/m K
$k_e^x, k_e^y, k_e^z$	equivalent thermal conductivity (east-west, north-south, top-bottom), W/m K
$k_i$	water saturation line constant
$k_\ell$	thermal conductivity (aqueous), W/m K
$k_{r\ell}, k_{rg}$	relative permeability (aqueous, gas)
$k_{r\ell b}, k_{r\ell f}, k_{r\ell m}$	aqueous relative permeability (bulk, fracture, matrix)
$\tilde{k}_s^u, \tilde{k}_s^s$	solid thermal conductivity tensor (unsaturated, saturated), W/m K
$K_D$	partition coefficient (solid-aqueous systems)
$K_{\ell g}$	partition coefficient (aqueous-gas systems), kg/m <sup>3</sup>

## Roman Symbols (contd)

$l(j)$	liquid water constant
$L_i$	liquid water constant
$m$	van Genuchten model curve-fitting parameter
$m_f, m_m$	van Genuchten model curve-fitting parameter (fracture, matrix)
$\dot{m}^w, \dot{m}^a$	mass source rate (water, air), kg/m <sup>3</sup> s
$M^w, M^a$	mass accumulation term (water, air), kg/m <sup>3</sup>
$M_{wt}^w, M_{wt}^a$	molecular weight (water, air), g/mol
$M_{wt}^A, M_{wt}^B$	molecular weight (component A, component B), g/mol
$n$	van Genuchten model parameter
$\mathbf{n}$	surface normal vector
$n_f, n_m$	van Genuchten model parameter (fracture, matrix)
$n(j)$	liquid water constant
$n_D, n_E, n_T$	porosity (diffusive, effective, total)
$n_{Df}, n_{Dm}$	porosity (diffusive-fracture, diffusive-matrix)
$n_D^*$	reference diffusive porosity
$P$	system pressure, Pa
$P^*$	reference pressure, Pa
$P_c^w, P_c^A, P_c^B$	critical pressure (water, component A, component B), Pa
$P_{cap}^*$	capillary pressure at residual saturation, Pa
$P_g^w, P_g^a$	gas-phase partial pressure (water, air), Pa
$P_g^*$	reference gas pressure, Pa
$P_l, P_g$	pressure (aqueous, gas), Pa
$P_r$	reduced pressure
$P_s^w$	saturation pressure (water), Pa

## Roman Symbols (contd)

$\dot{q}$	thermal energy source power density, W/m <sup>3</sup>
$\dot{Q}$	total energy source power density, W/m <sup>3</sup>
$\dot{Q}_{c,\gamma}$	species flux, mol/s m <sup>2</sup>
$\dot{Q}_{e,\gamma}$	diffusion heat flux, W/m <sup>2</sup>
$\dot{Q}_l, \dot{Q}_g, \dot{Q}_\gamma$	mass flux (aqueous, gas) kg/m <sup>2</sup> s
$r$	west-east coordinate (cylindrical coordinate systems), m
$R^w, R^a$	gas constant (water, air), J/kg K
$R^e$	energy conservation equation residual, W
$R^w, R^a$	mass conservation equation residual (water, air), kg/s
$\mathbf{R}$	vector of conservation equation residuals
$\dot{R}_c$	species reaction rate, 1/s
$\dot{s}_c$	species source, mol/m <sup>3</sup> s
$s_l, s_g$	saturation (aqueous, gas)
$s_{lb}, s_{lf}, s_{lm}$	effective aqueous saturation (bulk, fracture, matrix)
$s_l^*$	effective aqueous saturation
$s_{lf}^*, s_{lm}^*$	effective aqueous saturation (fracture, matrix)
$s_{lt}$	residual aqueous saturation
$s_{lrf}, s_{lrm}$	residual aqueous saturation (fracture, matrix)
$s_{st}$	entrapped air saturation
$S_s$	coefficient of specific storage, 1/m
$t$	time, s
$T$	temperature, °C or K
$T^*$	reference temperature, °C or K

## Roman Symbols (contd)

$T_c^A, T_c^B, T_c^w$	critical temperature (component A, component B, water), °C or K
$T_o$	273.15 K
$T_r$	reduced temperature
$u$	east-west Darcy velocity, m/s
$u_g^w, u_g^a$	gas-phase internal energy (water, air), J/kg
$u_l, u_g, u_s$	internal energy (aqueous, gas, solid), J/kg
$v$	north-south Darcy velocity, m/s
$V$	volume, m <sup>3</sup>
$V_l, V_g$	Darcy velocity vector (aqueous, gas), m/s
$w$	top-bottom Darcy velocity, m/s
$x$	west-east coordinate (Cartesian coordinate systems), m
$x$	independent variable
$x(j)$	liquid water constant
$x_g^w, x_g^a$	gas-phase mass fraction (water, air)
$x_l^w, x_l^a$	aqueous-phase mass fraction (water, air)
$y$	south-north coordinate (Cartesian coordinate systems), m
$Y, Y'$	water-vapor canonical function parameter
$z$	bottom-top coordinate (Cartesian and cylindrical coordinate systems), m
$\hat{z}$	bottom-top coordinate gradient
$z(j)$	liquid water constant
$Z$	water-vapor canonical function parameter
$Z_{ra}$	Rackett compressibility factor

## Greek Symbols

$\alpha$	van Genuchten model curve-fitting parameter, 1/m
$\alpha_f, \alpha_m$	van Genuchten model curve-fitting parameter (fracture, matrix), 1/m
$\alpha_L$	longitudinal hydraulic dispersivity, m
$\alpha_P$	pore compressibility, 1/Pa
$\alpha_T$	pore expansivity, 1/K; transverse hydraulic dispersivity, m
$\beta_p$	fluid compressibility, 1/Pa
$\Gamma$	control volume area, m <sup>2</sup>
$\xi$	Darcy velocity magnitude, m/s
$\eta_D$	diffusive water content = $n_E - (1 - s_l) n_D$
$\theta$	angular coordinate (cylindrical coordinate systems), radians
$\mu_g^w, \mu_g^a$	gas-phase component viscosity (water, air), Pa s
$\mu_l, \mu_g$	viscosity (aqueous, gas), Pa s
$\rho_c^w$	critical density (water), kg/m <sup>3</sup>
$\rho_g^w, \rho_g^a$	gas-phase component density (water, air), kg/m <sup>3</sup>
$\rho_{ls}, \rho_{ls}^*$	saturated density (aqueous, aqueous ref.), kg/m <sup>3</sup>
$\rho_l, \rho_g, \rho_s$	density (aqueous, gas, solid), kg/m <sup>3</sup>
$\rho_l^*$	aqueous reference density, kg/m <sup>3</sup>
$\sigma^{aw}$	air-water surface tension, N/m
$\tau_l, \tau_g$	tortuosity (aqueous, gas)
$\Phi_g^{ik}$	viscosity interaction parameter (gas)
$\chi_g^w, \chi_g^a$	gas-phase mole fraction (water, air)
$\chi_l^w, \chi_l^a$	aqueous-phase mole fraction (water, air)
$\psi^*$	minimum drainage capillary pressure head, m

## Greek Symbols (contd)

$\omega_{srk}$  Hankinson-Brobst-Thomson correlation parameter

## Subscripts

*B* bottom surface; bottom node  
*c* critical property; species  
*d* diffusion  
*D* diffusive  
*e* equivalent  
*E* east surface; east node; effective  
*f* fracture  
*g* gas phase  
*i* index i; component i  
*j* index j; component j  
*l* aqueous phase  
*m* minimum; matrix  
*N* north surface; north node  
*p* constant pressure  
*P* local node  
*r* residual  
*ra* Rackett  
*s* solid phase; saturation state  
*S* south surface; south node  
*T* top surface; top node; total  
*vap* vaporization  
*W* west surface; west node

### Subscripts (contd)

<i>WB</i>	west boundary surface
<i>wt</i>	weight
$\gamma$	surface indicator

### Superscripts

<i>a</i>	air component
<i>A</i>	component A
<i>aw</i>	air-water system
<i>B</i>	component B
<i>e</i>	energy
<i>min</i>	minimum
<i>n</i>	iteration index
<i>t</i>	time
<i>w</i>	water component
<i>x</i>	east-west direction
<i>y</i>	north-south direction
<i>z</i>	top-bottom direction
$\delta t$	time step
*	reference value; effective
.	per unit time
~	tensor

## Mathematical Symbols

<b>A</b>	bold lettering indicates vector or matrix
$\Sigma$	summation operator
$\int$	integral operator
$\partial$	partial differential operator
$\delta$	finite-difference operator
$\nabla$	divergence operator
$( )$	function operator
$  $	absolute value operator
$\overline{\square}$	surface interface-average operator
$\square$	upwind surface interface operator
$\max( , )$	maximum function operator

# Contents

Executive Summary .....	iii
Glossary of Symbols .....	v
1.0 Introduction .....	1.1
1.1 Yucca Mountain Hydrogeology Overview .....	1.1
1.2 Simulator Overview .....	1.4
2.0 Flow and Transport Theory .....	2.1
2.1 Application Scope .....	2.2
2.2 Governing Equations .....	2.3
2.2.1 Water Mass Conservation Equation .....	2.4
2.2.2 Air Mass Conservation Equation .....	2.4
2.2.3 Thermal Energy Conservation Equation .....	2.5
2.2.4 Species Mass Conservation Equation .....	2.6
2.3 Solution Options .....	2.6
2.3.1 Water .....	2.8
2.3.2 Air .....	2.9
2.3.3 Water-Air .....	2.10
2.3.4 Energy .....	2.11
2.3.5 Water-Energy .....	2.12
2.3.6 Air-Energy .....	2.13
2.3.7 Water-Air-Energy .....	2.14
3.0 Constitutive Functions .....	3.1
3.1 Gas-Phase Partial Pressure .....	3.1
3.1.1 Water-Vapor Partial Pressure .....	3.1
3.1.2 Air Partial Pressure .....	3.2
3.2 Density .....	3.2
3.2.1 Gas-Phase Density .....	3.3
3.2.2 Aqueous-Phase Density .....	3.4
3.3 Mass and Mole Fractions .....	3.4
3.3.1 Gas-Phase Mass Fraction .....	3.5
3.3.2 Aqueous-Phase Mass Fraction .....	3.5
3.4 Viscosity .....	3.6
3.4.1 Gas-Phase Viscosity .....	3.6

3.4.2	Aqueous-Phase Viscosity .....	3.7
3.5	Enthalpy and Internal Energy .....	3.8
3.5.1	Gas-Phase Enthalpy and Internal Energy .....	3.8
3.5.2	Aqueous-Phase Enthalpy and Internal Energy .....	3.9
3.6	Porosity and Tortuosity .....	3.11
3.7	Liquid Saturation .....	3.11
3.7.1	van Genuchten Model .....	3.11
3.7.2	Brooks and Corey Model .....	3.12
3.7.3	Leverett Model .....	3.13
3.7.4	Dual Porosity Model .....	3.14
3.8	Liquid and Gas Relative Permeability .....	3.15
3.8.1	Mualem Model .....	3.15
3.8.2	Burdine Model .....	3.16
3.8.3	Corey Model .....	3.17
3.8.4	Fatt and Klikoff Model .....	3.17
3.8.5	Dual Porosity Model .....	3.18
3.9	Thermal Conductivity .....	3.19
3.10	Gas-Phase Diffusivity .....	3.20
3.11	Species Transport Properties .....	3.21
4.0	Numerical Solution Method .....	4.1
4.1	Discretization of the Mass Conservation Equations .....	4.1
4.2	Discretization of the Energy Conservation Equation .....	4.6
4.3	Discretization of the Species Mass Conservation Equation .....	4.9
4.4	Boundary Conditions .....	4.12
4.4.1	Dirichlet Boundary Conditions .....	4.15
4.4.2	Neumann Boundary Conditions .....	4.17
4.5	Newton-Raphson Linearization Scheme .....	4.18
4.6	Linear Equation Solution .....	4.21
5.0	Code Architecture .....	5.1
6.0	References .....	6.1
Appendix - Numerical Values of Liquid Water, Water-Vapor, and Saturation Line		
Constants	.....	A.1

## Figures

1.1 Physiographic Features of Yucca Mountain and Surrounding Region .....	1.2
1.2 Generalized East-West Section Through Yucca Mountain Showing Conceptual Moisture-Flow System Under Natural Conditions .....	1.3
3.1 Water Saturation Pressure .....	3.2
3.2 Water-Vapor Density (saturated conditions) .....	3.3
3.3 Liquid Water Density (saturated conditions) .....	3.4
3.4 Water-Vapor (saturated conditions) and Air Viscosities .....	3.7
3.5 Gas-Phase Viscosity .....	3.7
3.6 Water-Vapor Enthalpy and Internal Energy (saturated conditions) .....	3.9
3.7 Aqueous-Phase Enthalpy and Internal Energy (saturated conditions) .....	3.10
3.8 van Genuchten Saturation Function ( $\alpha = 0.0305 \text{ cm}^{-1}$ , $n = 2$ ) .....	3.12
3.9 Brooks and Corey Saturation Function ( $\beta = 6.5$ , $\psi^* = 0.11 \text{ cm}$ ) .....	3.13
3.10 Leverett Saturation Function ( $P^*_{cap} = 632455 \text{ Pa}$ ) .....	3.14
3.11 Dual Porosity Saturation Function .....	3.15
3.12 Mualem Liquid Relative Permeability Function .....	3.16
3.13 Burdine Liquid Relative Permeability Function .....	3.16
3.14 Corey Relative Permeability Functions .....	3.17
3.15 Fatt and Klikoff Relative Permeability Functions .....	3.18
3.16 Dual Porosity Liquid Relative Permeability Function .....	3.19
3.17 Liquid Thermal Conductivity .....	3.20
4.1 X-Z Cartesian Coordinate System .....	4.2
4.2 X-Y Cartesian Coordinate System .....	4.2
4.3 R-Z Cylindrical Coordinate System .....	4.3
4.4 R- $\theta$ Cylindrical Coordinate System .....	4.3
4.5 X-Z Cartesian Coordinate System for <i>West</i> Boundary .....	4.13
4.6 X-Y Cartesian Coordinate System for <i>West</i> Boundary .....	4.13
4.7 R- $\theta$ Cylindrical Coordinate System for <i>West</i> Boundary .....	4.14
4.8 R-Z Cylindrical Coordinate System for <i>West</i> Boundary .....	4.14
5.1 MSTS-Logic Flow Chart .....	5.2

## 1.0 Introduction

Yucca Mountain, Nevada, has been selected by the U.S. Department of Energy (DOE) as a potential site for construction of a deep geologic repository for the permanent storage of high-level radioactive waste. The site must now be characterized (studied) to determine its suitability to contain the waste. The strategy for site characterization has been outlined in the Site Characterization Plan (SCP; DOE 1988) by the DOE Office of Civilian Radioactive Waste Management (OCRWM). Data collected during the site characterization phase of repository analysis will be used to analyze the performance of the repository with respect to the statutory requirements of the Nuclear Waste Policy Act (Public Law 97-425), the Nuclear Waste Policy Amendments Act (Public Law 100-203), 10 CFR 60, and 40 CFR 191. DOE is required to submit a license application to the U.S. Nuclear Regulatory Commission (NRC).

Performance assessment analyses are under way to determine if unfavorable conditions exist that would preclude licensing of a potential repository at Yucca Mountain. Another purpose of performance assessment analyses is to provide input to site characterization. Data that have been collected to date at Yucca Mountain provide initial estimates of hydraulic and geochemical properties. These initial estimates of Yucca Mountain properties provide the basis for OCRWM to begin development of performance assessment tools and strategies that will be used in the license submittal to NRC. Of primary importance is development of the conceptual and numerical models that are needed to increase current understanding of conditions at Yucca Mountain and to provide direction to the field and laboratory activities described in the SCP. Pacific Northwest Laboratory<sup>1</sup> has provided total systems performance analyses to assist DOE in assessing the performance of the potential repository based on current designs and hydrologic data.

### 1.1 Yucca Mountain Hydrogeology Overview

Yucca Mountain is located within the physiographic Basin and Range Province, which is characterized by mountain ranges trending generally north-south and intervening valleys. Yucca Mountain (Figure 1.1) is a prominent group of north-trending fault block ridges. Major structural geologic features of the mountain include the Solitario Canyon and Ghost Dance faults. The elevation of northern Yucca Mountain is approximately 1500 m, and the ridge is approximately 300 m above the valley floor. Yucca Mountain consists of a thick sequence of both welded and nonwelded volcanic tuffs that dip 5 to 10 degrees to the east (Montazer and Wilson 1984). The tuffs extend well below the water and form a thick unsaturated zone. The densely welded tuffs typically are highly fractured with low saturated matrix hydraulic conductivities (Peters and Klavetter 1988). The nonwelded tuffs that are vitric have few fractures and relatively highly saturated matrix hydraulic conductivities; the zeolitic nonwelded tuffs are characterized by relatively few fractures and low matrix hydraulic conductivities.

The unsaturated zone at Yucca Mountain is characterized by a low recharge rate. A conceptual model of flow through Yucca Mountain (Montazer and Wilson 1984) is presented in Figure 1.2. In the Montazer and Wilson conceptualization of flow through the mountain, a small fraction of the annual precipitation at the mountain migrates as recharge downward through the tuff units toward the water table. Some water movement within Yucca Mountain occurs as water vapor, which can move in an upward direction. Water-vapor movement will be more important when waste

---

<sup>1</sup> Pacific Northwest Laboratory is operated for the U.S. Department of Energy by Battelle Memorial Institute.

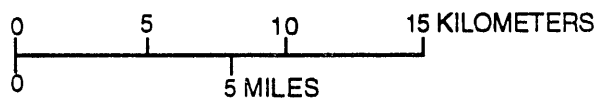
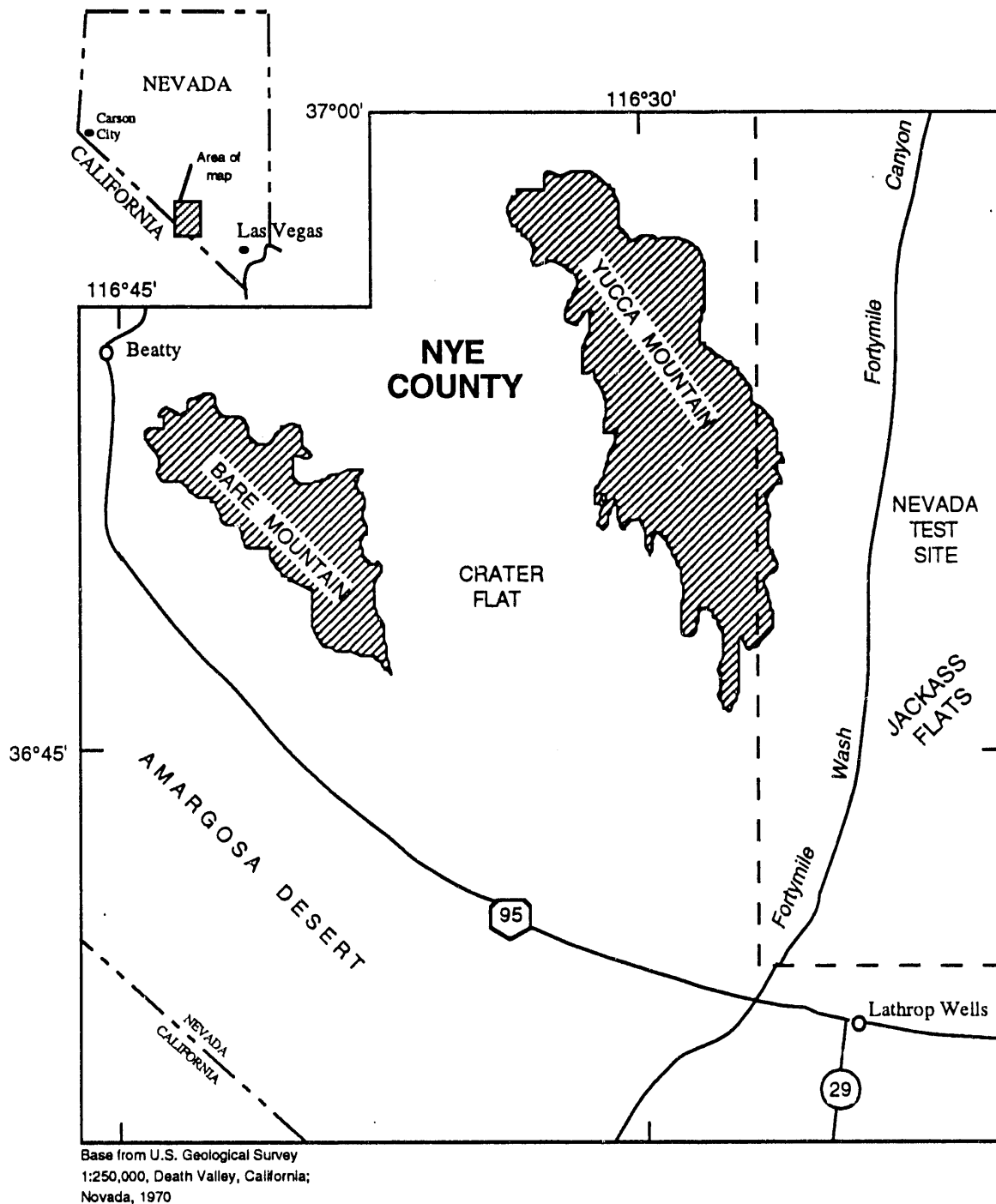


**Figure 1.1.** Physiographic Features of Yucca Mountain and Surrounding Region (modified from Montazer and Wilson 1984)

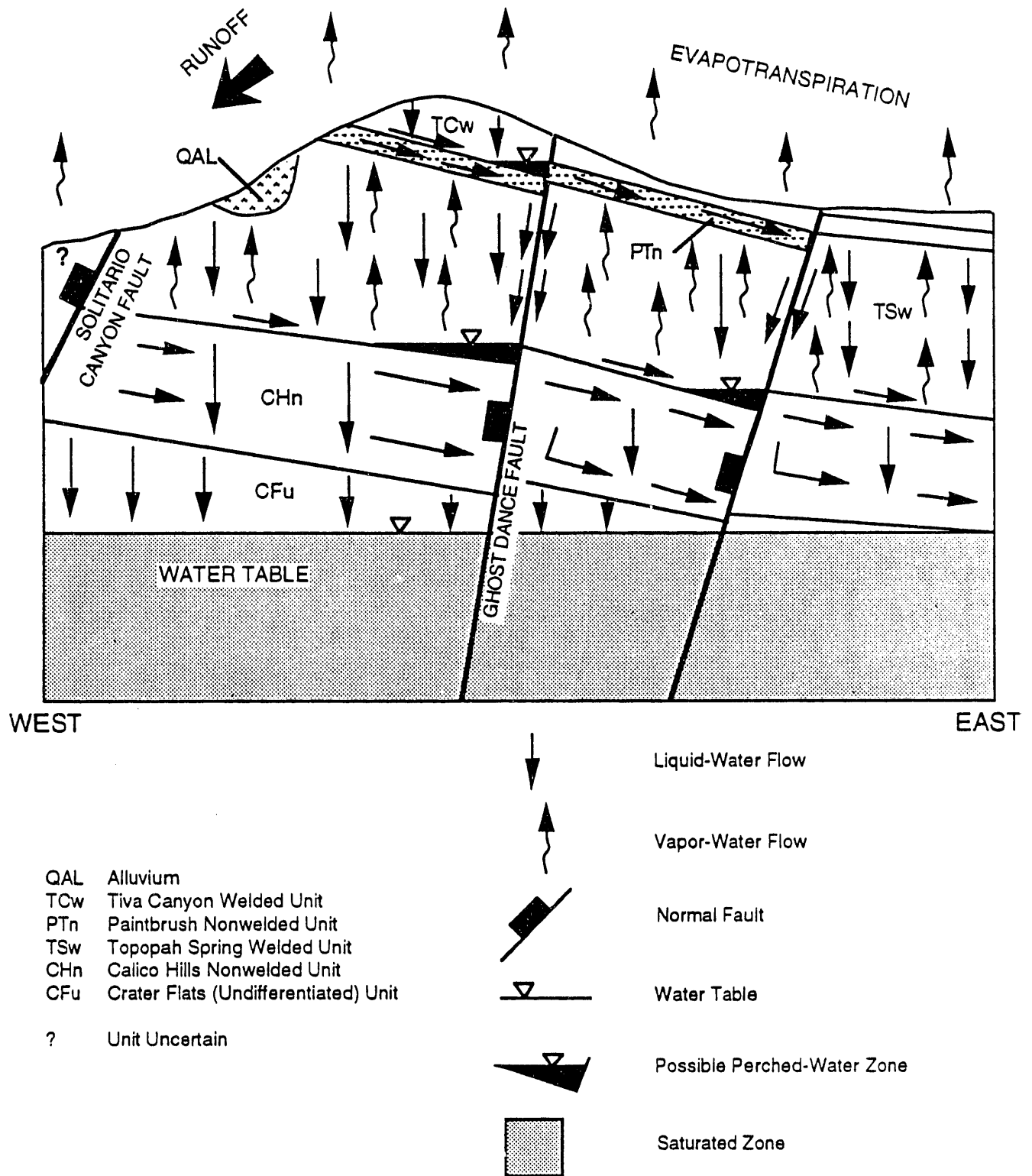


**Figure 1.2.** Generalized East-West Section Through Yucca Mountain Showing Conceptual Moisture-Flow System Under Natural Conditions (modified from Montazer and Wilson 1984)

is emplaced in the potential repository. Under ambient conditions, most of the liquid water likely moves predominantly in a vertical, downward direction, and its movement is influenced by interactions between the fractures and the matrix. The fractures present in the welded and nonwelded tuffs at Yucca Mountain represent heterogeneities where the flow properties vary by several orders of magnitude, depending on the local hydraulic conditions.

## 1.2 Simulator Overview

The site characterization studies conducted at the Yucca Mountain site necessitate numerical predictions of the thermal and hydrologic response of the subsurface environment to the potential nuclear waste repository. This thermal and hydrologic response of the repository environment is anticipated to include complex processes of countercurrent vapor and liquid migration, multiple-phase heat transfer, multiple-phase transport, and geochemical reactions. Numerical predictions of complex phenomena can be realized through empirical, semiempirical, or mechanistic-type models. Empirical and semiempirical models involve applying an expression of observed data from a particular system to predict the response of a similar system. Mechanistic models describe the fundamental processes of a particular system through mathematical expressions (known as the governing equations and constitutive equations). Whereas both general types of models can yield numerical predictions about the state of the subsurface system, the empirical and semiempirical models are generally limited in applicability to systems similar to those used to develop the empirical model. The mechanistic approach allows numerical predictions to be made of novel or untested systems over extended periods of time. This document describes the Multiphase Subsurface Transport Simulator (MSTS), a mechanistic numerical simulator for predicting the thermal and hydrologic flow and transport phenomena in fractured porous media.

Computer codes that simulate transport processes in geologic media are typically classified according to capabilities related to phases, components, and saturation levels. Under this classification strategy, MSTS would be classified as a two-phase, two-component numerical simulator, with a dilute species, for variably saturated geologic media. This classification arises because MSTS models two phases (aqueous and gas) and two components (water and air). In contrast, single-phase, single-component subsurface transport simulators typically model a single fluid (e.g., water or liquid organic) that is composed of a single component or completely miscible mixture. In reality, these types of single-phase simulators are pseudo-two-phase models, because a nonparticipating gas phase is assumed to exist. Another type of two-phase, two-component subsurface simulator is possible that should be distinguished from the MSTS code. These simulators typically model two immiscible fluid phases (e.g., water and liquid organic), and their applications differ significantly from those for MSTS. As with their single-phase, single-component counterparts, these simulators are restricted to modeling flows of weak thermal gradients without significant phase changes. Moreover, these types of two-phase simulators could be considered pseudo-three-phase models, because of the assumption of a nonparticipating gas phase.

Single-phase, single-component subsurface transport simulators are capable of modeling fluid flow, heat transfer, and mass transport (through a dilute species) in variably saturated media for numerous applications. The single-phase, single-component simulators, however, are inappropriate for modeling flow situations characterized by phase change or strong thermally driven flow fields. Typically for single-phase, single-component simulators capable of modeling variably saturated conditions, the presence of an air phase is acknowledged only through the functional dependence of the fluid hydraulic conductivity on relative saturation. A separate equation to determine the pressure in the vapor phase is not explicitly solved. The MSTS code specifically addresses the additional phenomena of air and water-vapor transport, two-phase heat transfer, and

two-phase mass transport by solving an additional conservation equation and phase-change-related constitutive equations. The requirements for modeling nonisothermal two-phase flow are motivated by the importance of accurately predicting the movement of liquid, vapor, heat, and species in the tuffaceous media within and surrounding the potential waste repository at Yucca Mountain.

The principal design goal for MSTS was that it contain the capabilities for generating numerical predictions of the complex flow and transport phenomena occurring in the subsurface environment at Yucca Mountain over a period of 10,000 years. Secondary design goals were that MSTS: 1) be accessible and exploitable to scientists and engineers familiar with subsurface environment phenomena but not necessarily numerical modeling technicalities; 2) have enough general applicability to attract or generate a user group that is capable of supporting training, maintenance, and enhancement activities; 3) be verified by comparisons with analytical solutions and benchmarked against existing simulators; 4) be validated against germane laboratory and field experiments; and 5) have controlled configuration and documentation under an appropriate quality assurance program. This document primarily describes those portions of the simulator and support software that are associated with the primary design goal. Issues relating to the secondary design goals and simulator use are described in the companion document called the "User's Guide and Reference" (Nichols and White 1992).

The source code for MSTS is written in FORTRAN 77, following the American National Standards Institute (ANSI) standards, and includes calls to machine-dependent time and data subroutines for numerous computing platforms. Input files for MSTS can be generated with either an interactive graphical user interface, for Macintosh systems (Nichols and White 1992), or a conventional text editor. The graphical user interface allows the user to specify simulation parameters through a controlled interactive environment. Output generated by MSTS is completely controlled by the user through input specifications and includes thermal and hydrologic field states and fluxes (e.g., temperatures, pressures, saturations, component mass fractions, Darcy velocities, and heat transfer rates). Species transport output also includes field states and fluxes. Special screen outputs can be requested by the user to trace histories of field and flux variables interactively during the simulation. Both spatial and temporal output of field and flux variables can be generated for subsequent graphical analysis.

An established quality assurance program is followed for the maintenance and control of the MSTS software. This program is designed to ensure documentation and verification of engineering and/or scientific software. The current version of MSTS has been verified against a selected series of problems for which analytical and/or numerical solutions were available. A portion of these problems are described in the "User's Guide and Reference" document (Nichols and White 1992). The subject quality assurance program has three principal components: software maintenance and control, software use, and software database management. The software maintenance and control component of the quality assurance program requires that a systematic procedure be adopted for distinguishing among versions of the software and recording all changes between versions. Furthermore, the program requires that systematic backups are performed, that new versions of the software are verified to ensure that changes were installed correctly, and that software continues to satisfy its design requirements. The software use component of the quality assurance program requires that all applications are reproducible by documenting versions and known errors or modifications for the software in use. This component also requires that appropriate testing has been performed and documented prior to using the software for application simulations. Moreover, any software transferred to a new computing environment for application-type simulations will be reverified and documented prior to performing application simulations. Because MSTS does not use databases, other than those constants used to compute physical properties, the database management component of the subject quality assurance program is not applicable to the software.

This software theory manual is divided into six principal sections. Section 2 describes the specific scope of applications addressable by the simulator and the governing conservation equations that mathematically describe multiphase flow, thermal transport, and species transport in fractured subsurface environments. Included in this section are discussions of the fundamental assumptions used to construct the mechanistic models in MSTs. Section 3 describes the constitutive equations that relate the principle unknowns (i.e., primary variables) to the coefficients (i.e., secondary variables) of the governing equations. Section 4 is dedicated to discussions of the numerical techniques used to solve the governing conservation equations. This section covers a broad spectrum of topics, including primary variables, secondary variables, variable switching, discretization techniques, linearization methods, boundary conditions, and linear equation solvers. Section 5 describes the code architecture, and the references are listed in Section 6.

## 2.0 Flow and Transport Theory

Design of MSTS was directed at predicting the thermal and hydrologic response of the subsurface environment surrounding the potential nuclear waste repository at Yucca Mountain, over a 10,000-year period. Required prediction capabilities include those for multiphase transport and radioactive decay of radionuclides and/or heavy metals. To numerically predict the thermal and hydrologic response of Yucca Mountain, mechanistic models are required that accurately describe multiphase fluid flow, interphase mass transfer, heat transfer, and species transport phenomena in subsurface environments. The Yucca Mountain subsurface environment consists of fractured or unfractured porous media filled or partially filled with either air or water. Furthermore, the subsurface environment will be assumed to consist of three phases: an aqueous phase composed of liquid water and dissolved air, a gas phase composed of water vapor and air, and a solid phase composed of the porous media. With this phase description, radionuclides or heavy metals are assumed to occur adsorbed on the solid phase and/or dissolved in the fluid phases. An important distinction exists between components and phases when describing multiphase and multicomponent subsurface transport phenomena. For example, conservation equations are written for component masses transported by phases; however, phase mass is not a conserved quantity.

Numerical models for subsurface transport yield quantitative descriptions of transport phenomena. Numerical models may be classified as empirical, semiempirical, or fundamental. Empirical models are typically developed from observed or experimentally measured quantities, and are generally used to predict the response of a particular system to a limited number of parameter variations. Empirical models are applicable only to systems that are roughly equivalent to the system used to develop the empirical model and associated data sets. Fundamental models describe phenomena through accepted physical laws (e.g., conservation of mass and conservation of energy). In general, fundamental models have a broader range of applicability than empirical models. Semiempirical models contain elements of both empirical and fundamental models. Typically, semiempirical models are formulated from fundamental principals for idealized systems with empirically derived parameters serving to adjust the model for real systems.

All three types of numerical models (empirical, semiempirical, and fundamental) are incorporated into MSTS in various degrees. Four fundamental equations that express the conservation of component mass, species mass, and energy form the simulator's governing equations. Empirical and semiempirical models relate the governing equations' principal unknowns (primary variables) to the equations' coefficients (secondary variables). These empirical and semiempirical equations are referred to collectively as the constitutive equations. An example of a semiempirical equation embedded in a governing fundamental equation is one that describes the component mass conservation equations. The conservation equations for water and air mass contain expressions of phase Darcy velocities. Darcy velocities or phase mass fluxes are computed from Darcy's semiempirical relationship that relates phase volumetric rates to phase pressure gradients and gravitational body forces. The functional relationship between aqueous-phase saturation and capillary pressure, commonly referred to as the soil characteristics, is an example of an empirical model that relates the primary variables of pressure to the second variable of aqueous-phase saturation.

Flow of air and water components in the subsurface environment is expressed in MSTS through component conservation equations. Mass conservation equations are fundamental equations that mathematically balance the amount of component mass entering and leaving a control volume with the time rate of change of the component's mass within the control volume. The component mass crossing the control volume surfaces is described by Darcy's flow equation for porous media, where Darcy's equation relates the phase mass flux to gradients in pressure head and

gravitational body forces. Component fluxes crossing a control volume surface are computed from phase mass fluxes by multiplying the component mass fraction for a particular phase by the Darcy mass flux for that phase. Diffusion of air and water component masses across the control volume surfaces is considered for the gas phase. Gas-phase diffusive flow of components is described by Fick's law, modified for porous media with saturation-dependent tortuosities. The time rate of change of a component mass within the control volume depends on the time rate of change of the following parameters: component mass fractions for both phases, phase saturations, phase densities, and diffusive porosity. The conservation equations for water and air mass, expressed in partial differential form, make up the governing equations for component flow in the subsurface environment. For isothermal systems, uncontaminated with radioactive or heavy metal elements, these conservation equations describe two-phase flow phenomena in porous media.

Because heat will be generated within the waste forms emplaced in the potential nuclear waste repository at Yucca Mountain, the ability to compute heat transport phenomena in the subsurface environment is critical to describing the thermal and hydrologic response of the repository. Analogous to mass flow, heat transfer in the subsurface environment is described with a conservation equation for energy. The energy conservation equation is a fundamental equation that mathematically balances the amount of energy entering the control volume with the time rate of change of energy within the control volume. Heat transfer crossing the control volume surfaces occurs by diffusion and/or advection. Diffusive heat transfer is described by Fick's law and assumed to occur through the aqueous and solid phases. Heat conduction through the gas phase is neglected. Furthermore, latent and sensible heat transfer contributions from components diffusing through the gas phase are ignored. Advective heat transfer includes both sensible and latent components. Interphase mass transfer of water and air is computed assuming thermodynamic equilibrium conditions exist. The time rate of change of energy within the control volume depends on the time rate of change of the following parameters: phase internal energies, phase saturations, phase densities, and diffusive porosity.

Transport of radionuclides or heavy metals in the subsurface environment is described by a species component conservation equation. A fundamental assumption associated with the species transport equation is that species concentrations remain dilute with respect to computing the physical properties of the aqueous and gas phases. The species conservation equation is a fundamental equation that mathematically balances the quantity of species mass entering the control volume with the time rate of change of species mass within the control volume. Species mass transport across the control volume surfaces occurs by molecular diffusion, hydrodynamic dispersion, and/or advection. Diffusive and advective transport of species mass is considered in both the aqueous and the gas phases and is dependent on the species concentration for a particular phase. Dispersive transport is considered only for the aqueous phase. Species partitioning among the solid, aqueous, and gas phases depends on the affinity of the species for each particular phase according to composition and local geochemistry. As with the energy equation, geochemical equilibrium is assumed in computing the species partitioning. The time rate of change of species mass within the control volume depends on the time rate of change of the following parameters: species concentration in each phase, phase saturations, and diffusive porosity.

## **2.1 Application Scope**

The four fundamental equations for conservation of component mass, energy, and species mass that compose MSTS essentially define the simulator's application scope. A fundamental restriction with respect to the MSTS application scope is that all applications are strictly limited to subsurface porous media environments. This restriction holds because of the application of Darcy's law to compute phase volumetric fluxes. Furthermore, driving forces for fluid flow are

limited to pressure gradients and gravitational body forces. MSTS is classified as a two-component, two-phase simulator. This classification implies that MSTS is capable of computing flow and transport processes only for subsurface systems that contain no more than two components and two phases. Moreover, components are confined to water and air, and phases are confined to aqueous and gas systems. Subsurface systems contaminated with significant concentrations of an organic compound would fall outside the application scope of MSTS. Low solubilities are assumed for expressing the quantity of air dissolved in the aqueous phase. Within the gas phase, component mass fractions are completely variable. Liquid saturations and relative permeabilities are computed neglecting hysteretic and air entrapment effects. The flow model for highly fractured systems assumes that the porous medium and fracture are continuously in thermal and hydraulic equilibrium. Although discrete fractures can be modeled with MSTS, the simulator is inappropriate for modeling transient fracture-matrix interactions with the dual porosity model.

The energy conservation equation expands the application scope by allowing thermal gradients to influence flow fields. The energy equation formulation allows for both sensible and latent heat transfer. Sensible heat transfer occurs by thermal diffusion through the solid and liquid phases and by advection through the fluid phase. Diffusive heat transfer through the gas phase is neglected. Latent heat transfer by evaporation and condensation processes is considered for the water component. Because interphase mass transfer computations depend on the assumption of thermodynamic equilibrium, MSTS is not applicable for systems requiring disequilibrium or kinetic modeling of the thermodynamic processes. Sensible and latent heat transfer associated with diffusing or dispersing components is neglected. Therefore, enhanced heat transfer by vapor migration under thermal gradient conditions must be included empirically in the effective thermal conductivity coefficient.

Species transport processes are solved by assuming loose coupling between multiphase fluid flow and species transport processes. Because of the strong dependence of phase pressures and temperature on the secondary variables that compose the fundamental equations for mass and energy conservation, these fluid flow and heat transport fundamental equations are solved simultaneously (coupled). The principal assumption associated with the species transport processes is that the species are numerically considered passive scalars. Physically, this assumption implies that the secondary variables of the mass and energy conservation equations are independent of species concentrations. A passive scalar species limits the applicability of the engineering simulator to dilute species concentrations. Species concentrations may be considered dilute whenever the physical, thermal, or transport properties of the transport fluid remain unaltered. The dilute concentration assumption and decoupled solution approach also allow consideration of multiple species and transport modeling of radioactive decay products. No accounting is made of chemical reaction and/or radioactive decay products.

## **2.2 Governing Equations**

Four partial differential equations form the governing equations that are assumed to mathematically describe the transport of water, air, thermal energy, and a dilute species in the subsurface environment at the potential Yucca Mountain waste repository. Each partial differential equation represents an expression of conservation of component mass, thermal energy, or species mass. The conservation equations balance the time rate of change in the conserved quantity within a control volume against the surface fluxes of the conserved quantity entering the control volume. The conserved quantities are water mass, air mass, thermal energy, and species mass. Transport of the four conserved quantities through a porous medium is modeled within two distinct phases, aqueous and gas. The aqueous phase is composed primarily of water, with relatively small amounts of dissolved air, whereas the gas phase is composed of various compositions of air and water vapor.

### 2.2.1 Water Mass Conservation Equation

The conservation equation for water mass, expressed in partial differential equation form, is shown in Equation (2.1). The term on the left-hand side of Equation (2.1) represents the time rate of change of water mass within the control volume. Water occurs within the soil pores as liquid in the aqueous phase and as vapor in the gas phase. Unconnected pore spaces are considered to be filled with liquid water but isolated from the continuous pore spaces, and therefore do not contribute to the water mass accumulation term. Interphase mass transfer of water between the aqueous and gas phases is computed by assuming thermodynamic equilibrium conditions. This equilibrium assumption implies that time scales for thermodynamic processes are significantly shorter than those associated with transport. The two gradient terms on the right-hand side of Equation (2.1) represent the mass flux of water mass into the control volume through aqueous and gas phases, respectively. Water mass flux occurs by advection in both phases and by diffusion through the gas phase. Advective transport is governed by Darcy's law for flow through porous media, where phase pressure gradients and gravitational forces drive the flow fields. For unsaturated porous media, advective transport depends on saturation-dependent relative permeabilities for each phase. Component diffusion rates through the liquid phases are neglected as a transport mechanism. Diffusion through the gas phase is governed by the classical mass diffusion equation, modified by the porous media tortuosity. The driving forces behind diffusive transport are component concentration or mass fraction gradients in the gas phase. The last term on the right-hand side of Equation (2.1) represents the water mass source rate within the control volume.

$$\begin{aligned} \frac{\partial}{\partial t} [n_D x_l^w \rho_l s_l + n_D x_g^w \rho_g s_g] = \nabla \left[ \frac{x_l^w \tilde{k} k_{rl} \rho_l}{\mu_l} (\nabla P_l + \rho_l g \hat{z}) \right] \\ + \nabla \left[ \frac{x_g^w \tilde{k} k_{rg} \rho_g}{\mu_g} (\nabla P_g + \rho_g g \hat{z}) + \tau_g n_D \rho_g s_g D_g^{aw} \nabla x_g^w \right] + \dot{m}^w \end{aligned} \quad (2.1)$$

### 2.2.2 Air Mass Conservation Equation

The conservation equation for air mass, expressed in partial differential equation form, is shown in Equation (2.2). The term on the left-hand side of Equation (2.2) represents the time rate of change of air mass in the control volume. Air occurs within the soil pores as dissolved air in the aqueous phase and as gaseous air in the gas phase. Occluded air within the aqueous phase is neglected, by assuming that air entrapped by imbibing water would eventually dissolve into the aqueous phase. Unconnected pore spaces are considered to be filled with liquid water but isolated from the continuous pore spaces, and therefore do not contribute to the air mass accumulation term. Interphase mass transfer of air between the aqueous and gas phases is computed by assuming thermodynamic equilibrium conditions. This equilibrium assumption implies that time scales for thermodynamic processes are significantly shorter than those associated with transport. The two gradient terms on the right-hand side of Equation (2.2) represent the mass flux of air mass into the control volume through aqueous and gas phases, respectively. Air mass flux occurs by advection in both phases and by diffusion through the gas phase. Advective transport is governed by Darcy's law for flow through porous media, where phase pressure gradients and gravitational forces drive the flow fields. For unsaturated porous media, advective transport depends on saturation-dependent relative permeabilities for each phase. Component diffusion rates through the aqueous phase are neglected as a transport mechanism. Diffusion through the gas phase is governed by the classical mass diffusion equation, modified by the porous media tortuosity. The driving forces behind

diffusive transport are component concentration or mass fraction gradients in the gas phase. The last term on the right-hand side of Equation (2.2) represents the air mass source rate within the control volume.

$$\begin{aligned} \frac{\partial}{\partial t} [n_D x_\ell^a \rho_\ell s_\ell + n_D x_g^a \rho_g s_g] = & \nabla \left[ \frac{x_\ell^a \tilde{k} k_{r\ell} \rho_\ell}{\mu_\ell} (\nabla P_\ell + \rho_\ell g \hat{z}) \right] \\ + \nabla \left[ \frac{x_g^a \tilde{k} k_{rg} \rho_g}{\mu_g} (\nabla P_g + \rho_g g \hat{z}) - \tau_g n_D \rho_g s_g D_g^{aw} \nabla x_g^w \right] + \dot{m}^a \end{aligned} \quad (2.2)$$

### 2.2.3 Thermal Energy Conservation Equation

The conservation equation for thermal energy, expressed in partial differential form, is shown in Equation (2.3), where phase velocities are defined by Equations (2.4) and (2.5), for the aqueous and gas phases, respectively. The term on the left-hand side of Equation (2.3) represents the time rate of change of heat content in the control volume. The total heat contained in the control volume depends directly on temperature, liquid saturations, phase compositions, and soil physical properties. For the thermal energy conservation equation, a modified aqueous-phase saturation applies that accounts for the thermal capacitance of unconnected pore spaces, which are assumed to be filled with liquid water. Internal energies and densities of the aqueous phase are those for pure liquid water. This assumption follows directly from the principal assumption of relatively low solubilities of air in the aqueous phase. Disparately, the internal energy of the gas phase is strongly dependent on phase composition. The first term on the right-hand side of Equation (2.3) represents heat transfer into the control volume by advection. Analogous to the evaluation of internal energies, the enthalpy of the aqueous phase is that for pure liquid water, whereas the gas-phase enthalpy is strongly dependent on phase composition. The second term on the right-hand side of Equation (2.3) represents heat transfer by conduction and mechanical dispersion. The equivalent conductivity tensor represents the combination of solid- and liquid-phase conductivities along with the mechanical dispersion coefficient. Typically, the mechanical dispersion tensor is neglected by assigning zero to the longitudinal and transverse dispersivities. Thermal conductivity through the gas phase is neglected. The last three terms on the right-hand side of Equation (2.3) represent internal heat generation quantities from thermal energy sources and sinks within the control volume, and the change in internal energy associated with water and air mass sources and sinks within the control volume, respectively. The internal heat generation quantities from mass sources represent the enthalpy associated with a mass source.

$$\begin{aligned} \frac{\partial}{\partial t} [ (1 - n_T) \rho_s u_s + \eta_D \rho_\ell u_\ell + n_D s_g \rho_g u_g ] = \\ - \nabla [ \rho_\ell h_\ell \mathbf{V}_\ell + \rho_g h_g \mathbf{V}_g ] \\ + \nabla [ \tilde{k}_e \nabla T ] + \dot{q} + h^w \dot{m}^w + h^a \dot{m}^a \end{aligned} \quad (2.3)$$

where

$$\mathbf{V}_\ell = A \frac{\tilde{k} k_{r\ell}}{\mu_\ell} (\nabla P_\ell + \rho_\ell g \hat{z}) \quad (2.4)$$

$$\mathbf{V}_g = A \frac{\tilde{k} k_{rg}}{\mu_g} (\nabla P_g + \rho_g g \hat{z}) \quad (2.5)$$

### 2.2.4 Species Mass Conservation Equation

The conservation equation for species mass, expressed in partial differential equation form, is shown in Equation (2.6). The term on the left-hand side of Equation (2.6) represents the time rate of change of total species mass within a control volume. Interphase species mass transfer between solid and fluid phases is computed by assuming that thermodynamic and geochemical equilibrium conditions apply. These equilibrium condition assumptions require that time scales for thermodynamic and geochemical phenomena be small when compared with those for transport phenomena. For transport through geologic media, these assumptions are generally appropriate. The first term on the right-hand side of Equation (2.6) represents the migration of species mass into the control volume by advection through the aqueous and gas phases. Advective transport is dependent on the species concentration and Darcy velocity within each phase. The second term on the right-hand side of Equation (2.6) represents the hydrodynamic dispersion of species in the aqueous phase. The third term on the right-hand side of Equation (2.6) represents the diffusion of species mass into the control volume in the aqueous and gas phases. Typically, diffusion coefficients for the gas phase will be several orders of magnitude greater than those for the aqueous phase. Species diffusion fluxes are phase-specific and depend on the gradients in species phase concentrations, phase pore areas, and phase tortuosities. The fourth term on the right-hand side of Equation (2.6) represents the generation of species within the control volume. The last term on the right-hand side of Equation (2.6) represents the radioactive decay or consumption rate of species mass.

$$\begin{aligned} \frac{\partial C}{\partial t} = & -\nabla [C_\ell \mathbf{V}_\ell + C_g \mathbf{V}_g] + \nabla [s_\ell n_D \tilde{D}_{h_\ell} \nabla C_\ell] \\ & + \nabla [\tau_\ell s_\ell n_D D_{d_\ell} \nabla C_\ell + \tau_g s_g n_D D_{d_g} \nabla C_g] + \dot{s}_c - \dot{R}_c C \end{aligned} \quad (2.6)$$

### 2.3 Solution Options

One of the design goals for MSTS was to create an efficient numerical simulator for predicting flow and transport phenomena in the subsurface environment. Because of the diversity of subsurface flow problems, a single-solution option would result in a numerical simulator that was computationally inefficient for a majority of problems. For example, if the simulation problem involved generating predictions of radionuclide transport by water under isothermal conditions, then it would be superfluous to include gas-phase transport and heat transfer in the solution scheme. The preferred solution scheme in terms of computational efficiency would be to sequentially solve the water mass conservation and species mass conservation equations. However, if the simulation problem involves nonisothermal aspects and if species transport through the gas phase is significant, then the solution scheme would require the coupled solution of both component mass conservation equations and the energy equation, along with the sequential solution of the species transport equation. To avoid simulating the negligible aspects of a particular subsurface flow and transport problem, several solution options are available with MSTS. This approach yields a simulator that matches computational effort to the problem characteristics.

Solution modes or options are characterized by the specific solved conservation equations. The conservation equations are divided into coupled and auxiliary conservation equations according

to their interdependencies. The governing conservation equations for water mass, air mass, and energy are considered coupled equations because they are solved simultaneously. The species mass conservation equation is considered an auxiliary equation because it is solved sequentially to the coupled conservation equations. The lowest-order solution modes are those that involve the solution of a single coupled conservation equation (e.g., water mass conservation, air mass conservation, or energy conservation). These lower-order solution modes generally require more assumptions about the subsurface system to be applicable. The next-higher-order solution modes are those that involve the coupled solution of a pair of conservation equations. These solution modes typically eliminate one of the primary assumptions associated with a single-equation solution mode. The highest-order solution mode requires the coupled solution of both component mass conservation equations and the energy conservation equation. The computational effort increases roughly with the square of the coupled equations solved (i.e., three coupled equations require eight times the computational effort required for a single equation). All solution modes can include the solution of the auxiliary species conservation equation.

Solution modes are chosen by the user according to the coupled conservation equations selected for solution. Considerable computational savings may be achieved through the proper choice of a solution mode for a particular application. Choosing lower-order solution modes (i.e., those with fewer equations) generally requires that some assumptions be made about the problem. Some assumptions are obvious (e.g., eliminating the air mass conservation equation for isothermal water flow problems, or eliminating the energy conservation equation for isothermal problems). Other assumptions require previous modeling experience, experimental evidence, or field observations to support the elimination of a specific equation. For example, what thermal gradients constitute the inclusion of vapor transport through the gas phase to accurately predict heat transfer rates? Answering this type of question requires specific property information about the porous media and anticipated thermal gradients.

The following subsections (Sections 2.3.1 through 2.3.7) describe the seven solution modes available in MSTS. Each subsection is labeled with a solution mode title, followed by a brief general description of the solution mode and the type of problems to which it applies. Each subsection also contains primary, secondary, and velocity variable lists. Primary variables refer to the principal unknowns for the solution mode. The numbers of primary variables and equations solved always coincide. Fixed primary variables refer to primary variables that must be specified according to the problem assumptions. Fixed primary variables are specified, not computed. For example, the gas-phase pressure for a water flow problem solved in the "Water" mode might be fixed to atmospheric conditions, or 101325.0 Pa. Secondary variables are physical properties, transport properties, and saturations that are computed from the unknown and fixed primary variables. Fixed secondary variables are physical properties, transport properties, and saturations, required for the solved equations, that are independent of the unknown primary variables. For example, liquid viscosities are generally considered independent of liquid pressures. Velocities refer to flow velocities or diffusion mass fluxes computed by MSTS from the solution of the unknown pressure field. Fixed velocities are those velocities or diffusion mass fluxes computed for inactive phases from fixed pressure fields, soil characteristics, and transport properties.

### 2.3.1 Water

Description: The "Water" mode solves saturated and unsaturated water flow problems without a participating gas phase. This approach has been traditionally used to solve soil physics problems. Soil characteristics are computed for a two-phase air-water system using nonhysteretic relations. Physical properties may be specified invariant or dependent on aqueous pressure. Species transport in the aqueous phase may be modeled by additionally solving the species mass conservation equation.

Application: Appropriate applications for the "Water" mode include saturated and unsaturated water flow problems with negligible thermal and gas pressure gradients.

Specification: Solution Schemes and Options Card

Governing Equations

Thermal Energy Conservation Equation: off

Water Conservation Equation: on

Air Conservation Equation: off

Species Conservation Equation: off / on

Options

Binary Diffusion: off

Fixed Properties: off / on

Liquid Phase: on

Gas Phase: off

Vapor Pressure Lowering: off

Primary Variables: aqueous pressure

Fixed Primary Variables: gas pressure, temperature

Secondary Variables: aqueous-phase density, aqueous-phase saturation, aqueous-phase relative permeability, porosity, aqueous-phase tortuosity

Fixed Secondary Variables: aqueous-phase viscosity

Fluxes: aqueous-phase velocity

### 2.3.2 Air

Description: The "Air" mode solves unsaturated subsurface gas flow problems with static saturation fields. Liquid saturations are temporally invariant, and are either specified or computed from initial fields of aqueous pressure and gas pressure. Fixed physical properties are temporally invariant, computed from the initial fields of aqueous pressure, gas pressure, and temperature. Vapor-diffusive transport and convective mass transport may be computed through the gas phase for spatially variant temperature fields. Conservation of water mass and energy is not ensured for vapor transport problems. Gas-phase density, gas-phase mass fraction and vapor diffusivities may be specified invariant or dependent on gas pressure. Species transport in the gas phase can be modeled by additionally solving the species mass conservation equation.

Application: Appropriate applications for the "Air" mode include unsaturated subsurface gas flow problems with invariant liquid saturation and temperature fields. Density-driven gas flows resulting from steady thermal gradients are an appropriate problem for this mode. For these types of applications, the influence of both temperature and vapor mass fractions on gas-phase properties could be investigated. An inappropriate application, however, would result if either the liquid saturation or the thermal fields were significantly altered by the transport of vapor or heat through the gas phase.

Specification: Solution Schemes and Options Card

Governing Equations

Thermal Energy Conservation Equation: off

Water Conservation Equation: off

Air Conservation Equation: on

Species Conservation Equation: off / on

Options

Binary Diffusion: off / on

Fixed Properties: off / on

Liquid Phase: off

Gas Phase: on

Vapor Pressure Lowering: off / on

Primary Variables: gas pressure

Fixed Primary Variables: aqueous pressure, temperature

Secondary Variables: water-vapor partial pressure, air partial pressure, water-vapor density, air density, gas-phase density, water-vapor mass/mole fraction, air mass/mole fraction, gas-phase viscosity, water-vapor diffusivity

Fixed Secondary Variables: aqueous-phase saturation

Fluxes: gas-phase velocity, water-vapor diffusion mass flux

### 2.3.3 Water-Air

Description: The "Water-Air" mode solves saturated and unsaturated water flow problems with a participating gas phase. Soil characteristics are computed for a two-phase air-water system using nonhysteretic relations. Physical properties are temporally invariant, computed from the initial fields of aqueous pressure, gas pressure, and temperature. Water-vapor transport through the gas phase is computed for spatially variant temperature fields. Phase densities, mass fractions, and vapor diffusivities may be specified invariant or dependent on pressure. Species transport in the aqueous and gas phases can be modeled by additionally solving the species mass conservation equation.

Application: Appropriate applications for the "Water-Air" mode include saturated and unsaturated water flow problems with steady or negligible thermal gradients. This mode differs from the "Water" mode because it is applicable to problems involving gas pressure gradients. For steady thermal conditions, this mode is appropriate for predicting the transport of water vapor by diffusion and advection through the gas phase. The mode becomes inappropriate when the liquid and mass transport influence the thermal field. Because heat transfer associated with vaporization and condensation may be significant, thermal effects should be considered carefully before this mode is applied to a simulation problem.

Specification: Solution Schemes and Options Card

Governing Equations

Thermal Energy Conservation Equation: off

Water Conservation Equation: on

Air Conservation Equation: on

Species Conservation Equation: off / on

Options

Binary Diffusion: off / on

Fixed Properties: off / on

Liquid Phase: on

Gas Phase: on

Vapor Pressure Lowering: off / on

Primary Variables: aqueous pressure, gas pressure

Fixed Primary Variables: temperature

Secondary Variables: water-vapor partial pressure, air partial pressure, water-vapor density, air density, gas-phase density, aqueous-phase density, air mass/mole fraction, water-vapor mass/mole fraction, aqueous-phase air mass/mole fraction, gas-phase viscosity, aqueous-phase saturation, gas-phase saturation, aqueous-phase relative permeability, gas-phase relative permeability, porosity, aqueous-phase tortuosity, gas-phase tortuosity, water-vapor diffusivity

Fixed Secondary Variables: aqueous-phase viscosity

Fluxes: aqueous-phase velocity, gas-phase velocity, water-vapor diffusion mass flux

## 2.3.4 Energy

Description: The "Energy" mode solves heat transfer problems for saturated and unsaturated subsurface flow problems. Constant aqueous- and gas-phase flow fields may be prescribed. Diffusive heat transfer occurs through the solid and liquid phases. Advective heat transfer occurs through the fluid phases. No heat transfer occurs by vapor diffusion through the gas phase. System pressures, phase saturations, and relative permeabilities are invariant. Mass continuity is not ensured for specified flow fields. Physical properties may be specified as invariant or dependent on temperature.

Application: Appropriate applications for the "Energy" mode include subsurface heat transfer through saturated and unsaturated porous media. Fixed saturation and fluid flow fields are the principal assumptions associated with this mode. Saturation levels and Darcy flow velocities may be specified for the aqueous and gas phases through the initial pressure fields and soil characteristics. An appropriate application for this mode could involve heat transfer through completely dry or completely saturated porous media, or heat transfer through partially saturated porous media with relatively high liquid mass flux rates. Without adjusting the porous media thermal conductance for heat transfer enhancement by vapor diffusion, this mode would be inappropriate for predicting heat transfer for partially saturated media with low liquid mass flux rates. The mode would also be inappropriate for conditions where the thermal field affected the saturation fields (e.g., heat-pipe-type flow phenomena).

Specification: Solution Schemes and Options Card

Governing Equations

Thermal Energy Conservation Equation: on

Water Conservation Equation: off

Air Conservation Equation: off

Species Conservation Equation: off

Options

Binary Diffusion: off

Fixed Properties: off / on

Liquid Phase: off / on

Gas Phase: off / on

Vapor Pressure Lowering: off

Primary Variables: temperature

Fixed Primary Variables: aqueous pressure, gas pressure

Secondary Variables: water-vapor partial pressure, air partial pressure, water-vapor density, air density, gas-phase density, aqueous-phase density, water-vapor mass/mole fraction, air mass/mole fraction, aqueous-phase air mass fraction, water-vapor enthalpy, air enthalpy, gas-phase enthalpy, aqueous-phase enthalpy, water-vapor internal energy, air internal energy, gas-phase internal energy, aqueous-phase internal energy, aqueous-phase thermal conductivity, solid-phase thermal conductivity, equivalent thermal conductivity

Fixed Secondary Variables: aqueous-phase saturation

Fluxes: thermal flux

### 2.3.5 Water-Energy

Description: The "Water-Energy" mode solves aqueous flow and heat transfer problems for saturated and unsaturated subsurface flow systems. Aqueous-phase flow fields are computed assuming a nonparticipating gas phase. Soil characteristics are computed for an air-water system using nonhysteretic relations. Diffusive heat transfer occurs through the solid and aqueous phases. Advective heat transfer occurs through the aqueous phase. No heat transfer occurs by vapor diffusion through the gas phase. Physical properties may be specified invariant or dependent on aqueous pressure and temperature. Species transport in the aqueous phase may be modeled by additionally solving the species mass conservation equation.

Application: Appropriate applications for the "Water-Energy" mode include water flow and heat transfer through saturated and unsaturated porous media. Typical applications would involve concurrent solutions of the aqueous-pressure and temperature fields. Transport of heat and water vapor through the gas phase is assumed negligible with this mode. An appropriate application for this mode is the solution of a density-driven aqueous flow through porous media. Inappropriate problems include those characterized with high latent heat transfer rates through the gas phase.

Specification: Solution Schemes and Options Card

Governing Equations

Thermal Energy Conservation Equation: on

Water Conservation Equation: on

Air Conservation Equation: off

Species Conservation Equation: off / on

Options

Binary Diffusion: off

Fixed Properties: off / on

Liquid Phase: on

Gas Phase: off / on

Vapor Pressure Lowering: off

Primary Variables: aqueous pressure, temperature

Fixed Primary Variables: gas pressure

Secondary Variables: aqueous-phase density, aqueous-phase viscosity, aqueous-phase enthalpy, aqueous-phase internal energy, aqueous-phase thermal conductivity, solid-phase thermal conductivity, equivalent thermal conductivity, aqueous-phase saturation, trapped gas saturation, aqueous-phase relative permeability, porosity, aqueous-phase tortuosity

Fluxes: aqueous-phase velocity, thermal flux

### 2.3.6 Air-Energy

Description: The "Air-Energy" mode solves unsaturated subsurface gas flow and heat transfer problems with static saturation fields. Liquid saturations are temporally invariant, and are either specified or computed from initial fields of aqueous pressure and gas pressure. Diffusive heat transfer occurs through the solid and liquid phases. Advective heat transfer occurs through the gas phase. No heat transfer occurs by vapor diffusion through the gas phase. Conservation of water mass is not ensured for vapor transport problems. Physical properties may be specified invariant or dependent on gas pressure and temperature. Species transport in the gas phase may be modeled by additionally solving the species mass conservation equation.

Application: Appropriate applications for the "Air-Energy" mode include gas flow and heat transfer through unsaturated porous media. Density-driven gas flows resulting from transient or steady thermal fields are an appropriate problem for this mode. Fixed liquid saturation fields may be specified for the aqueous phase through the initial aqueous- and gas-pressure fields and the soil characteristics. For these types of applications, the influence of both temperature and vapor mass fractions on gas-phase properties may be investigated. An inappropriate application, however, would result if the liquid saturation fields were significantly altered by the transport of vapor or neat through the gas phase.

Specification: Solution Schemes and Options Card

Governing Equations

Thermal Energy Conservation Equation: on

Water Conservation Equation: off

Air Conservation Equation: on

Species Conservation Equation: off / on

Options

Binary Diffusion: off / on

Fixed Properties: off / on

Liquid Phase: off

Gas Phase: on

Vapor Pressure Lowering: off / on

Primary Variables: gas pressure, temperature

Fixed Primary Variables: aqueous pressure

Secondary Variables: water-vapor partial pressure, air partial pressure, water-vapor density, air density, gas-phase density, water-vapor mass/mole fraction, air mass/mole fraction, gas-phase viscosity, water-vapor enthalpy, air enthalpy, gas-phase enthalpy, aqueous-phase enthalpy, water-vapor internal energy, air internal energy, gas-phase internal energy, aqueous-phase internal energy, aqueous-phase thermal conductivity, solid-phase thermal conductivity, equivalent thermal conductivity, water-vapor diffusivity

Fixed Secondary Variables: aqueous-phase saturation

Fluxes: gas-phase velocity, water-vapor diffusion mass flux, thermal flux

### 2.3.7 Water-Air-Energy

**Description:** The "Water-Air-Energy" mode solves aqueous flow and heat transfer problems for saturated and unsaturated subsurface flow systems. Aqueous-phase flow fields are computed assuming a participating gas phase. Soil characteristics are computed for an air-water system using nonhysteretic relations. Diffusive heat transfer occurs through the solid and aqueous phases. Advective heat transfer occurs through the aqueous and gas phases. Diffusive heat transfer through the gas phase includes both sensible and latent components for water vapor. No heat transfer occurs by vapor diffusion through the gas phase. Physical properties may be specified invariant or dependent on aqueous pressure, gas pressure, and temperature. Species transport in the aqueous and gas phases can be modeled by additionally solving the species mass conservation equation.

**Application:** Appropriate applications for the "Water-Air-Energy" mode include aqueous and gas flow and heat transfer through saturated and unsaturated porous media. Because of the coupled solution of the water, air, and energy equations, this mode is applicable to problems involving both sensible and latent heat transfer through the gas phase (e.g., heat-pipe-type flows). This mode eliminates the isothermal assumptions associated with the "Water-Air" mode and the assumptions of zero latent heat transfer associated with the "Water-Energy" mode, at the expense of additional computational effort.

**Specification:** Solution Schemes and Options Card

Governing Equations

Thermal Energy Conservation Equation: on

Water Conservation Equation: on

Air Conservation Equation: on

Species Conservation Equation: off / on

Options

Binary Diffusion: off / on

Fixed Properties: off / on

Liquid Phase: on

Gas Phase: on

Vapor Pressure Lowering: off / on

**Primary Variables:** aqueous pressure (water-vapor mass fraction), gas pressure, temperature

**Secondary Variables:** water-vapor partial pressure, air partial pressure, water-vapor density, air density, gas-phase density, aqueous-phase density, air mass/mole fraction, water-vapor mass/mole fraction, aqueous-phase air mass/mole fraction, gas-phase viscosity, aqueous-phase viscosity, water-vapor enthalpy, air enthalpy, gas-phase enthalpy, aqueous-phase enthalpy, water-vapor internal energy, air internal energy, gas-phase internal energy, aqueous-phase internal energy, aqueous-phase thermal conductivity, solid-phase thermal conductivity, equivalent thermal conductivity, aqueous-phase saturation, gas-phase saturation, trapped gas saturation, aqueous-phase relative permeability, gas-phase relative permeability, porosity, aqueous-phase tortuosity, gas-phase tortuosity, water-vapor diffusivity

**Fluxes:** aqueous-phase velocity, gas-phase velocity, water-vapor diffusion mass flux, thermal flux

## 3.0 Constitutive Functions

Constitutive functions relate the coefficients of the governing equations (secondary variables) to the principal unknowns of the governing equations (primary variables). For the thermodynamic, physical, hydrologic, and geochemical systems to be completely specified, all of the secondary variables must be computable from the selected set of primary variables. Secondary variables include hydrologic parameters (e.g., saturation, relative permeability), soil properties (e.g., porosity, tortuosity), fluid properties (e.g., viscosity, density, enthalpy), thermodynamic properties (e.g., saturation vapor pressures, vapor mass fractions), and transport properties (e.g., dispersion coefficients, diffusion coefficients, partition coefficients). This section describes and references the constitutive functions applied in MSTS to relate secondary with primary variables. Several of the constitutive functions described in this section incorporate secondary variables in the functional descriptions of other secondary variables. The calculation sequences for secondary variables in MSTS are specifically structured to avoid using uncomputed secondary variables in expressions of other secondary variables. Because of the modular structure of MSTS, constitutive functions for a particular parameter can be supplanted with another theory or actual experimental data, when available. As part of the modular design, MSTS incorporates "stand alone" subroutines for the constitutive functions, allowing advanced users to modify or supplant constitutive functions without concern for the particulars of the numerical schemes.

### 3.1 Gas-Phase Partial Pressure

When liquid and gas phases exist under thermodynamic equilibrium, the partial pressure of water vapor in the gas phase equals the saturated water-vapor pressure (van Wylen and Sonntag 1978). In the absence of the liquid phase, the water-vapor partial pressure may be computed from the gas-phase mole fraction and gas-phase pressure. The partial pressure of air in the gas phase is estimated with Dalton's partial pressure law for ideal gases, as shown in Section 3.1.2. Strong capillary pressures lower the saturated water-vapor pressure, through an effect referred to as vapor pressure lowering (Nitao 1988).

#### 3.1.1 Water-Vapor Partial Pressure

For multiphase (i.e., both liquid and gas phases are present) and thermodynamic equilibrium conditions, the water-vapor partial pressure equals the saturated water-vapor pressure. Saturated vapor pressures are computed as a function of temperature from the steam table equations (ASME<sup>1</sup> 1967), according to Equation (3.1). The numerical values of the saturation line constants are listed in Table A.3 of the Appendix. The saturated water-vapor pressure function is shown in graphical form in Figure 3.1. In the absence of an aqueous phase, the water-vapor partial pressure is computed from the water-vapor mass fraction, gas-phase component molecular weights, and total gas pressure (van Wylen and Sonntag 1978) according to Equations (3.2) and (3.3). Refer to Section 3.3 for gas-phase mass fraction constitutive functions. Under conditions of high capillary pressures, water molecules are bound more tightly than for free surfaces, and vapor pressure lowering occurs. Vapor pressure lowering effectively lowers the vapor pressure above the pore water (i.e., raises the pore-water boiling point), as shown in Equation (3.4) (Nitao 1988).

---

<sup>1</sup> American Society of Mechanical Engineers.

$$P_g^w = P_c^w \exp \left[ \frac{T_c^w}{T} \left( \frac{\sum_{i=1}^5 k_i \left(1 - \frac{T}{T_c^w}\right)^i}{1 + k_6 \left(1 - \frac{T}{T_c^w}\right) + k_7 \left(1 - \frac{T}{T_c^w}\right)^2} \right) - \frac{\left(1 - \frac{T}{T_c^w}\right)}{k_8 \left(1 - \frac{T}{T_c^w}\right)^2 + k_9} \right] \quad (3.1)$$

$$\chi_g^w = \frac{\frac{x_g^w}{M_{wt}^w}}{\sum_{i=w, a} \frac{x_g^i}{M_{wt}^i}} \quad (3.2)$$

$$P_g^w = \chi_g^w P_g \quad (3.3)$$

$$P_g^w = P_g^w \exp \left( \frac{P_l - P_g}{\rho_l R^w T} \right) \quad (3.4)$$

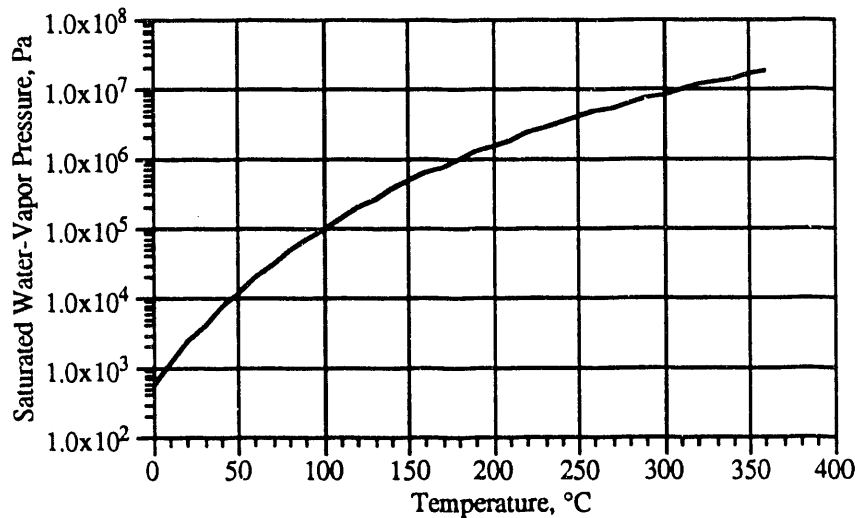


Figure 3.1. Water Saturation Pressure

### 3.1.2 Air Partial Pressure

The air partial pressure is computed from Dalton's partial pressure law for ideal gas mixtures (van Wylen and Sonntag 1978), according to Equation (3.5).

$$P_g^a = P_g - P_g^w \quad (3.5)$$

### 3.2 Density

Gas-phase densities are computed using Dalton's ideal gas law for mixtures, where component partial pressures sum to the total gas-phase pressure, and component densities sum to the total gas-phase density. The assumption of low liquid-phase solubilities, taken with the engineering simulator, allows the aqueous-phase densities to be computed for pure liquid water.

### 3.2.1 Gas-Phase Density

Water-vapor component density is computed as a function of temperature and water-vapor partial pressure from the steam table equations (ASME 1967), according to Equation (3.6). The numerical values of the water-vapor constants are listed in Tables A.2 and A.4 of the Appendix. The numerical indices for the water-vapor density function are listed in Table A.5 of the Appendix. The water-vapor density function for saturated conditions is shown in graphical form in Figure 3.2. Air component density is computed from the ideal gas law according to Equation (3.7). The gas-phase density equals the sum of the individual gas-phase component densities (van Wylen and Sonntag 1978), according to Equation (3.8).

$$\rho_g^w = \frac{1}{v_g^w} \left[ \frac{l_1 T_r}{P_r} - \sum_{i=1}^5 \left\{ i P_r^{(i-1)} \sum_{j=1}^{n(i)} B_{ij} X^z(i,j) \right\} - \sum_{i=6}^8 \left\{ \frac{(i-2) P_r^{(1-i)} \sum_{j=1}^{n(i)} B_{ij} X^z(i,j)}{P_r^{(2-i)} \sum_{k=1}^{l(i)} b_{ik} X^x(i,j)} + 11 \left( \frac{P_r}{\beta_L} \right)^{10} \sum_{i=0}^6 B_{9i} X^i \right\} \right]^{-1} \quad (3.6)$$

where

$$X = \exp\{b(1 - T_r)\}$$

$$\beta_L = L_0 + L_1 T_r + L_2 T_r^2$$

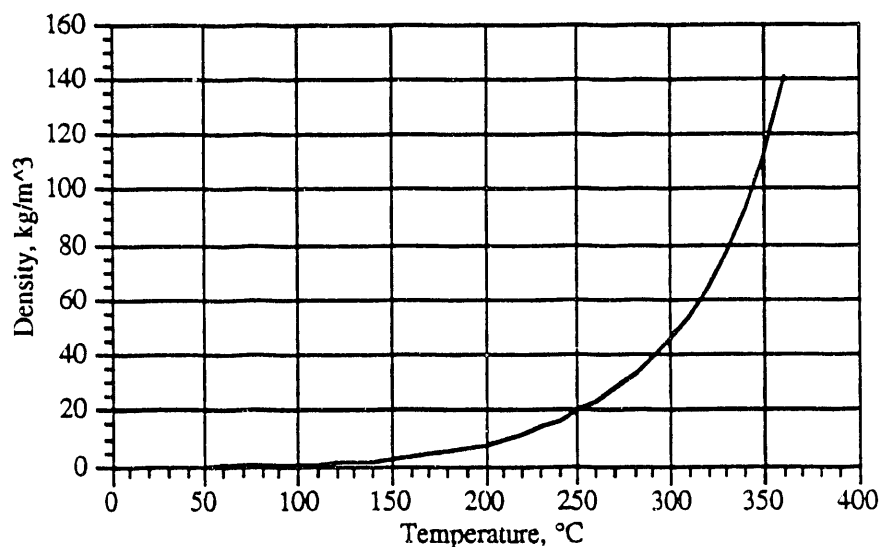


Figure 3.2. Water-Vapor Density (saturated conditions)

$$\rho_g^a = \frac{P_g^a}{R^a T} \quad (3.7)$$

$$\rho_g = \rho_g^w + \rho_g^a \quad (3.8)$$

### 3.2.2 Aqueous-Phase Density

Aqueous-phase density is computed as a function of temperature and pressure from the steam table equations (ASME 1967), according to Equation (3.9). The numerical values of the liquid water constants are listed in Table A.1 of the Appendix. The aqueous-phase density function for saturated conditions is shown in graphical form in Figure 3.3.

$$\rho_l = \frac{1}{v_l^w} \left[ A_{11} a_5 Z^{-5/17} + \left\{ \begin{array}{l} A_{12} + A_{13} T_r + A_{14} T_r^2 \\ + A_{15} (a_6 - T_r)^{10} + A_{16} (a_7 + T_r^{19})^{-1} \end{array} \right\}^{-1} \right. \\ \left. - (a_8 + T_r^{11})^{-1} (A_{17} + 2 A_{18} P_r + 3 A_{19} P_r^2) \right. \\ \left. - A_{20} T_r^{18} (a_9 + T_r^2) (-3 (a_{10} + P_r)^{-4} + a_{11}) \right. \\ \left. + 3 A_{21} (a_{12} - T_r) P_r^2 + 4 A_{22} T_r^{-20} P_r^3 \right] \quad (3.9)$$

where

$$Z = Y + (a_3 Y^2 - 2 a_4 T_r + 2 a_5 P_r)^{1/2}$$

$$Y = 1 - a_1 T_r^2 - a_2 T_r^{-6}$$

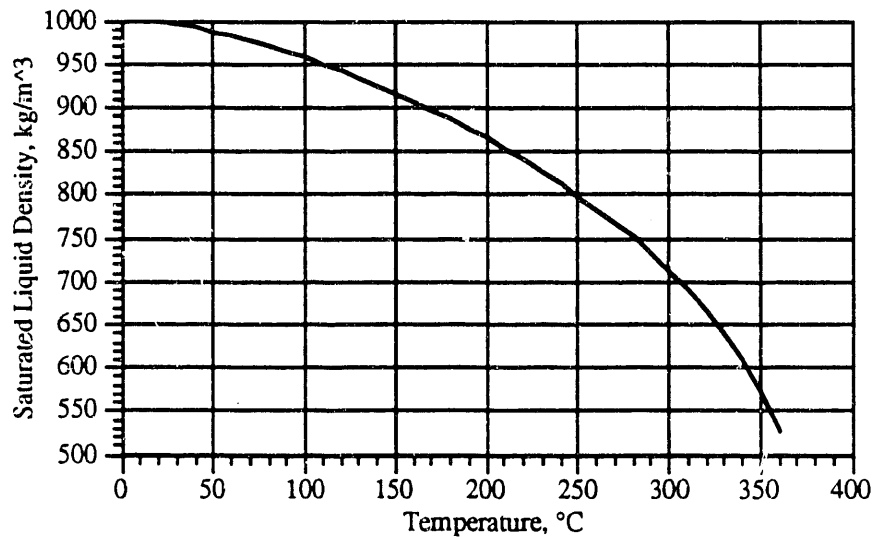


Figure 3.3. Liquid Water Density (saturated conditions)

### 3.3 Mass and Mole Fractions

Gas-phase mass fraction is computed directly from the ratio of component gas density to gas-phase density (van Wylen and Sonntag 1978). Aqueous-phase mass fraction is computed assuming thermodynamic and geochemical equilibrium exists between the gas and aqueous phases. Mole fraction is computed from the component mass fractions and component molecular weights (van Wylen and Sonntag 1978), according to Equation (3.10), where the summation occurs over the water and air components. Superscripts *i* and *k* indicate components, whereas the subscript *j* indicates phases. Mass fraction may be computed from the component mole fractions and

component molecular weights (van Wylen and Sonntag 1978), according to Equation (3.11), where the summation occurs over the two components water and air:

$$\chi_j^i = \frac{\frac{x_j^i}{M_{wt}^i}}{\sum_{k=w, a} \frac{x_j^k}{M_{wt}^k}} \text{ for } i = w, a \text{ and } j = \ell, g \quad (3.10)$$

$$\chi_j^i = \frac{\chi_j^i M_{wt}^i}{\sum_{k=w, a} \chi_j^k M_{wt}^k} \text{ for } i = w, a \text{ and } j = \ell, g \quad (3.11)$$

### 3.3.1 Gas-Phase Mass Fraction

For multiphase (i.e., both liquid and gas phases are present) and thermodynamic equilibrium conditions, the gas-phase mass fraction is computed from the ratio of component gas density to total gas-phase density (van Wylen and Sonntag 1978), according to Equation (3.12) for water. By definition, the component gas-phase mass fractions sum to one; therefore, the air mass fraction is computed according to Equation (3.13). In the absence of a particular liquid phase, the component vapor mass fraction becomes the primary variable for the governing mass conservation equation.

$$x_g^w = \frac{\rho_g^w}{\rho_g} \quad (3.12)$$

$$x_g^a = 1 - x_g^w \quad (3.13)$$

### 3.3.2 Aqueous-Phase Mass Fraction

Aqueous-phase mass fractions are computed by assuming thermodynamic equilibrium conditions between gaseous air and dissolved air in the aqueous phase. Under chemical equilibrium conditions, the concentration of a component in the gas phase is proportional to the concentration/solubility of the component in the aqueous phase (Sandler 1989). The proportionality constant, Henry's constant, relates the component partial pressure in the gas phase with the component's mole fraction in the aqueous phase (Sandler 1989). Using Henry's law, the partial pressure of air in the gas phase is related to the mole fraction of air in the aqueous phase according to Equation (3.14). Henry's constant depends on the solute-solvent pair, temperature, and pressure. At higher solute concentrations, the linear relationship fails, because Henry's constant becomes dependent on concentration. Assuming a linear form for Henry's law is equivalent to assuming low aqueous solubilities for air, which is a fundamental assumption for MSTs. Air solubilities in the aqueous phase can be complex functions of temperature. By definition, the aqueous-phase mass fractions sum to one; therefore, the water mass fraction is computed according to Equation (3.15). Aqueous-phase mass fractions are computed from aqueous-phase mole fractions, according to Equation (3.11).

$$\chi_{\ell}^a = \frac{p_g^a}{H_{g\ell}^a} \quad (3.14)$$

$$\chi_i^w = 1 - \chi_i^a \quad (3.15)$$

### 3.4 Viscosity

Gas-phase viscosity is dependent on composition, temperature, and pressure. Gas-phase viscosity is computed in MSTS with an extension of the Chapman-Enskog theory for multicomponent gas mixtures at low densities (Reid et al. 1987). Aqueous-phase viscosity is assumed independent of composition and is computed for pure water as a function of both temperature and pressure.

#### 3.4.1 Gas-Phase Viscosity

Gas phases modeled with MSTS can be composed of various compositions of air and water vapor; therefore, the gas-phase viscosity function depends on the mixture composition and system temperature. Gas-phase viscosity is computed using an extension, proposed by Wilke, of the Chapman-Enskog theory for multicomponent gas mixtures at low densities (Bird et al. 1960). The semiempirical expression developed by Wilke relates component vapor viscosities, composition mole fractions, and component molecular weights to a mixture viscosity, according to Equations (3.16) and (3.17), where the component vapor viscosities are computed as a function of temperature and pressure. Water-vapor viscosity is computed from the International Formulation Committee (IFC) steam table formulations (ASME 1967), according to Equations (3.18) and (3.19), with viscosity in micropoise, density in g/cm<sup>3</sup>, and temperature in °C. Air component viscosity is computed as a function of temperature from empirical correlations (ASHRAE<sup>2</sup> 1977), according to Equation (3.20), with viscosity in Pa s and temperature in K. The functions for air viscosity and water-vapor viscosity for saturated conditions are shown graphically in Figure 3.4. The gas-phase viscosity function is shown graphically in Figure 3.5 for a temperature of 60°C.

$$\mu_g = \sum_{i=w,a} \frac{\chi_g^i \mu_g^i}{\sum_{k=w,a} \chi_g^k \Phi_g^{i,k}} \quad (3.16)$$

$$\Phi_g^{i,k} = \frac{1}{\sqrt{8}} \left( 1 + \frac{M_{wt}^i}{M_{wt}^k} \right)^{-1/2} \left[ 1 + \left( \frac{\mu_g^i}{\mu_g^k} \right)^{1/2} \left( \frac{M_{wt}^k}{M_{wt}^i} \right)^{1/4} \right]^2 \quad (3.17)$$

Superheated steam at 1-bar pressure in the temperature range 100°C to 700°C:

$$\mu_g^w = 0.407 T + 80.4 \quad (3.18)$$

Superheated steam from 1-bar pressure to saturation pressure in the temperature range 100°C to 300°C:

$$\mu_g^w = 0.407 T + 80.4 - \rho_g^w (1858 - 5.9 T) \quad (3.19)$$

---

<sup>2</sup> American Society of Heating, Refrigerating, and Air Conditioning Engineers.

$$\mu_g = 2.6693 \times 10^{-6} \frac{(M_{wt}^a T)^{1/2}}{(3.617)^2 \left[ 1.188 - \frac{0.051}{97.0} T \right]} \quad (3.20)$$

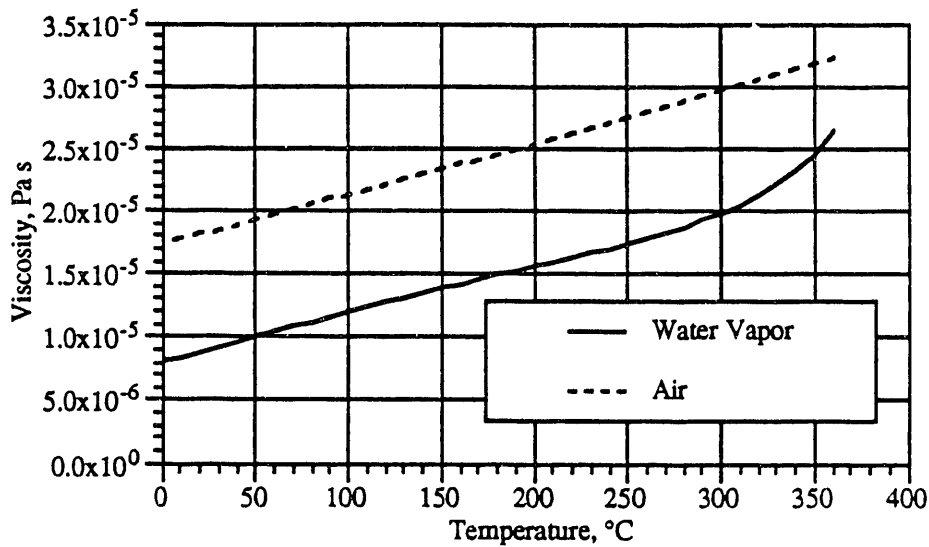


Figure 3.4. Water-Vapor (saturated conditions) and Air Viscosities

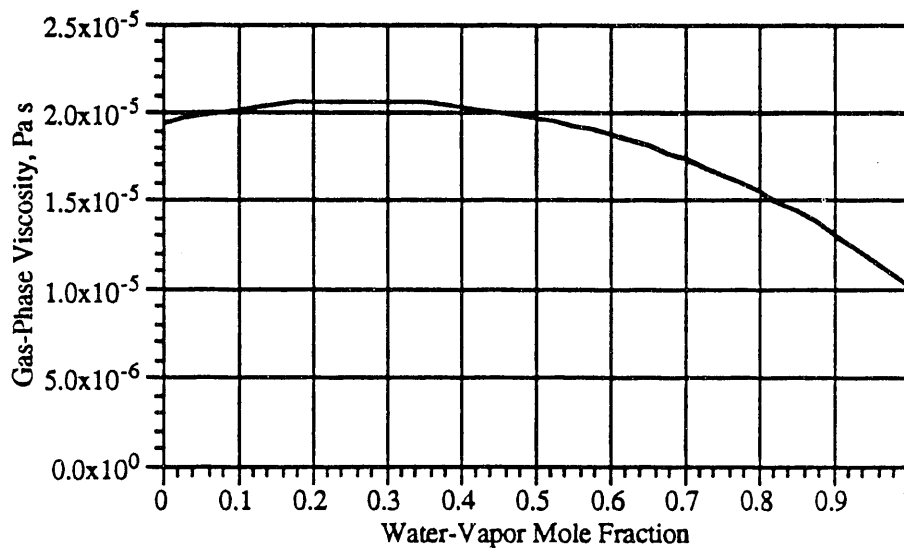


Figure 3.5. Gas-Phase Viscosity

### 3.4.2 Aqueous-Phase Viscosity

Aqueous-phase viscosity is computed for pure liquid water as a function of temperature only from the IFC steam table formulation (ASME 1967), according to Equation (3.21) for liquid water along the saturation line from 0°C to 300°C, with viscosity in micropoise and temperature in K.

$$\mu_l = 241.4 [247.8 / (T - 140)] \quad (3.21)$$

### 3.5 Enthalpy and Internal Energy

Gas-phase enthalpy and internal energy are computed from component enthalpies and internal energies using a mass fraction weighting scheme (Falta et al. 1990). Aqueous-phase enthalpy and internal energy are assumed independent of solute composition and are computed for pure liquid water as functions of temperature and pressure.

#### 3.5.1 Gas-Phase Enthalpy and Internal Energy

Gas-phase enthalpy and internal energy are computed from component enthalpies and internal energies with a mass fraction weighting scheme (Falta et al. 1990), according to Equations (3.22) and (3.23), where the summation occurs over the water and air components. Water-vapor enthalpy is computed using the IFC steam table formulations (ASME 1967), according to Equation (3.24), where the reference state equals the internal energy of liquid water at 0.01°C. The numerical values of the water-vapor constants are listed in Tables A.2 and A.4 of the Appendix. The water-vapor enthalpy and internal energy functions for saturated conditions are shown graphically in Figure 3.6. The water-vapor internal energy is computed from the water-vapor enthalpy using the thermodynamic property relationship (van Wylen and Sonntag 1978) shown in Equation (3.25).

$$h_g = \sum_{i=w, a} x_g^i h_g^i \quad (3.22)$$

$$u_g = \sum_{i=w, a} x_g^i u_g^i \quad (3.23)$$

$$\begin{aligned} \frac{h_g^w \rho_c^w}{P_c^w} = & B_0 T_r - \sum_{i=1}^5 B_{0i} (i-2) T_r^{i-1} - \sum_{j=1}^5 P_r^j \sum_{i=1}^{n(j)} B_{ji} (1 + z(j,i) b \theta) X^{z(j,i)} \\ & - \sum_{j=6}^8 \left[ \frac{\sum_{u=1}^{n(j)} B_{ju} X^{z(j,u)} \left( [1 + z(j,i) b T_r] - \frac{b T_r \sum_{k=1}^{l(j)} x(j,k) b_{jk} X^{x(j,k)}}{\beta^{2-j} + \sum_{k=1}^{l(j)} b_{jk} X^{x(j,k)}} \right)}{P_r^{2-j} + \sum_{k=1}^{l(j)} b_{jk} X^{x(j,k)}} \right] \\ & + \beta \left( \frac{\beta}{\beta_L} \right)^{10} \sum_{j=0}^6 \left[ \left[ 1 + T_r \left( \frac{10 \beta'_L}{\beta_L} \right) + j b \right] B_{9j} X^j \right] \end{aligned} \quad (3.24)$$

where

$$T_r = \frac{T}{T_c^w}$$

$$P_r = \frac{P}{P_c^w}$$

$$X = \exp\{b(1 - T_r)\}$$

$$\beta_L = L_0 + L_1 T_r + L_2 T_r^2$$

$$\beta_L' = L_1 + 2 L_2 \theta$$

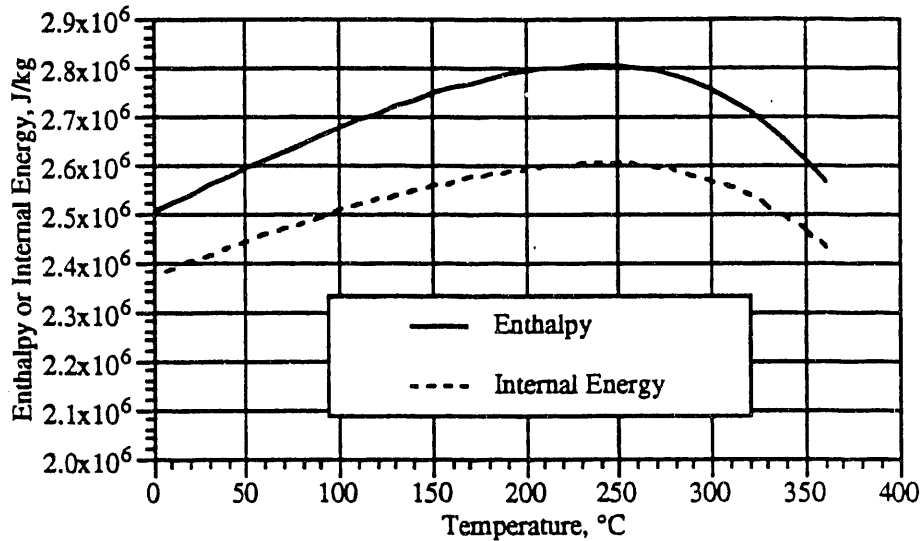


Figure 3.6. Water-Vapor Enthalpy and Internal Energy (saturated conditions)

$$u_g^w = h_g^w - \frac{P_g^w}{\rho_g^w} \quad (3.25)$$

Air that is involved in subsurface flow and transport is considered a noncondensable gas. The enthalpy of air, therefore, is computed as a function of temperature and pressure from the thermodynamic property relationship for enthalpy (van Wylen and Sonntag 1978) shown in Equation (3.26). By neglecting the variation with temperature in the constant-volume specific heat, and designating a reference point as the internal energy at 0°C, the air internal energy is computed (van Wylen and Sonntag 1978) according to Equation (3.27).

$$h_g^a = u_g^a + \frac{P_g^a}{\rho_g^a} \quad (3.26)$$

$$u_g^a = c_v^a T \quad (3.27)$$

### 3.5.2 Aqueous-Phase Enthalpy and Internal Energy

Aqueous-phase enthalpy and internal energy are computed independent of compositional effects (i.e., for pure water). The IFC steam table formulations (ASME 1967) are used to compute the enthalpy of liquid water, where the reference state is defined as the internal energy of liquid water at 0.01°C, as shown in Equation (3.28). The numerical values of the liquid water constants are listed in Table A.1 of the Appendix. The aqueous-phase enthalpy function for saturated

conditions is shown in graphical form in Figure 3.7. Differences between liquid enthalpy and internal energy are neglected.

$$\begin{aligned}
 \frac{h_g^w \rho_c^w}{P_c^w} &= A_0 T_r - \sum_{i=1}^{10} (i-2) A_i T_r^{i-1} \\
 + A_{11} \left[ Z \left( 17 \left( \frac{Z}{29} - \frac{Y}{12} \right) + 5 T_r \frac{Y}{12} \right) + a_4 T_r - (a_3 - 1) T_r Y Y \right] Z^{-5/17} \\
 &+ \left\{ A_{12} - A_{14} T_r^2 + A_{15} (9 T_r + a_6) (a_6 - T_r)^9 \right. \\
 &\quad \left. + A_{16} (20 T_r^{19} + a_7) (a_7 + T_r^{19})^2 \right\} \beta \\
 &- (12 T_r^{11} + a_8) (a_8 + T_r^{11})^2 (A_{17} P_r + A_{18} P_r^2 + A_{19} P_r^3) \\
 &+ A_{20} T_r^{18} (17 a_9 + 19 T_r^2) \{ (a_{10} + P_r)^3 + a_{11} P_r \} \\
 &+ A_{21} a_{12} P_r^3 + 21 A_{22} T_r^{20} P_r^4
 \end{aligned} \tag{3.28}$$

where

$$Z = Y + (a_3 Y^2 - 2 a_4 T_r + 2 a_5 P_r)^{1/2}$$

$$Y = 1 - a_1 T_r^2 - a_2 T_r^6$$

$$Y' = -2 a_1 T_r + 6 a_2 T_r^7$$

$$T_r = \frac{T}{T_c^w}$$

$$P_r = \frac{P_g^w}{P_c^w}$$

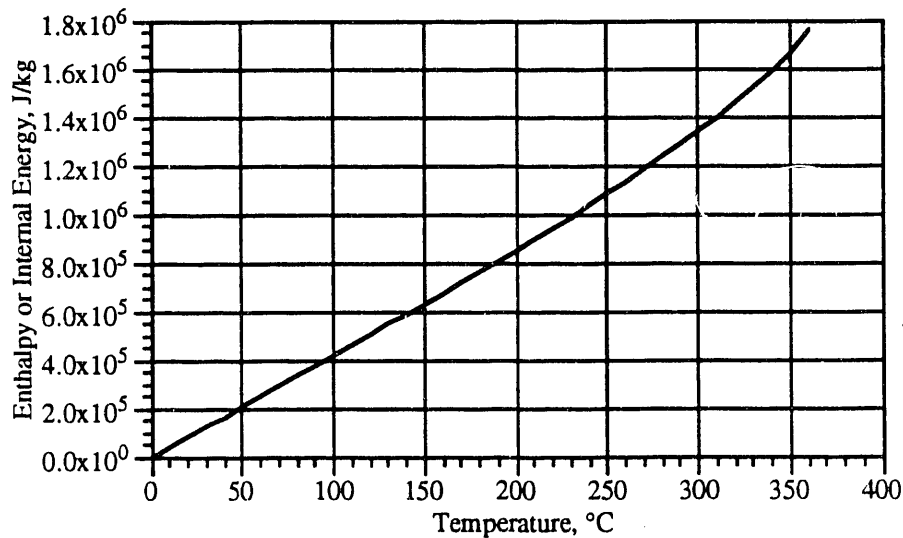


Figure 3.7. Aqueous-Phase Enthalpy and Internal Energy (saturated conditions)

### 3.6 Porosity and Tortuosity

Soil porosity in MSTS is described with three distinct porosities: effective, diffusive, and total. The effective porosity refers to interconnected pores that contribute to convective fluid flow. The diffusive porosity refers to all interconnected pores. Total porosity refers to both isolated and connected pore volumes. Isolated pore spaces are assumed to be filled with liquid water. All saturations are defined with respect to the diffusive porosity of the porous medium. Changes in the diffusive porosity occur through changes in pressure and temperature (Falta et al. 1990), according to Equation (3.29). The porous media compressibility may be computed from the coefficient of specific storage, as shown in Equation (3.30), where the liquid water compressibility, water reference density, and coefficient of specific storage are referenced at the same temperature.

$$n_D = n_D^* [1 + \alpha_P (P - P^*) + \alpha_T (T - T^*)] \quad (3.29)$$

$$\alpha_P = \frac{S_s}{\rho_l^* g} - n_D \beta_P \quad (3.30)$$

Gas diffusion flux through soils is calculated by modifying the diffusion flux through air by a gas tortuosity factor (Jury et al. 1991). Millington and Quirk (1959) established tortuosity expressions based on theoretical pore-size distribution models for partially saturated and fully saturated air-water systems. Tortuosity models in MSTS use the approach of Millington and Quirk for two-phase systems, according to Equations (3.31) and (3.32) for the aqueous-phase and gas-phase tortuosities, respectively.

$$\tau_l = (n_D)^{10/3} (s_l)^{4/3} \quad (3.31)$$

$$\tau_g = (n_D)^{10/3} (s_g)^{4/3} \quad (3.32)$$

### 3.7 Liquid Saturation

Liquid saturation is computed using nonhysteretic empirical functions dependent on gas-aqueous capillary pressures, where the gas-aqueous capillary pressure equals the difference between the gas- and aqueous-phase pressures. Several empirical relationships between liquid saturation and capillary pressure, described in this section, are predefined in MSTS. These empirical relationships consist of the van Genuchten, Brooks and Corey, Leverett, and dual porosity models. Saturation path histories and nonwetting fluid entrapment effects are neglected. Liquid saturation in MSTS is defined as the ratio of aqueous-phase water content to diffusive porosity. The liquid and gas saturations in MSTS sum to one.

#### 3.7.1 van Genuchten Model

The van Genuchten (1980) function relates the gas-aqueous capillary pressure, in terms of head, to an effective liquid saturation with two correlation parameters  $\alpha$  and  $n$ , as shown in Equations (3.33) and (3.34). The effective liquid saturation is defined in terms of the actual liquid saturation and a minimum residual saturation, as shown in Equation (3.35). An example of the van Genuchten function for fixed values of  $\alpha$  and  $n$  is shown graphically in Figure 3.8.

$$s_l^* = \left[ 1 + \left( \alpha \left[ \frac{P_g - P_l}{g \rho_l^*} \right]^n \right)^{\left( \frac{1}{n} - 1 \right)} \right] \text{ for } \left[ \frac{P_g - P_l}{g \rho_l^*} \right] > 0 \quad (3.33)$$

$$s_l^* = 1 \text{ for } \frac{[P_g - P_l]}{g \rho_l} \leq 0 \quad (3.34)$$

$$s_l^* = \frac{s_l - s_{lr}}{1 - s_{lr}} \quad (3.35)$$

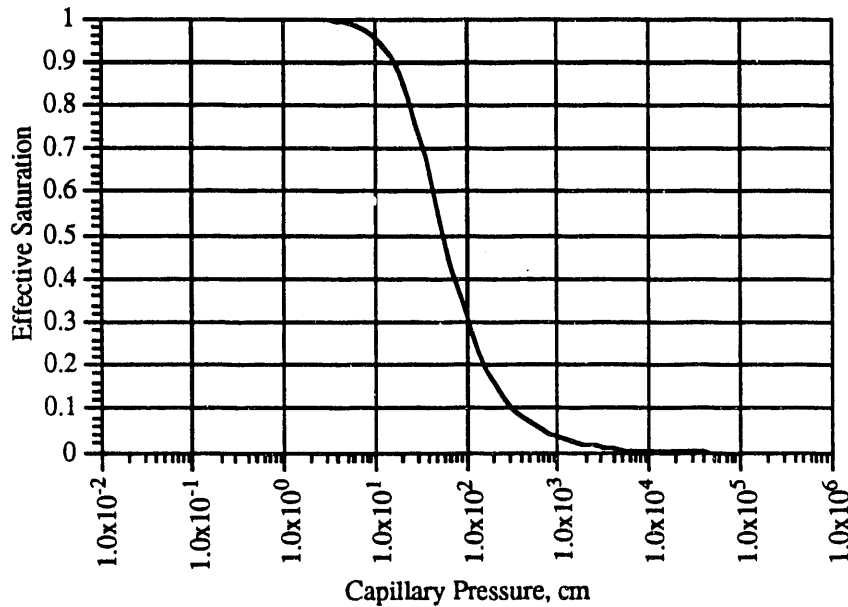


Figure 3.8. van Genuchten Saturation Function ( $\alpha = 0.0305 \text{ cm}^{-1}$ ,  $n = 2$ )

### 3.7.2 Brooks and Corey Model

The Brooks and Corey (1966) function relates the gas-aqueous capillary pressure, in terms of head, to an effective liquid saturation with two correlation parameters, as shown in Equations (3.36) and (3.37). The first correlation parameter ( $\psi^*$ ) is referred to as the air-entry head and is defined as the minimum drainage capillary pressure head for which a continuous nonwetting phase exists. The second correlation parameter ( $\beta$ ) is related to the pore-size distribution of the porous medium. The effective liquid saturation is defined in terms of the actual liquid saturation and a minimum residual saturation, as shown in Equation (3.38). An example of the Brooks and Corey function for fixed values of  $\psi^*$  and  $\beta$  is shown graphically in Figure 3.9.

$$s_l^* = \left[ \frac{\left( \frac{P_g - P_l}{g \rho_l^*} \right)^{-\beta}}{\psi^*} \right] \text{ for } \left( \frac{P_g - P_l}{g \rho_l^*} \right) < \psi^* \quad (3.36)$$

$$s_l^* = 1 \text{ for } \left( \frac{P_g - P_l}{g \rho_l^*} \right) \geq \psi^* \quad (3.37)$$

$$s_l^* = \frac{s_l - s_{lr}}{1 - s_{lr}} \quad (3.38)$$

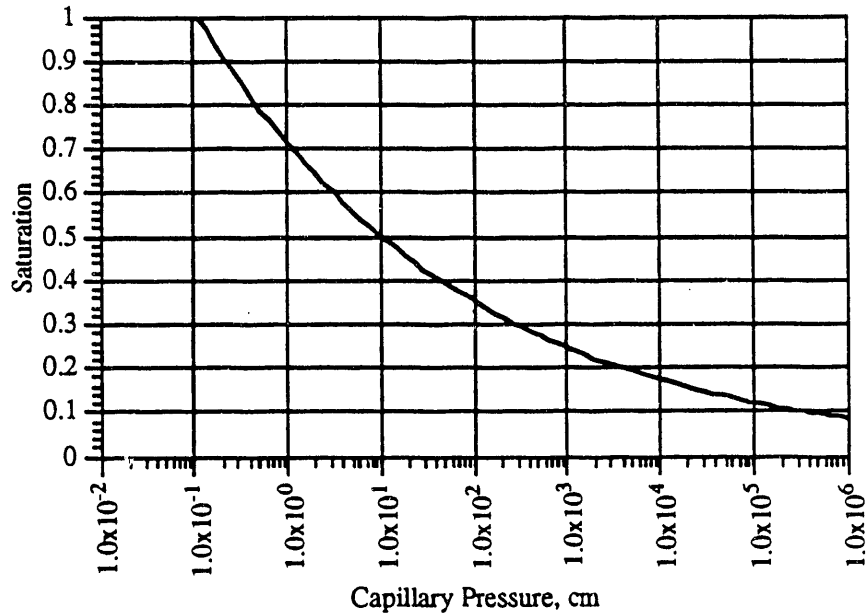


Figure 3.9. Brooks and Corey Saturation Function ( $\beta = 6.5$ ,  $\psi^* = 0.11$  cm)

### 3.7.3 Leverett Model

The Leverett function (Leverett 1941; Udell and Fitch 1985) relates the gas-aqueous capillary pressure to an effective liquid saturation with one correlation parameter ( $P_{cap}^*$ ) and an expression for the surface tension of water as a function of temperature, as shown in Equations (3.39) and (3.40). The correlation parameter is related to the capillary pressure head at the residual saturation. The effective liquid saturation is defined in terms of the actual liquid saturation and a minimum residual saturation, as shown in Equation (3.41). An example of the Leverett function for a temperature of 50°C is shown graphically in Figure 3.10.

$$P_g - P_l = P_{cap}^* \sigma^{aw} f \quad (3.39)$$

$$f = 1.417 (1 - s_l^*) - 2.120 (1 - s_l^*)^2 + 1.263 (1 - s_l^*)^3 \quad (3.40)$$

$$s_l^* = \frac{s_l - s_{lr}}{1 - s_{lr}} \quad (3.41)$$

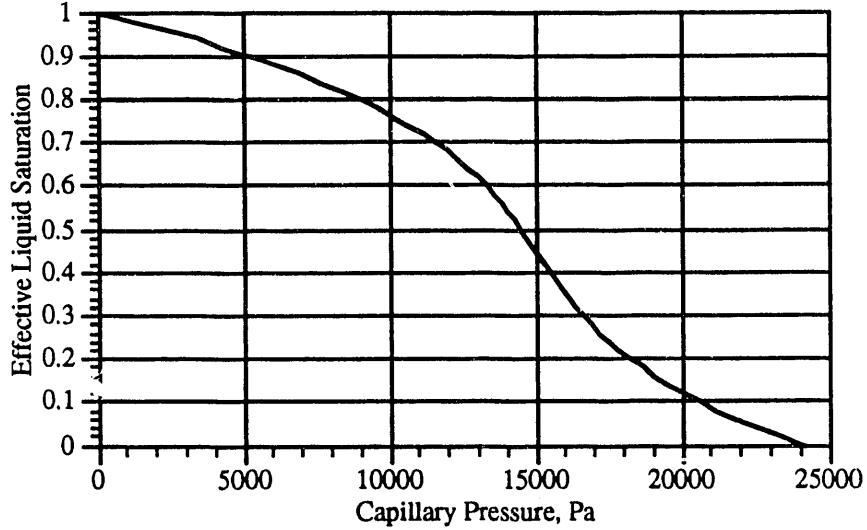


Figure 3.10. Leverett Saturation Function ( $P^*_{cap} = 632455$  Pa)

### 3.7.4 Dual Porosity Model

The dual porosity (equivalent continuum) model (Klavetter and Peters 1986; Nitao 1988) relates the bulk saturation of a fractured porous medium to an effective gas-aqueous capillary pressure through two functions of capillary pressure and liquid saturation, one for the fractures and one for the matrix, as shown in Equation (3.42). The primary assumption associated with dual porosity models is that fracture and matrix pressures are in equilibrium, which ignores transient fracture-matrix interactions. Fracture and matrix saturations are computed with van Genuchten functions that relate equivalent saturations to capillary pressures as shown in Equations (3.43) through (3.46). The effective liquid saturation is defined in terms of the actual liquid saturation and a minimum residual saturation, as shown in Equations (3.47) and (3.48) for fracture and matrix components, respectively. An example of the dual porosity saturation function is shown graphically in Figure 3.11, where  $n_{Df} = 0.43$ ,  $n_{Dm} = 0.11$ ,  $s_{\ell_{rf}} = 0.045$ ,  $s_{\ell_{rm}} = 0.052$ ,  $\alpha_f = 14.5 \text{ m}^{-1}$ ,  $\alpha_m = 0.0033 \text{ m}^{-1}$ ,  $n_f = 2.68$ , and  $n_m = 1.798$ .

$$s_{\ell_b} = \frac{s_{\ell_f} n_{Df} + s_{\ell_m} (1 - n_{Df}) n_{Dm}}{n_{Df} + (1 - n_{Df}) n_{Dm}} \quad (3.42)$$

$$s_{\ell_f}^* = \left[ 1 + \left( \alpha_f \left[ \frac{P_g - P_\ell}{g \rho_\ell^*} \right] \right)^{n_f} \right]^{-m_f} \text{ for } \left[ \frac{P_g - P_\ell}{g \rho_\ell^*} \right] > 0 \quad (3.43)$$

$$s_{\ell_f}^* = 1 \text{ for } \left[ \frac{P_g - P_\ell}{g \rho_\ell} \right] \leq 0 \quad (3.44)$$

$$s_{\ell_m}^* = \left[ 1 + \left( \alpha_m \left[ \frac{P_g - P_\ell}{g \rho_\ell^*} \right] \right)^{n_m} \right]^{-m_m} \text{ for } \left[ \frac{P_g - P_\ell}{g \rho_\ell^*} \right] > 0 \quad (3.45)$$

$$s_{\ell_m}^* = 1 \text{ for } \left[ \frac{P_g - P_\ell}{g \rho_\ell} \right] \leq 0 \quad (3.46)$$

$$s_{lf}^* = \frac{s_{lf} - s_{lrf}}{1 - s_{lrf}} \quad (3.47)$$

$$s_{lm}^* = \frac{s_{lm} - s_{lrm}}{1 - s_{lrm}} \quad (3.48)$$

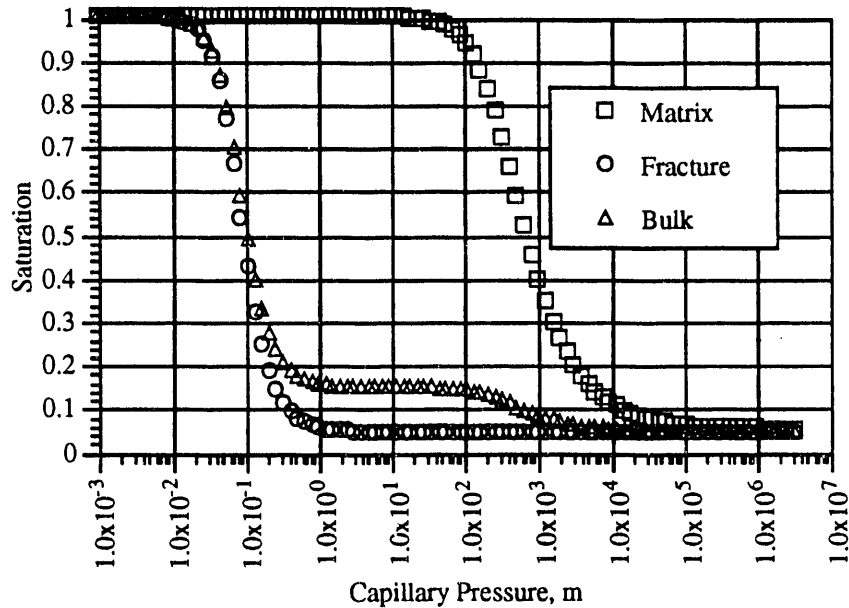


Figure 3.11. Dual Porosity Saturation Function

### 3.8 Liquid and Gas Relative Permeability

Liquid relative permeability and gas relative permeability are computed using nonhysteretic empirical functions dependent on liquid saturation. Several empirical relationships between liquid relative permeability and liquid saturation, described in this section, are predefined in MSTs. Saturation path histories and nonwetting fluid entrapment effects are neglected.

#### 3.8.1 Mualem Model

An expression for the liquid relative permeability as a function of liquid saturation can be derived from Mualem's pore distribution model from knowledge of the soil-water retention functions (Mualem 1976). The Mualem model for predicting liquid relative permeability has been applied to the van Genuchten and Brooks and Corey models of soil-water retention. The integrations yield closed-form expressions that relate liquid relative permeability to liquid saturation as shown in Equations (3.49) and (3.50) for the van Genuchten and Brooks and Corey soil-water retention functions, respectively. Examples of the Mualem liquid relative permeability function for both soil-water retention functions are shown graphically in Figure 3.12, where  $m = 2$  and  $\beta = 6.5$ .

$$k_{rl} = (s_l^*)^{1/2} \left[ 1 - \left( 1 - (s_l^*)^{1/m} \right)^m \right]^2 \quad (3.49)$$

$$k_{rl} = (s_l^*)^{\left(\frac{5}{2} + \frac{2}{\beta}\right)} \quad (3.50)$$

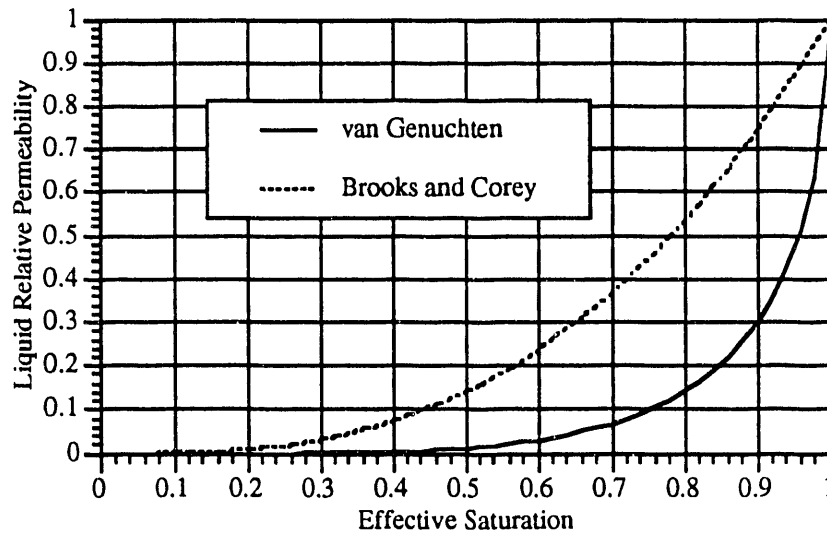


Figure 3.12. Mualem Liquid Relative Permeability Function

### 3.8.2 Burdine Model

An expression for the liquid relative permeability as a function of liquid saturation can be derived from Burdine's pore distribution model from knowledge of the soil-water retention functions (Burdine 1953). The Burdine model for predicting liquid relative permeability has been applied to the van Genuchten and Brooks and Corey models of soil-water retention. The integrations yield closed-form expressions that relate liquid relative permeability to liquid saturation, as shown in Equations (3.51) and (3.52) for the van Genuchten and Brooks and Corey soil-water retention functions, respectively. Examples of the Burdine liquid relative permeability function for both soil-water retention models are shown graphically in Figure 3.13, where  $m = 2$  and  $\beta = 6.5$ .

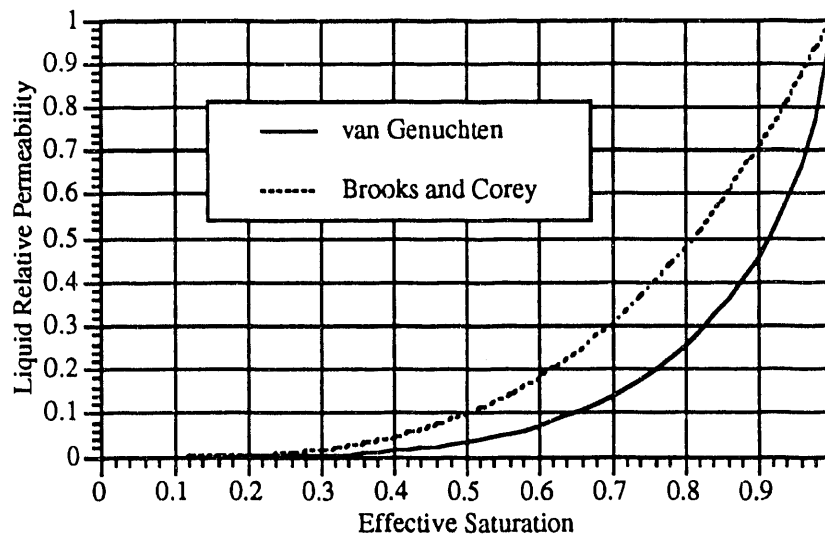


Figure 3.13. Burdine Liquid Relative Permeability Function

$$k_{r\ell} = (s_{\ell}^*)^2 \left[ 1 - \left( 1 - (s_{\ell}^*)^{\frac{1}{m}} \right)^m \right] \quad (3.51)$$

$$k_{r\ell} = (s_{\ell}^*)^{\left(3 + \frac{2}{\beta}\right)} \quad (3.52)$$

### 3.8.3 Corey Model

Liquid and gas relative permeabilities can be expressed as functions of a modified effective liquid saturation according to the empirical model developed by Corey (Pruess 1987) as shown in Equations (3.53) and (3.54) for liquid and gas, respectively. The effective liquid saturation is defined for the Corey relative permeability model as shown in Equation (3.55), where both the residual and the entrapped air saturations are included. Examples of Corey functions for liquid relative permeability and gas relative permeability are shown graphically in Figure 3.14.

$$k_{r\ell} = (s_{\ell}^*)^4 \quad (3.53)$$

$$k_{rg} = (1 - s_{\ell}^*)^2 (1 - (s_{\ell}^*)^2) \quad (3.54)$$

$$s_{\ell}^* = \frac{s_{\ell} - s_{\ell r}}{1 - s_{\ell r} - s_{sr}} \quad (3.55)$$

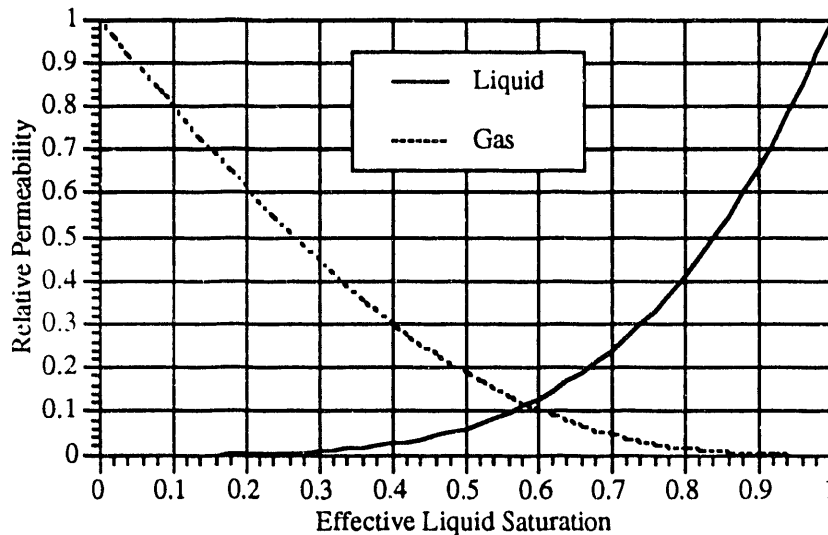


Figure 3.14. Corey Relative Permeability Functions

### 3.8.4 Fatt and Klikoff Model

Liquid and gas relative permeabilities can be expressed as functions of the effective liquid saturation according to the empirical model developed by Fatt and Klikoff (1959), as shown in Equations (3.56) and (3.57) for liquid and gas, respectively. The effective liquid saturation is defined for the Fatt and Klikoff model as shown in Equation (3.58). Examples of Fatt and Klikoff functions for liquid relative permeability and gas relative permeability are shown graphically in Figure 3.15.

$$k_{r\ell} = (s_{\ell}^*)^3 \quad (3.56)$$

$$k_{rg} = (1 - s_{\ell}^*)^3 \quad (3.57)$$

$$s_{\ell}^* = \frac{s_{\ell} - s_{\ell r}}{1 - s_{\ell r}} \quad (3.58)$$

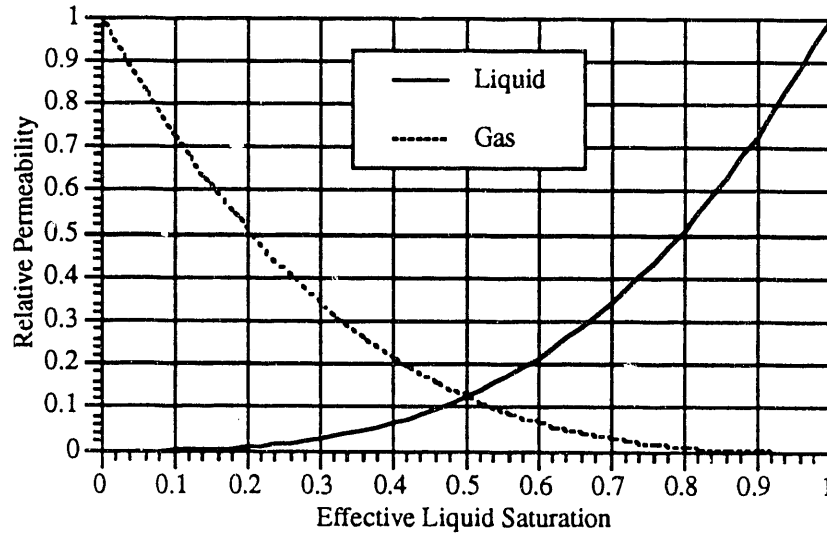


Figure 3.15. Fatt and Klikoff Relative Permeability Functions

### 3.8.5 Dual Porosity Model

The dual porosity (equivalent continuum) model (Klavetter and Peters 1986; Nitao 1988) relates the bulk liquid relative permeability to the liquid relative permeabilities for the fracture and matrix, as shown in Equation (3.59). The primary assumption associated with dual porosity models is that fracture and matrix pressures are in equilibrium, which ignores transient fracture-matrix interactions. For the dual porosity model, the van Genuchten water retention model is integrated with the Mualem pore distribution model to obtain expressions for the fracture and matrix relative permeabilities as functions of the fracture and matrix effective saturations, as shown in Equations (3.60) and (3.61), respectively. The effective liquid saturation is defined in terms of the actual liquid saturation and a minimum residual saturation, as shown in Equations (3.47) and (3.48) for fracture and matrix components, respectively. An example of the dual porosity liquid relative permeability function is shown graphically in Figure 3.16, where  $n_{Df} = 0.43$ ,  $n_{Dm} = 0.11$ ,  $s_{\ell rf} = 0.045$ ,  $s_{\ell rm} = 0.052$ ,  $\alpha_f = 14.5 \text{ m}^{-1}$ ,  $\alpha_m = 0.0033 \text{ m}^{-1}$ ,  $n_f = 2.68$ ,  $n_m = 1.798$ ,  $\tilde{k}_f = 8.25 \times 10^{-5} \text{ m/s}$ , and  $\tilde{k}_m = 3.01 \times 10^{-12} \text{ m/s}$ .

$$k_{r\ell b} = \frac{\tilde{k}_f k_{r\ell f}(n_{Df}) + \tilde{k}_m k_{r\ell m}(1 - n_{Df})}{\tilde{k}_f(n_{Df}) + \tilde{k}_m(1 - n_{Df})} \quad (3.59)$$

$$k_{r\ell f} = (s_{\ell f}^*)^{1/2} \left[ 1 - \left( 1 - (s_{\ell f}^*)^{1/m_f} \right)^{m_f} \right]^2 \quad (3.60)$$

$$k_{r\ell m} = (s_{\ell m}^*)^{1/2} \left[ 1 - \left( 1 - (s_{\ell m}^*)^{1/m_m} \right)^{m_m} \right]^2 \quad (3.61)$$

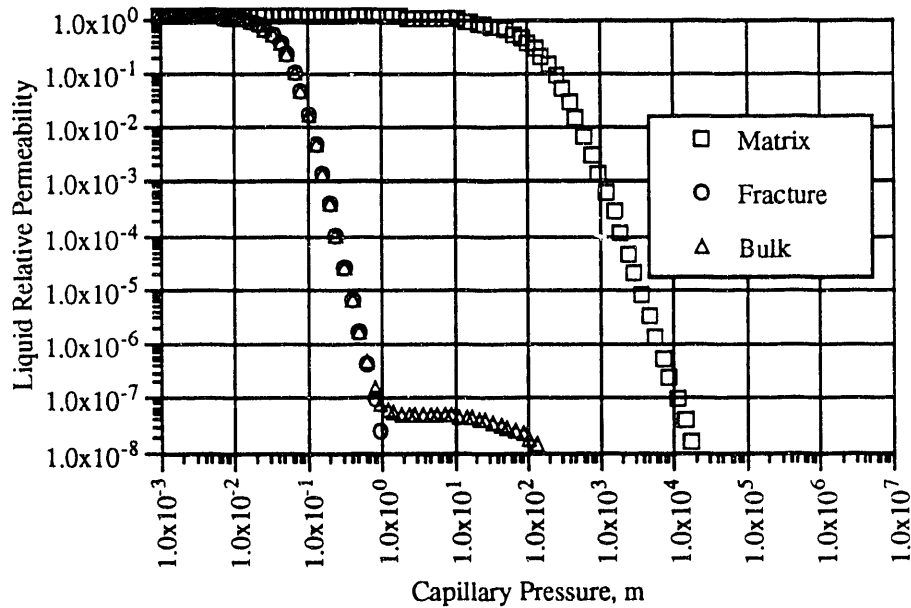


Figure 3.16. Dual Porosity Liquid Relative Permeability Function

### 3.9 Thermal Conductivity

The thermal conductivity of a two-phase system in a solid porous medium will depend on the volumetric proportions of the fluid and solid components, the arrangement of the solid particles, the interfacial contact between the solid and fluid phases, and the thermal conductivities of the phase components (Jury et al. 1991). For geologic media, the thermal conductivity of the solid phase is generally an order of magnitude greater than that of the aqueous phase and approximately two orders of magnitude greater than that of the gas phase. Data for two-phase systems (Jury et al. 1991) reveal important features of the dependence of porous media thermal conductivity on the above variables. Thermal conductivity increases with increasing surface contact between soil particles and increasing bulk density. The presence of liquid water between soil particles greatly improves the thermal contact between particles and displaces the gas phase, which has relatively poor thermal conductivity. The greatest rate of increase in thermal conductivity with increasing saturation occurs at the lower saturations; for higher-saturation conditions, the approach to the saturated conductivity is asymptotic.

For two-phase systems, liquid-to-solid surface contacts depend on liquid saturations. The combined thermal conductivity for a two-phase system in a solid porous medium would, in general, be a complex function of porosity, liquid saturations, phase thermal conductivities, and saturation histories. Without an experimentally verified model to account for these dependencies, the overall conductivity can be approximated with a parallel model. The parallel model combines the thermal conductivities of the individual phases through volumetric weighted averages, as shown in Equation (3.62). With this model, the combined thermal conductivity is computed by assuming parallel conduction paths through each phase. Because the gas-phase conduction pathway contributes negligibly to the combined thermal conductivity, the gas-phase term was excluded from Equation (3.62).

The thermal conductivity of the solid phase can be an anisotropic property, which is a thermal characteristic of the porous media. Because the solid-phase thermal conductivity is an anisotropic property, combined thermal conductivity is necessarily anisotropic. The thermal

conductivity of water is computed from the steam table formulations (ASME 1967) as a function of temperature, according to Equation (3.63), with thermal conductivity in mW/m K, temperature in K, and pressure in bar. The liquid thermal conductivity function is shown graphically in Figure 3.17.

The effective thermal conductivity may also be expressed as a function of the unsaturated and saturated thermal conductivities and liquid saturation. One model scales the effective thermal conductivity linearly between the unsaturated and saturated values as a function of the liquid saturation, as shown in Equation (3.64). Another model (Somerton et al. 1973, 1974) scales the effective thermal conductivity as the square root of the liquid saturation between the unsaturated and saturated values, as shown in Equation (3.65).

$$\tilde{k}_e = \tilde{k}_s (1 - n_T) + k_\ell [n_T - n_D (1 - s_\ell)] \quad (3.62)$$

$$\begin{aligned} k_\ell = & a_0 + a_1 \left(\frac{T}{T_o}\right) + a_2 \left(\frac{T}{T_o}\right)^2 + a_3 \left(\frac{T}{T_o}\right)^3 + a_4 \left(\frac{T}{T_o}\right)^4 \\ & + (P - P_s^w) \left[ b_0 + b_1 \left(\frac{T}{T_o}\right) + b_2 \left(\frac{T}{T_o}\right)^2 + b_3 \left(\frac{T}{T_o}\right)^3 \right] \\ & + (P - P_s^w)^2 \left[ c_0 + c_1 \left(\frac{T}{T_o}\right) + c_2 \left(\frac{T}{T_o}\right)^2 + c_3 \left(\frac{T}{T_o}\right)^3 \right] \end{aligned} \quad (3.63)$$

$$\tilde{k}_e = \tilde{k}_s^u + s_\ell (\tilde{k}_s^s - \tilde{k}_s^u) \quad (3.64)$$

$$\tilde{k}_e = \tilde{k}_s^u + \sqrt{s_\ell} (\tilde{k}_s^s - \tilde{k}_s^u) \quad (3.65)$$

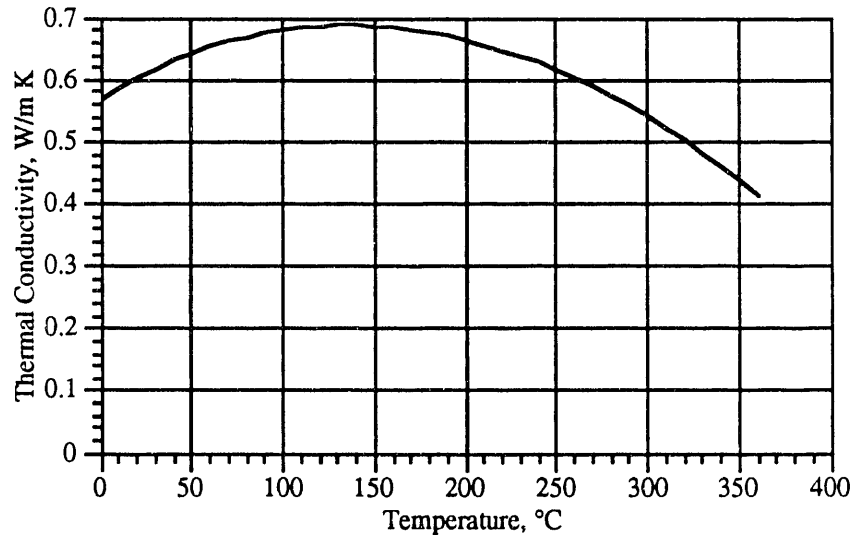


Figure 3.17. Liquid Thermal Conductivity

### 3.10 Gas-Phase Diffusivity

Gas-phase components diffuse according to gradients in gas-phase concentrations, gas-phase saturations, porous-media-dependent hydrogeological properties, and component diffusivities. Two-phase systems require binary diffusivities, because each component diffuses through a two-component mixture (e.g., air/water vapor). Because of the requirement for mass conservation, the net mass diffusive fluxes across the surfaces of a control volume necessarily sum

to zero, as shown in Equation (3.66). Therefore, the diffusive flux of the air component may be computed from known diffusive fluxes of the water component. Binary diffusivities for air/water-vapor mixtures may be computed as a function of temperature and pressure from a reference binary diffusivity according to a method by Vargaftik (Falta et al. 1990), as shown in Equation (3.67).

$$\tau_g n_D \rho_g s_g D_g^{aw} \nabla x_g^w + \tau_g n_D \rho_g s_g D_g^{aw} \nabla x_g^a = 0 \quad (3.66)$$

$$D_g^{aw} = D_g^{aw*} \left( \frac{P_g^*}{P_g} \right) \left( \frac{T}{T^*} \right)^{1.8} \quad (3.67)$$

### 3.11 Species Transport Properties

The total concentration of species may be split into volumetric phase concentrations according to Equation (3.68). Volumetric phase concentrations are interrelated through partition coefficients. The aqueous-gas partitioning coefficient describes the ratio of concentration of a species in the aqueous phase to that in the gas phase (Weeks et al. 1982) according to Equation (3.69). The solid-aqueous distribution coefficient describes the ratio of species concentration adsorbed on the solid phase to species concentration in the aqueous phase according to Equation (3.70). Combining Equations (3.68) through (3.70) yields expressions for volumetric phase concentrations in terms of total species concentrations, as shown in Equations (3.71) through (3.73) for the aqueous, gas, and solid phases, respectively.

$$C = n_D s_\ell C_\ell + n_D s_g C_g + (1 - n_T) C_s \quad (3.68)$$

$$K_{\ell g} = \frac{C_\ell}{C_g \rho_\ell} \quad (3.69)$$

$$K_D = \frac{C_s \rho_\ell}{C_\ell \rho_s} \quad (3.70)$$

$$C_\ell = \frac{C}{\left[ n_D s_\ell + \frac{n_D s_g}{K_{\ell g} \rho_\ell} + (1 - n_T) \frac{K_D \rho_s}{\rho_\ell} \right]} \quad (3.71)$$

$$C_g = \frac{C}{\left[ n_D s_\ell K_{\ell g} \rho_\ell + n_D s_g + (1 - n_T) K_D K_{\ell g} \rho_s \right]} \quad (3.72)$$

$$C_s = \frac{C}{\left[ \frac{n_D s_\ell K_D \rho_s}{\rho_\ell} + \frac{n_D s_g}{K_D K_{\ell g} \rho_s} + (1 - n_T) \right]} \quad (3.73)$$

Molecular diffusion coefficients are dependent on the solvent-solute pair. Generally, molecular diffusion of species through liquid phases is negligible compared with the convection transport mechanisms. An expression for gas-phase diffusivities for nonpolar gas pairs has been developed by Slattery and Bird (1958), as shown in Equation (3.74), with temperature in K and pressure in atm.

$$D_g^{AB} = 2.745 \times 10^{-4} \left[ \frac{(P_c^A P_c^B)^{1/3} (T_c^A T_c^B)^{5/12} \left( \frac{1}{M_{wt}^A} + \frac{1}{M_{wt}^B} \right)^{1/2}}{P} \right] \left[ \frac{T}{(T_c^A T_c^B)^{1/2}} \right]^{1.823} \quad (3.74)$$

Under the assumption of relatively fast mixing times along a direction normal to the direction of mean convection, a special case of convective-dispersive transport occurs. Under these conditions, the variations in pore velocities produce a hydrodynamic dispersion of solutes, which may be described mathematically with a form identical to the diffusion flux (Bear 1972). The hydrodynamic dispersion coefficient that relates the dispersion flux to the gradient in species concentration is a second-order symmetric tensor, which is a function of both the media and the fluid. The components of the dispersion coefficients along the principal orthogonal axis of the computational domain are computed from the principal velocity components and two experimentally determined parameters referred to as the longitudinal and transverse dispersivities as shown in Equations (3.75) through (3.81).

$$\dot{D}_{h\ell}^x = \alpha_L u' + \alpha_T (v' + w') \quad (3.75)$$

$$\dot{D}_{h\ell}^y = \alpha_L v' + \alpha_T (w' + u') \quad (3.76)$$

$$\dot{D}_{h\ell}^z = \alpha_L w' + \alpha_T (u' + v') \quad (3.77)$$

$$u' = \frac{u^2}{\xi} \quad (3.78)$$

$$v' = \frac{v^2}{\xi} \quad (3.79)$$

$$w' = \frac{w^2}{\xi} \quad (3.80)$$

$$\xi = (u^2 + v^2 + w^2)^{1/2} \quad (3.81)$$

## 4.0 Numerical Solution Method

The governing conservation equations of MSTS (see Section 2.2) are discretized to algebraic form with an integrated finite-difference method (Patankar 1980). Transformation of the partial differential conservation equations into algebraic form requires that the physical domain be spatially discretized into a computational domain composed of a number of nonoverlapping control volumes. Each control volume surrounds a single grid point, which defines the position of intrinsic property variables (e.g., temperature, species concentration, pressure, saturation, density, and viscosity). The conservation equations are integrated over the control volume by assuming a piecewise profile that expresses the variation in the primary variable between grid points. The resulting expressions from integrating the conservation equations are nonlinear algebraic equations containing the primary variables for a group of grid points. The integral finite-difference method conserves quantities such as mass, energy, and species over each control volume and the entire computational domain.

Discretization of the partial differential conservation equations has been implemented in MSTS for two orthogonal computational grid systems. For the Cartesian grid system, coordinate directions follow the "right-hand" rule and are labeled  $x$ ,  $y$ , and  $z$ . Positive and negative directions along the  $x$ -axis are referred to as *east* and *west*, respectively. Similarly, positive and negative directions along the  $y$ -axis are referred to as *north* and *south*, respectively. The  $z$ -axis is assumed aligned with the negative gravitational vector, where positive and negative directions are referred to as *top* and *bottom*, respectively. For cylindrical grid systems, the coordinate directions are labeled  $r$ ,  $\theta$ , and  $z$ , where  $r$  represents the radial distance,  $\theta$  the azimuthal angle, and  $z$  the vertical distance. Direction nomenclature remains the same between the two coordinate systems by substituting the  $x$ -axis direction labels for those of the  $r$ -axis, and the  $y$ -axis direction labels for those of the  $\theta$ -axis. Computational grids may be constructed for either grid system using one, two, or three dimensions. Geometric variables for the Cartesian coordinate system are shown in Figures 4.1 and 4.2; geometric variables for the cylindrical coordinate system are shown in Figures 4.3 and 4.4.

The algebraic expressions that result from discretizing the conservation equations are nonlinear. Liquid saturation, relative permeability, and physical properties during phase transitions are the parameters most responsible for these nonlinearities. The nonlinear algebraic forms of the conservation equations are converted to a linear form using a multivariable, residual-based, Newton-Raphson iteration technique (Kreyszig 1979). The technique will generally yield quadratic convergence of the residuals with iteration, given initial estimates of the primary variables that are sufficiently close to the solution. Each iteration requires the solution of the linearized algebraic form of the conservation equations. Depending on the order of the computational domain, the linearized form of the conservation equations are either tridiagonal or block-banded.

### 4.1 Discretization of the Mass Conservation Equations

The water mass and air mass conservation equations are discretized by integrating the respective partial differential equations, Equations (2.1) and (2.2), over the control volume. The accumulation terms for these integrals are shown generically in Equation (4.1), where the accumulation mass for the water and air conservation equations are shown in Equations (4.2) and (4.3), respectively. Similarly, the source is spatially discretized as shown in Equation (4.4).

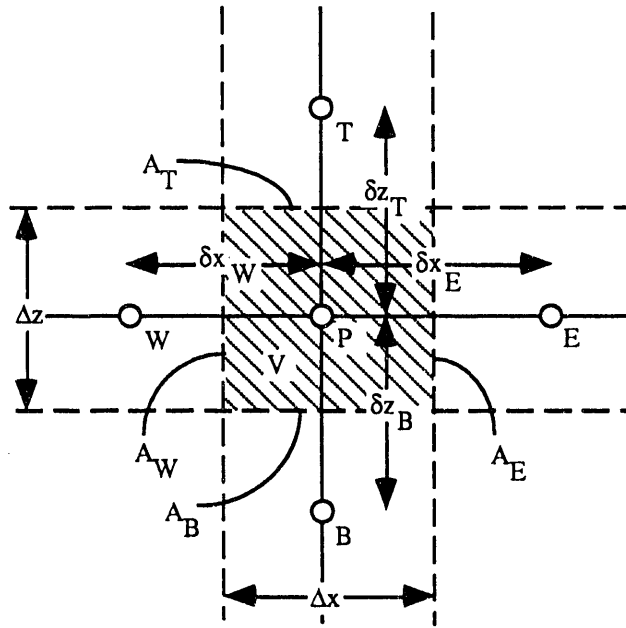


Figure 4.1. X-Z Cartesian Coordinate System

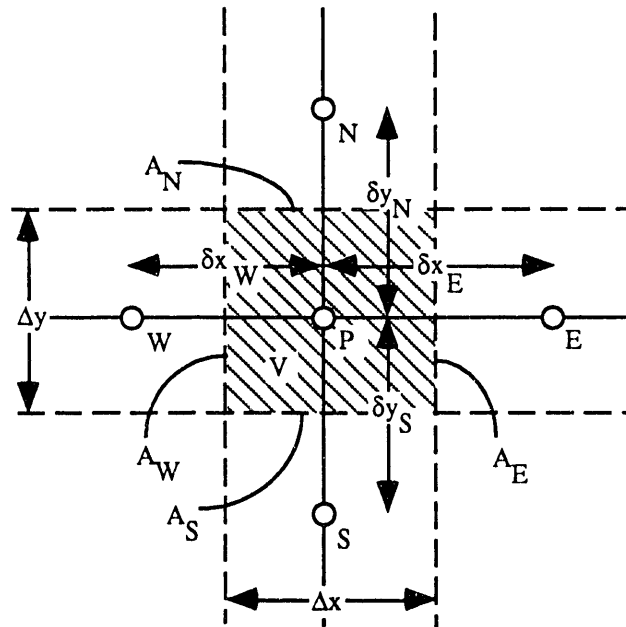
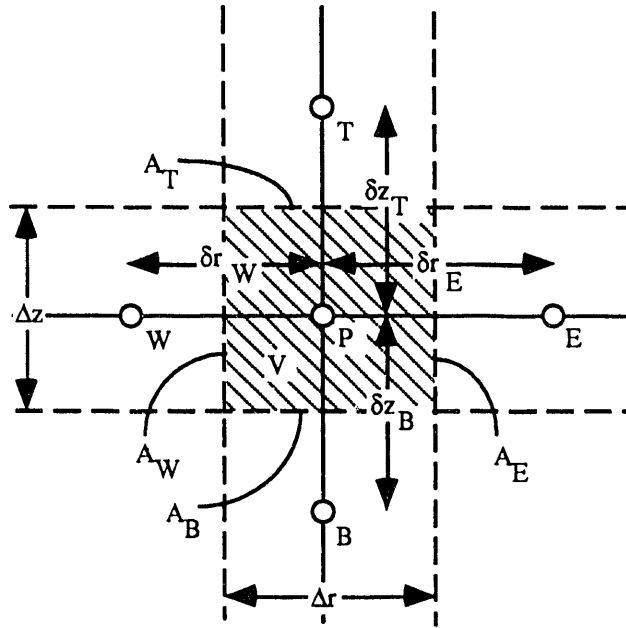
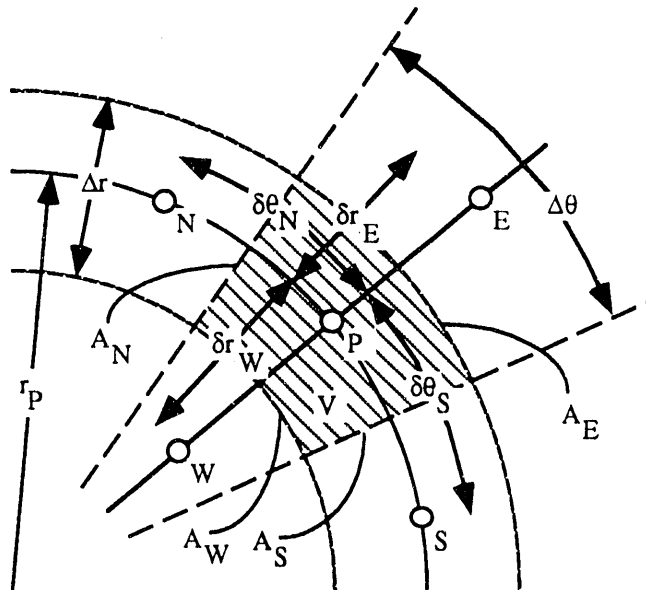


Figure 4.2. X-Y Cartesian Coordinate System



**Figure 4.3.** R-Z Cylindrical Coordinate System



**Figure 4.4.** R- $\theta$  Cylindrical Coordinate System

$$\frac{\partial}{\partial t} \int_V M^i dV = \frac{\partial}{\partial t} V M^i \text{ for } i = w, a \quad (4.1)$$

$$M^w = n_D x_\ell^w \rho_\ell s_\ell + n_D x_g^w \rho_g s_g \quad (4.2)$$

$$M^a = n_D x_\ell^a \rho_\ell s_\ell + n_D x_g^a \rho_g s_g \quad (4.3)$$

$$\frac{\partial}{\partial t} \int_V \dot{m}^i dV = V \dot{m}^i \text{ for } i = w, a \quad (4.4)$$

The surface flux terms are composed of a Darcy flux and a diffusive flux. Discretization of the surface flux terms is shown generically in Equation (4.5), where the volumetric integrals are first converted to surface integrals, then approximated as summations over the surface areas between adjoining nodes. Darcy flux terms for the aqueous and gas phases are shown in Equations (4.6) and (4.7), respectively. Diffusive flux terms for water and air components are shown in Equations (4.8) and (4.9), respectively.

$$\begin{aligned} & \int_V [\nabla \mathbf{F}_\ell^i + \nabla \mathbf{F}_g^i + \nabla \mathbf{J}_g^i] dV \\ &= \int_\Gamma [\mathbf{F}_\ell^i + \mathbf{F}_g^i + \mathbf{J}_g^i] \cdot \mathbf{n} d\Gamma \\ &= \sum_\gamma [\mathbf{F}_{\ell, \gamma}^i + \mathbf{F}_{g, \gamma}^i + \mathbf{J}_{g, \gamma}^i] A_\gamma \\ & \text{for } i = w, a; \text{ for } \gamma = W, E, S, N, B, T \end{aligned} \quad (4.5)$$

$$\mathbf{F}_\ell^i = - \frac{x_\ell^i \tilde{k} k_{r\ell} \rho_\ell}{\mu_\ell} (\nabla P_\ell + \rho_\ell g \hat{z}) \text{ for } i = w, a \quad (4.6)$$

$$\mathbf{F}_g^i = - \frac{x_g^i \tilde{k} k_{rg} \rho_g}{\mu_g} (\nabla P_g + \rho_g g \hat{z}) \text{ for } i = w, a \quad (4.7)$$

$$\mathbf{J}_g^w = - \tau_g n_D \rho_g s_g D_g^{aw} \nabla x_g^w \quad (4.8)$$

$$\mathbf{J}_g^a = 1 - \mathbf{J}_g^w \quad (4.9)$$

The discretized forms of the Darcy flux terms have the same general form for the various combinations of air and water components, and aqueous and gas phases. For example, the discretized forms (Cartesian coordinate system) of the Darcy flux term of the water component in the aqueous phase are shown in Equations (4.10) through (4.12) for the *west*, *south*, and *bottom* surfaces, respectively. The discretized forms (cylindrical coordinate system) of the Darcy flux term

of the water component in the aqueous phase are shown in Equations (4.13) through (4.15) for the *west*, *south*, and *bottom* surfaces, respectively. The terms delimited with brackets and topped with bars indicate interface averages, where the double bar indicates a user-specified choice between arithmetic, harmonic, geometric, upwind, or "linear k" weighting; the arrowed bar indicates upwind or donor-cell weighting; and the single bar indicates arithmetic averaging.

$$F_{z,w}^w = - \left[ \overline{\frac{k^x k_{rl}}{\mu_l}} \right] \left[ \overrightarrow{\rho_l x_l^w} \right] \frac{(P_l, P - P_l, w)}{\delta x_w} \quad (4.10)$$

$$F_{z,s}^w = - \left[ \overline{\frac{k^y k_{rl}}{\mu_l}} \right] \left[ \overrightarrow{\rho_l x_l^w} \right] \frac{(P_l, P - P_l, s)}{\delta y_s} \quad (4.11)$$

$$F_{z,B}^w = - \left[ \overline{\frac{k^z k_{rl}}{\mu_l}} \right] \left[ \overrightarrow{\rho_l x_l^w} \right] \left[ \frac{(P_l, P - P_l, B)}{\delta z_B} + \left[ \overline{\rho_l g} \right] \right] \quad (4.12)$$

$$F_{r,w}^w = - \left[ \overline{\frac{k^x k_{rl}}{\mu_l}} \right] \left[ \overrightarrow{\rho_l x_l^w} \right] \frac{(P_l, P - P_l, w)}{\delta r_w} \quad (4.13)$$

$$F_{r,s}^w = - \left[ \overline{\frac{k^y k_{rl}}{\mu_l}} \right] \left[ \overrightarrow{\rho_l x_l^w} \right] \frac{(P_l, P - P_l, s)}{r_p \delta \theta_s} \quad (4.14)$$

$$F_{r,B}^w = - \left[ \overline{\frac{k^z k_{rl}}{\mu_l}} \right] \left[ \overrightarrow{\rho_l x_l^w} \right] \left[ \frac{(P_l, P - P_l, B)}{\delta z_B} + \left[ \overline{\rho_l g} \right] \right] \quad (4.15)$$

As with the Darcy flux terms, the discretized forms of the diffusive flux terms have the same general form among the various combinations of air and water components, and aqueous and gas phases. For example, the discretized forms (Cartesian coordinate system) of the diffusive flux term of the water component in the gas phase are shown in Equations (4.16) through (4.18) for the *west*, *south*, and *bottom* surfaces, respectively. The discretized forms (cylindrical coordinate system) of the diffusive flux term of the water component in the gas phase are shown in Equations (4.19) through (4.21) for the *west*, *south*, and *bottom* surfaces, respectively.

$$J_{g,w}^w = - \left[ \overline{\tau_g n_D \rho_g s_g D_g^{aw}} \right] \frac{x_{g,P}^w - x_{g,w}^w}{\delta x_w} \quad (4.16)$$

$$J_{g,s}^w = - \left[ \overline{\tau_g n_D \rho_g s_g D_g^{aw}} \right] \frac{x_{g,P}^w - x_{g,s}^w}{\delta y_s} \quad (4.17)$$

$$J_{g,B}^w = - \left[ \overline{\tau_g n_D \rho_g s_g D_g^{aw}} \right] \frac{x_{g,P}^w - x_{g,B}^w}{\delta z_B} \quad (4.18)$$

$$\mathbf{J}_{g,W}^w = - \frac{\overline{[\tau_g n_D \rho_g s_g D_g^{aw}]}}{\delta r_W} \frac{x_{g,P}^w - x_{g,W}^w}{\delta r_W} \quad (4.19)$$

$$\mathbf{J}_{g,S}^w = - \frac{\overline{[\tau_g n_D \rho_g s_g D_g^{aw}]}}{r_P \delta \theta_S} \frac{x_{g,P}^w - x_{g,S}^w}{r_P \delta \theta_S} \quad (4.20)$$

$$\mathbf{J}_{g,B}^w = - \frac{\overline{[\tau_g n_D \rho_g s_g D_g^{aw}]}}{\delta z_B} \frac{x_{g,P}^w - x_{g,B}^w}{\delta z_B} \quad (4.21)$$

Temporal discretization is fully implicit first-order finite difference, as shown generically for mass conservation by Equation (4.22), where time levels are indicated with superscripts. The implicit temporal discretization ensures numerical stability. The unknowns for the mass conservation equations are the primary variables at the grid node points for the new time step. For three-dimensional domains, the number of unknowns associated with a mass conservation equation for an interior node equals seven; for two-dimensional domains, the number of unknowns equals five; and for one-dimensional domains, the number of unknowns equals three. The discretized mass conservation equation, Equation (4.22), may be expressed in residual form as shown in Equation (4.23).

$$\begin{aligned} & V \left[ \frac{(M^i)^{t+\delta t} - (M^i)^t}{\delta t} \right] - V (\dot{m}^i)^{t+\delta t} = \\ & - \sum_{\gamma} \left[ (\mathbf{F}_{\ell, \gamma}^i)^{t+\delta t} + (\mathbf{F}_{g, \gamma}^i)^{t+\delta t} + (\mathbf{J}_{g, \gamma}^i)^{t+\delta t} \right] A_{\gamma} \\ & \text{for } i = w, a; \text{ for } \gamma = W, E, S, N, B, T \end{aligned} \quad (4.22)$$

$$\begin{aligned} (R^i)^{t+\delta t} & \equiv V \left[ \frac{(M^i)^{t+\delta t} - (M^i)^t}{\delta t} \right] - V (\dot{m}^i)^{t+\delta t} \\ & + \sum_{\gamma} \left[ (\mathbf{F}_{\ell, \gamma}^i)^{t+\delta t} + (\mathbf{F}_{g, \gamma}^i)^{t+\delta t} + (\mathbf{J}_{g, \gamma}^i)^{t+\delta t} \right] A_{\gamma} \\ & \text{for } i = w, a; \text{ for } \gamma = W, E, S, N, B, T \\ & \text{where } (R^i)^{t+\delta t} = 0 \end{aligned} \quad (4.23)$$

## 4.2 Discretization of the Energy Conservation Equation

Discretization of the energy conservation equation follows that of the mass conservation equations except for the advection terms. Integration of the heat content or accumulation term for the energy conservation equation over the control volume yields the expressions shown in Equations (4.24) and (4.25). Integration of the thermal source terms over the control volume yields the expression shown in Equation (4.26).

$$\frac{\partial}{\partial t} \int_V E dV = \frac{\partial}{\partial t} V E \quad (4.24)$$

$$E = (1 - n_T) \rho_s u_s + \eta_D \rho_\ell u_\ell + n_D s_g \rho_g u_g \quad (4.25)$$

$$\int_V [\dot{q} + h^w \dot{m}^w + h^a \dot{m}^a] dV = \int_V \dot{Q} dV = V \dot{Q} \quad (4.26)$$

The thermal energy conservation equation contains both diffusive and advective surface flux terms. Spatial discretization of the surface flux terms begins by converting the volumetric integrals into surface integrals, then approximating the surface integrals as summations over the surface areas between adjacent nodes, as shown in Equations (4.27) and (4.28) for the diffusive and advective flux terms, respectively. For the thermal energy equation, the diffusive flux terms are central differenced, whereas the advective flux terms are upwind or donor-cell differenced. The discretized forms of the diffusive flux terms (Cartesian coordinate system) are shown in Equations (4.29) through (4.31), for the *west*, *south*, and *bottom* surfaces, respectively. The discretized forms of the diffusive flux terms (cylindrical coordinate system) are shown in Equations (4.32) through (4.34), for the *west*, *south*, and *bottom* surfaces, respectively. The bracket with double bars indicates a user-specified interface average. The discretized forms of the advective flux terms (Cartesian coordinate system) are given in Equations (4.35) through (4.37), for the *west*, *south*, and *bottom* surfaces, respectively. The discretized forms of the advective flux terms (cylindrical coordinate system) are given in Equations (4.38) through (4.40), for the *west*, *south*, and *bottom* surfaces, respectively.

$$\begin{aligned} \int_V \nabla [\tilde{k}_e \nabla T] dV &= \int_\Gamma [\tilde{k}_e \nabla T] \cdot \mathbf{n} d\Gamma \\ &= \sum_\gamma [\tilde{k}_e \nabla T] A_\gamma \text{ for } \gamma = W, E, S, N, B, T \end{aligned} \quad (4.27)$$

$$\begin{aligned} \int_V \nabla [\rho_\ell h_\ell \mathbf{V}_\ell + \rho_g h_g \mathbf{V}_g] dV &= \int_\Gamma [\rho_\ell h_\ell \mathbf{V}_\ell + \rho_g h_g \mathbf{V}_g] \cdot \mathbf{n} d\Gamma \\ &= \sum_\gamma [\rho_\ell h_\ell \mathbf{V}_\ell + \rho_g h_g \mathbf{V}_g] A_\gamma \text{ for } \gamma = W, E, S, N, B, T \end{aligned} \quad (4.28)$$

$$\mathbf{D}_{e,W} = - \frac{[\overline{k_e^x}] (T_P - T_W)}{\delta x_W} \quad (4.29)$$

$$\mathbf{D}_{e,S} = - \frac{[\overline{k_e^y}] (T_P - T_S)}{\delta y_S} \quad (4.30)$$

$$\mathbf{D}_{e,B} = - \frac{[\overline{k_e^z}] (T_P - T_B)}{\delta z_B} \quad (4.31)$$

$$D_{e,W} = -\overline{[k_e^x]} \frac{(T_P - T_W)}{\delta r_W} \quad (4.32)$$

$$D_{e,S} = -\overline{[k_e^y]} \frac{(T_P - T_S)}{r_P \delta \theta_S} \quad (4.33)$$

$$D_{e,B} = -\overline{[k_e^z]} \frac{(T_P - T_B)}{\delta z_B} \quad (4.34)$$

$$F_{e,W} = \sum_{j=L, g} [(\rho_{j,W} h_{j,W}) \max[u_{j,W}, 0] - (\rho_{j,P} h_{j,P}) \max[-u_{j,W}, 0]] \quad (4.35)$$

$$F_{e,S} = \sum_{j=L, g} [(\rho_{j,S} h_{j,S}) \max[v_{j,S}, 0] - (\rho_{j,P} h_{j,P}) \max[-v_{j,S}, 0]] \quad (4.36)$$

$$F_{e,B} = \sum_{j=L, g} [(\rho_{j,B} h_{j,B}) \max[w_{j,B}, 0] - (\rho_{j,P} h_{j,P}) \max[-w_{j,B}, 0]] \quad (4.37)$$

$$F_{e,W} = \sum_{j=L, g} [(\rho_{j,W} h_{j,W}) \max[u_{j,W}, 0] - (\rho_{j,P} h_{j,P}) \max[-u_{j,W}, 0]] \quad (4.38)$$

$$F_{e,S} = \sum_{j=L, g} [(\rho_{j,S} h_{j,S}) \max[r_P v_{j,S}, 0] - (\rho_{j,P} h_{j,P}) \max[-r_P v_{j,S}, 0]] \quad (4.39)$$

$$F_{e,B} = \sum_{j=L, g} [(\rho_{j,B} h_{j,B}) \max[w_{j,B}, 0] - (\rho_{j,P} h_{j,P}) \max[-w_{j,B}, 0]] \quad (4.40)$$

Substituting the expressions for diffusive and advective surface flux, Equations (4.29) through (4.40), into the discretized surface integrals allows the thermal energy conservation equation to be expressed in spatially discretized form according to Equation (4.41). Temporal discretization is fully implicit first-order finite difference, according to Equation (4.42), where time levels are indicated with superscripts. The unknowns for the energy conservation equation are new time-step temperatures at each grid point. Expressed in residual form, the fully discretized energy conservation equation is shown in Equation (4.43).

$$\frac{\partial}{\partial t} V E - V \dot{Q} + \sum_{\gamma} [D_{e,\gamma} + F_{e,\gamma}] A_{\gamma} = 0 \text{ for } \gamma = W, E, S, N, B, T \quad (4.41)$$

$$V \left[ \frac{E^{t+\delta t} - E^t}{\delta t} \right] - V \dot{Q}^{t+\delta t} + \sum_{\gamma} [D_{e,\gamma}^{t+\delta t} + F_{e,\gamma}^{t+\delta t}] A_{\gamma} = 0 \text{ for } \gamma = W, E, S, N, B, T \quad (4.42)$$

$$(R^{e\gamma})^{t+\delta t} \equiv V \left[ \frac{E^{t+\delta t} - E^t}{\delta t} \right] - V \dot{Q}^{t+\delta t} + \sum_{\gamma} [D_{e,\gamma}^{t+\delta t} + F_{e,\gamma}^{t+\delta t}] A_{\gamma} = 0$$

for  $\gamma = W, E, S, N, B, T$

where  $(R^{e\gamma})^{t+\delta t} = 0$  (4.43)

### 4.3 Discretization of the Species Mass Conservation Equation

Discretization of the species mass conservation equation, Equation (2.6), follows an approach similar to that of the energy conservation equation, except that the advection and diffusion terms are combined with the power-law scheme proposed by Patankar (1980). Integration of the mass accumulation term, species source term, and reaction/decay term over the control volume yields the expression shown in Equation (4.44).

$$\frac{\partial}{\partial t} \int_V C dV - \int_V \dot{s}_c dV + \int_V \dot{R}_c C dV = \frac{\partial}{\partial t} C V - \dot{s}_c V + \dot{R}_c C V \quad (4.44)$$

The species mass conservation equation contains both advection and diffusion transport terms. The advection terms have an inseparable link with the diffusion terms; therefore, the two are considered a single transport term. Spatial discretization of the surface flux terms, both advective and diffusive, begins by converting the volumetric integrals into surface integrals, then approximating the control volume surface integrals as summations over the surface areas between adjacent nodes. These expressions are shown in Equations (4.45) and (4.46) for the diffusive terms and in Equation (4.47) for the advective terms. Defining the diffusive conductance for the aqueous and gas phases allows a compact expression of the power-law scheme, as shown in Equations (4.48) through (4.50) for a Cartesian coordinate system and Equations (4.51) through (4.53) for a cylindrical coordinate system.

$$\begin{aligned} \int_V \nabla [ \tau_j s_j n_D D_{dj} \nabla C_j ] dV &= \int_{\Gamma} [ \tau_j s_j n_D D_{dj} \nabla C_j ] \cdot \mathbf{n} dI \\ &= \sum_{\gamma} [ \tau_j s_j n_D D_{dj} \nabla C_j ] A_{\gamma} \\ &\text{for } \gamma = W, E, S, N, B, T; \text{ for } j = \ell, g \end{aligned} \quad (4.45)$$

$$\begin{aligned} \int_V \nabla [ s_j n_D \tilde{D}_{h\ell} \nabla C_j ] dV &= \int_{\Gamma} [ s_j n_D \tilde{D}_{h\ell} \nabla C_j ] \cdot \mathbf{n} dI \\ &= \sum_{\gamma} [ s_j n_D \tilde{D}_{h\ell} \nabla C_j ] A_{\gamma} \\ &\text{for } \gamma = W, E, S, N, B, T; \text{ for } j = \ell, g \end{aligned} \quad (4.46)$$

$$\begin{aligned} \int_V \nabla C_j V dV &= \int_{\Gamma} [ C_j V ] \cdot \mathbf{n} dI = \sum_{\gamma} C_j V A_{\gamma} \\ &\text{for } \gamma = W, E, S, N, B, T; \text{ for } j = \ell, g \end{aligned} \quad (4.47)$$

$$D_{j,w} = \frac{[ \tau_j s_j n_D D_{dj} + s_{\ell} n_D \tilde{D}_{h\ell}^X ]}{\delta x_w} \text{ for } j = \ell, g \quad (4.48)$$

$$D_{j,S} = \frac{\tau_j s_j n_D D_{d_j} + s_\ell n_D D_{h_\ell}^y}{\delta y_S} \text{ for } j = \ell, g \quad (4.49)$$

$$D_{j,B} = \frac{\tau_j s_j n_D D_{d_j} + s_\ell n_D D_{h_\ell}^z}{\delta z_B} \text{ for } j = \ell, g \quad (4.50)$$

$$D_{j,W} = \frac{\tau_j s_j n_D D_{d_j} + s_\ell n_D D_{h_\ell}^x}{\delta r_W} \text{ for } j = \ell, g \quad (4.51)$$

$$D_{j,S} = \frac{\tau_j s_j n_D D_{d_j} + s_\ell n_D D_{h_\ell}^y}{r_P \delta \theta_S} \text{ for } j = \ell, g \quad (4.52)$$

$$D_{j,B} = \frac{\tau_j s_j n_D D_{d_j} + s_\ell n_D D_{h_\ell}^z}{\delta z_B} \text{ for } j = \ell, g \quad (4.53)$$

The exact solution to the steady-state, no-source, no-species-decay, species conservation equation yields a solution that is dependent on the local grid Peclet number. The Peclet number for a particular phase is defined as the ratio of Darcy velocity to diffusion conductance for that phase, and represents the ratio of strengths of convection and diffusion. The nature of the exact solution may be understood by considering the variation of the species concentration between two grid points for various Peclet numbers. If the Peclet number equals zero, then diffusion transport dominates and the species concentration varies linearly with distance between two nodes. If the Peclet number equals 1 or -1, then both diffusion and advection transport influence the species concentration profile, where the diffusion profile is skewed toward the upstream value of species concentration. For large absolute values of the Peclet number, advection transport dominates, and the upstream value of the species concentration dominates the species concentration profile between nodes. The power-law scheme provides an excellent approximation to the exact solution without excessive computational expense. Discretization of the convection-diffusion terms of the species mass conservation equation requires an equation of the form shown in Equation (4.54), for an interior node. Compact expressions of the "a" and "b" coefficients of Equation (4.54) are given for the power-law scheme in Equations (4.55) through (4.60) for a Cartesian coordinate system and in Equations (4.61) through (4.66) for a cylindrical coordinate system. As indicated by Equation (4.67) for a Cartesian coordinate system, by Equation (4.68) for a cylindrical coordinate system, and by Equation (4.69), temporal discretization is fully implicit first-order finite difference.

$$a_P C_P - a_W C_W - a_E C_E - a_S C_S - a_N C_N - a_B C_B - a_T C_T = b_P \quad (4.54)$$

$$a_W = a_{\ell,W} + a_{g,W}$$

$$a_{j,W} = D_{j,W} \max \left[ 0, \left( 1 - \frac{0.1 |u_{j,W}|}{D_{j,W}} \right)^5 \right] + \max [0, u_{j,W}]$$

$$\text{for } j = \ell, g \quad (4.55)$$

$$\begin{aligned}
a_E &= a_{\ell,E} + a_{g,E} \\
a_{j,E} &= D_{j,E} \max \left[ 0, \left( 1 - \frac{0.1 |u_{j,E}|}{D_{j,E}} \right)^5 \right] + \max [0, -u_{j,E}] \\
&\text{for } j = \ell, g
\end{aligned} \tag{4.56}$$

$$\begin{aligned}
a_S &= a_{\ell,S} + a_{g,S} \\
a_{j,S} &= D_{j,S} \max \left[ 0, \left( 1 - \frac{0.1 |v_{j,S}|}{D_{j,S}} \right)^5 \right] + \max [0, v_{j,S}] \\
&\text{for } j = \ell, g
\end{aligned} \tag{4.57}$$

$$\begin{aligned}
a_N &= a_{\ell,N} + a_{g,N} \\
a_{j,N} &= D_{j,N} \max \left[ 0, \left( 1 - \frac{0.1 |v_{j,N}|}{D_{j,N}} \right)^5 \right] + \max [0, -v_{j,N}] \\
&\text{for } j = \ell, g
\end{aligned} \tag{4.58}$$

$$\begin{aligned}
a_B &= a_{\ell,B} + a_{g,B} \\
a_{j,B} &= D_{j,B} \max \left[ 0, \left( 1 - \frac{0.1 |w_{j,B}|}{D_{j,B}} \right)^5 \right] + \max [0, w_{j,B}] \\
&\text{for } j = \ell, g
\end{aligned} \tag{4.59}$$

$$\begin{aligned}
a_T &= a_{\ell,T} + a_{g,T} \\
a_{j,T} &= D_{j,T} \max \left[ 0, \left( 1 - \frac{0.1 |w_{j,T}|}{D_{j,T}} \right)^5 \right] + \max [0, -w_{j,T}] \\
&\text{for } j = \ell, g
\end{aligned} \tag{4.60}$$

$$\begin{aligned}
a_W &= a_{\ell,W} + a_{g,W} \\
a_{j,W} &= D_{j,W} \max \left[ 0, \left( 1 - \frac{0.1 |u_{j,W}|}{D_{j,W}} \right)^5 \right] + \max [0, u_{j,W}] \\
&\text{for } j = \ell, g
\end{aligned} \tag{4.61}$$

$$\begin{aligned}
a_E &= a_{\ell,E} + a_{g,E} \\
a_{j,E} &= D_{j,E} \max \left[ 0, \left( 1 - \frac{0.1 |u_{j,E}|}{D_{j,E}} \right)^5 \right] + \max [0, -u_{j,E}] \\
&\text{for } j = \ell, g
\end{aligned} \tag{4.62}$$

$$\begin{aligned}
a_S &= a_{\ell,S} + a_{g,S} \\
a_{j,S} &= D_{j,S} \max \left[ 0, \left( 1 - \frac{0.1 |r_P v_{j,S}|}{D_{j,S}} \right)^5 \right] + \max [0, r_P v_{j,S}] \\
&\text{for } j = \ell, g
\end{aligned} \tag{4.63}$$

$$\begin{aligned}
a_N &= a_{\ell,N} + a_{g,N} \\
a_{j,N} &= D_{j,N} \max \left[ 0, \left( 1 - \frac{0.1 |r_P v_{j,N}|}{D_{j,N}} \right)^5 \right] + \max [0, -r_P v_{j,N}] \\
&\text{for } j = \ell, g
\end{aligned} \tag{4.64}$$

$$\begin{aligned}
a_B &= a_{\ell,B} + a_{g,B} \\
a_{j,B} &= D_{j,B} \max \left[ 0, \left( 1 - \frac{0.1 |w_{j,B}|}{D_{j,B}} \right)^5 \right] + \max [0, w_{j,B}] \\
&\text{for } j = \ell, g
\end{aligned} \tag{4.65}$$

$$\begin{aligned}
a_T &= a_{\ell,T} + a_{g,T} \\
a_{j,T} &= D_{j,T} \max \left[ 0, \left( 1 - \frac{0.1 |w_{j,T}|}{D_{j,T}} \right)^5 \right] + \max [0, -w_{j,T}] \\
&\text{for } j = \ell, g
\end{aligned} \tag{4.66}$$

$$\begin{aligned}
a_P &= a_{\ell,P} + a_{g,P} + \frac{V}{\delta t} + \dot{R}_c^{t+\delta t} \\
a_{j,P} &= a_{j,E} + a_{j,W} + a_{j,S} + a_{j,N} + a_{j,B} + a_{j,T} + u_{j,E} - u_{j,W} + v_{j,S} - v_{j,N} + w_{j,B} - w_{j,T} \\
&\text{for } j = \ell, g
\end{aligned} \tag{4.67}$$

$$\begin{aligned}
a_P &= a_{\ell,P} + a_{g,P} + \frac{V}{\delta t} + \dot{R}_c^{t+\delta t} \\
a_{j,P} &= a_{j,E} + a_{j,W} + a_{j,S} + a_{j,N} + a_{j,B} + a_{j,T} + u_{j,E} - u_{j,W} + r_P v_{j,S} - r_P v_{j,N} + w_{j,B} - w_{j,T} \\
&\text{for } j = \ell, g
\end{aligned} \tag{4.68}$$

$$b_P = \frac{C_P^t V}{\delta t} + \dot{s}_c^{t+\delta t} \tag{4.69}$$

#### 4.4 Boundary Conditions

The discretization approaches described above for the mass, energy, and species conservation equations were for nodes positioned within the interior of the computational domain. For nodes located adjacent to the domain boundary, the discretization of the governing equations differs to account for conditions at the boundary. Boundary conditions are specified either with field variables (e.g., aqueous pressure, gas pressure, temperature, vapor mass fraction, or species concentration) or with surface fluxes (e.g., aqueous-phase mass fluxes, gas-phase mass fluxes, heat fluxes, or species fluxes) on the boundary surfaces. Boundary conditions of the former type are referred to as Dirichlet, whereas the latter type are referred to as Neumann. Special boundary conditions such as the unit-gradient, saturated, zero-flux, and seepage-face boundaries typically can be reduced to either a Dirichlet- or a Neumann-type boundary. For example, the saturated boundary is equivalent to specifying phase pressures at the boundary surface to create saturated conditions. Default boundary conditions for MSTs are zero-flux Neumann-type boundaries. Geometric definitions differ between interior and boundary nodes. Definitions of geometric parameters for boundary nodes with *west* boundary surfaces are shown in Figures 4.5 through 4.8

for both Cartesian and cylindrical coordinate systems. Definitions of geometric parameters for boundary nodes with other boundary surfaces can be inferred from those shown for *west* boundary surfaces.

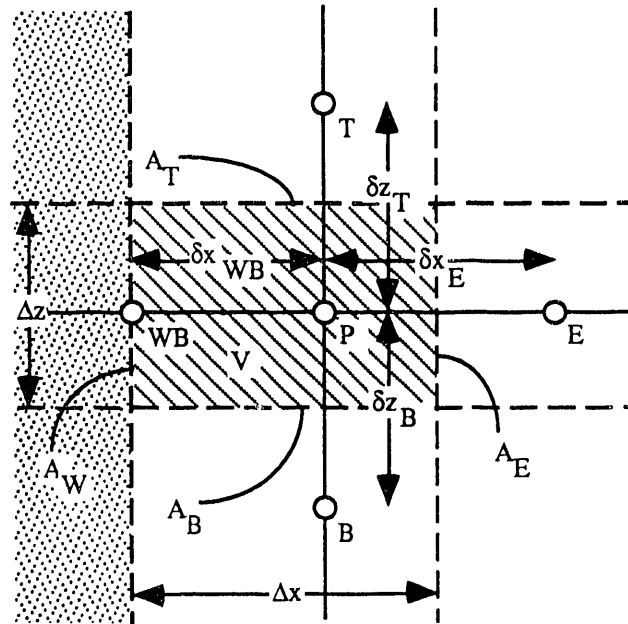


**Figure 4.5.** X-Z Cartesian Coordinate System for *West* Boundary

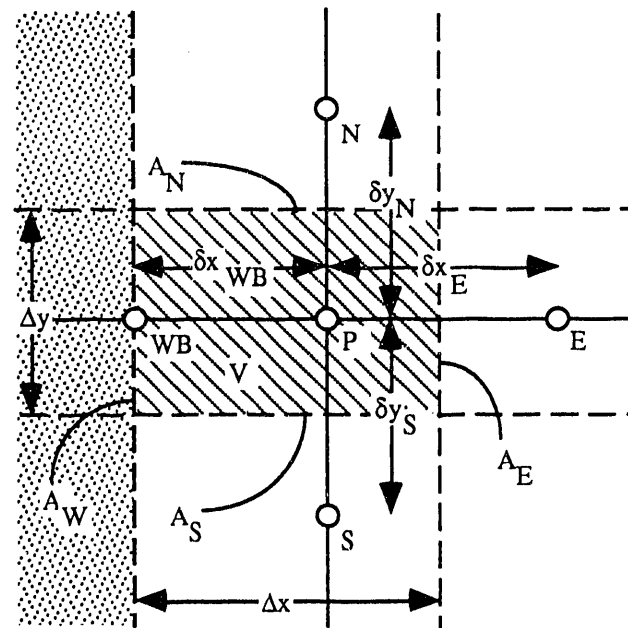


**Figure 4.6.** X-Y Cartesian Coordinate System for *West* Boundary

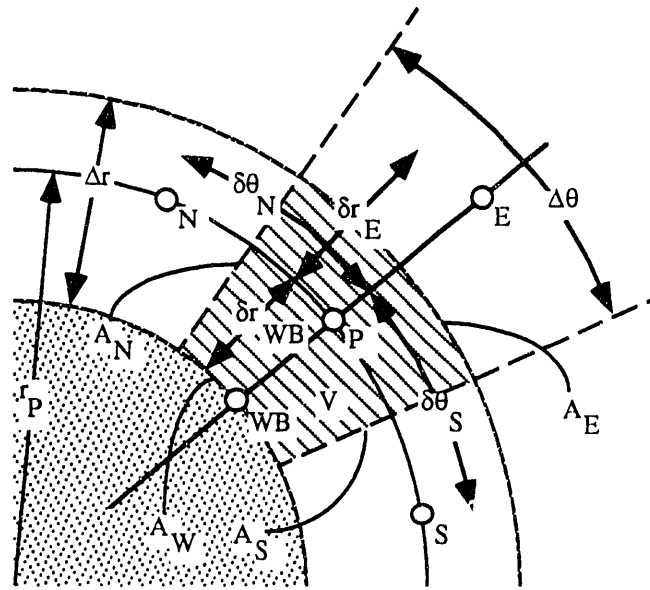


Figure 4.7. R- $\theta$  Cylindrical Coordinate System for *West Boundary*

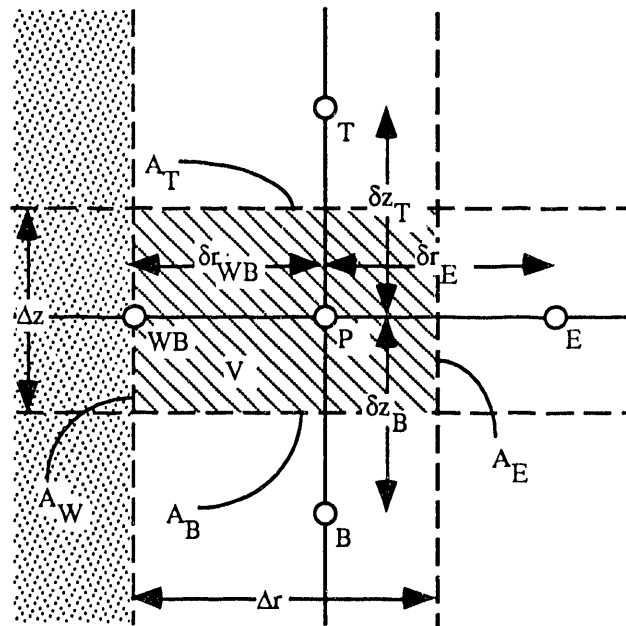


Figure 4.8. R-Z Cylindrical Coordinate System for *West Boundary*

#### 4.4.1 Dirichlet Boundary Conditions

Implementation of Dirichlet boundary conditions requires relatively few modifications to the discretized governing conservation equations. Dirichlet boundary conditions are equivalent to specifying a field variable on a particular boundary surface. Depending on the solution option, one or more of the following primary field variables can be specified on boundary surfaces: aqueous pressure, gas pressure, water-vapor mass fraction, temperature, and species concentration. In addition to specifying primary field variables, a number of secondary variables must be specified to completely establish the boundary conditions. The number of required secondary variables will depend on the solution option and primary field variables specified on the boundary surfaces. If, for example, the solution option involved only the solution of the water conservation equation, then the required secondary variables with a specified aqueous pressure would include the aqueous-phase density and mass fraction of air dissolved in the aqueous phase.

Aqueous-pressure boundary conditions directly affect the aqueous-phase surface flux. As an example, the discretized forms of water or air mass flux, associated with the aqueous phase, on a *west* boundary surface are shown in Equations (4.70) and (4.71) for Cartesian and cylindrical coordinate systems. Because the interfacial terms for aqueous-phase density and mass fraction parameters are upwind weighted, specification of aqueous pressure on a boundary surface requires the additional specification of these two secondary variables on the boundary surface. The intrinsic permeability, relative permeability, and aqueous-phase viscosity terms are evaluated from the boundary node primary variables.

$$\mathbf{F}_{\ell, w}^i = - \left[ \frac{k^x k_{r\ell}}{\mu_\ell} \right] \left[ \overrightarrow{\rho_\ell x_\ell^i} \right] \frac{(P_{\ell, WB} - P_{\ell, P})}{\delta x_{WB}} \text{ for } i = w, a \quad (4.70)$$

$$\mathbf{F}_{\ell, w}^i = - \left[ \frac{k^x k_{r\ell}}{\mu_\ell} \right] \left[ \overrightarrow{\rho_\ell x_\ell^i} \right] \frac{(P_{\ell, WB} - P_{\ell, P})}{\delta r_{WB}} \text{ for } i = w, a \quad (4.71)$$

Gas-pressure boundary conditions directly affect the gas-phase surface flux. As an example, the discretized forms of water or air mass flux, associated with the gas phase, on a *west* boundary surface are shown in Equations (4.72) and (4.73) for Cartesian and cylindrical coordinate systems. Because the interfacial terms for gas-phase density and mass fraction parameters are upwind weighted, specification of gas pressure on a boundary surface requires the additional specification of these two secondary variables on the boundary surface. The intrinsic permeability, relative permeability, and gas-phase viscosity terms are evaluated from the boundary node primary variables.

$$\mathbf{F}_{g, w}^i = - \left[ \frac{k^x k_{rg}}{\mu_g} \right] \left[ \overrightarrow{\rho_g x_g^i} \right] \frac{(P_{g, WB} - P_{g, P})}{\delta x_{WB}} \text{ for } i = w, a \quad (4.72)$$

$$\mathbf{F}_{g, w}^i = - \left[ \frac{k^x k_{rg}}{\mu_g} \right] \left[ \overrightarrow{\rho_g x_g^i} \right] \frac{(P_{g, WB} - P_{g, P})}{\delta r_{WB}} \text{ for } i = w, a \quad (4.73)$$

Water-vapor boundary conditions directly affect the diffusive gas-phase surface flux. As an example, the discretized form of the water mass flux, associated with binary diffusion through the gas phase, on a *west* boundary surface is shown in Equations (4.74) and (4.75) for Cartesian and cylindrical coordinate systems. The tortuosity, gas-phase density, gas-phase saturation, and binary

diffusion coefficient are all evaluated from the boundary node primary variables. No additional secondary variables are required for vapor mass fraction boundary conditions.

$$\mathbf{J}_{g,W}^w = -[\tau_g n_D \rho_g s_g D_g^{aw}] \frac{x_{g,WB}^w - x_{g,P}^w}{\delta x_{WB}} \quad (4.74)$$

$$\mathbf{J}_{g,W}^w = -[\tau_g n_D \rho_g s_g D_g^{aw}] \frac{x_{g,WB}^w - x_{g,P}^w}{\delta r_{WB}} \quad (4.75)$$

Temperature boundary conditions directly affect both the diffusive and the advective surface heat flux. As an example, the discretized forms of the diffusive and advective heat fluxes on a *west* boundary surface are shown in Equations (4.76) and (4.77) for a Cartesian coordinate system and in Equations (4.78) and (4.79) for a cylindrical coordinate system. For the diffusive heat flux, the effective thermal conductivity is evaluated from the boundary node primary variables. Because of the donor-cell averaging scheme used with the advective heat flux terms, phase density and phase enthalpy must additionally be specified at the surface boundary. Phase enthalpies that are specified for boundary surfaces must be defined according to the same reference states used internally by MSTS to compute the air, liquid water, and vapor water enthalpies. The reference state for computing air enthalpies and internal energies is the internal energy of air at 1 atm, 0°C, and the reference state for computing water enthalpies is the internal energy of liquid water at 1 atm, 0.01°C.

$$\mathbf{D}_{e,W} = -[k_e^x] \frac{(T_P - T_{WB})}{\delta x_{WB}} \quad (4.76)$$

$$\mathbf{F}_{e,W} = \sum_{j=\ell, g} [(\rho_{j,WB} h_{j,WB}) \max[u_{j,WB}, 0] - (\rho_{j,P} h_{j,P}) \max[-u_{j,WB}, 0]] \quad (4.77)$$

$$\mathbf{D}_{e,W} = -[k_e^x] \frac{(T_P - T_{WB})}{\delta r_{WB}} \quad (4.78)$$

$$\mathbf{F}_{e,W} = \sum_{j=\ell, g} [(\rho_{j,WB} h_{j,WB}) \max[u_{j,WB}, 0] - (\rho_{j,P} h_{j,P}) \max[-u_{j,WB}, 0]] \quad (4.79)$$

Species concentration boundary conditions directly affect the diffusive, dispersive, and advective species surface flux. As an example, the discretized form of the species combined diffusion-dispersion coefficient for a *west* boundary surface is shown in Equations (4.80) and (4.81) for Cartesian and cylindrical coordinate systems. The tortuosity, saturation, porosity, and diffusion coefficient are evaluated from the boundary node primary variables. The hydraulic dispersion coefficient is computed from boundary surface velocities and boundary node velocities. A species concentration boundary condition also modifies the form of the discretized governing equation, as shown in Equation (4.82) for both Cartesian and cylindrical coordinate systems, where the term associated with the species concentration on the *west* boundary surface becomes a known quantity and appears on the right-hand side of the equation.

$$D_{j,W} = \frac{[\tau_j s_j n_D D_{dj} + s_\ell n_D D_{h_\ell}^x]}{\delta x_{WB}} \text{ for } j = \ell, g \quad (4.80)$$

$$D_{j,W} = \frac{[\tau_j s_j n_D D_{dj} + s_\ell n_D D_{h_\ell}^x]}{\delta r_{WB}} \text{ for } j = \ell, g \quad (4.81)$$

$$a_P C_P - a_E C_E - a_S C_S - a_N C_N - a_B C_B - a_T C_T = b_P + a_W C_W \quad (4.82)$$

#### 4.4.2 Neumann Boundary Conditions

Neumann-type boundary conditions are accommodated by substituting the specified surface fluxes directly into the discretized form of the conservation equation. Neumann-type boundary conditions may be specified for aqueous-phase surface flux, gas-phase surface flux, diffusive thermal energy surface flux, advective thermal energy surface flux per phase, combined advective and diffusive thermal energy surface flux, and combined advective and diffusive species surface flux in each phase.

Aqueous surface flux boundary conditions are defined by specifying the following parameters on the boundary surface: aqueous-phase mass flux and air mass fraction in the aqueous phase. As an example, the air and water component mass fluxes on a *west* boundary surface are computed from these parameters, as shown in Equation (4.83) for both Cartesian and cylindrical coordinate systems. The aqueous-phase air mass fraction remains an interfacial average computed with upwind logic.

$$\mathbf{F}_{\ell,W}^i = [\overline{\rho_\ell x_\ell^i}] u_{\ell,WB} \text{ for } i = w, a \quad (4.83)$$

Gas surface flux boundary conditions are defined by specifying the following parameters on the boundary surface: gas-phase mass flux and water-vapor mass fraction in the gas phase. As an example, the air and water component mass fluxes on a *west* boundary surface are computed from these parameters, as shown in Equation (4.84) for both Cartesian and cylindrical coordinate systems. The gas-phase vapor mass fraction remains an interfacial average computed with upwind logic.

$$\mathbf{F}_{g,W}^i = [\overline{\rho_g x_g^i}] u_{g,WB} \text{ for } i = w, a \quad (4.84)$$

Neumann-type thermal boundary conditions may be specified for various components of the total surface heat flux. If a diffusive thermal surface flux is specified, then the diffusive component of the thermal flux term is reformulated. As an example, for a Neumann-type diffusive thermal boundary condition specified on a *west* boundary surface, the discretized form of the diffusive heat flux term would appear as shown in Equation (4.85). The advective components of the thermal surface flux may be specified individually per phase or collectively. Neumann-type advective thermal boundary conditions require the specification of phase densities, phase enthalpies, and phase Darcy velocities. For a Neumann-type advective thermal boundary condition specified on a *west* boundary surface, the discretized form of the advective heat flux term would appear as shown in Equation (4.86). In practice, the phase densities and phase Darcy velocities are specified as Neumann-type surface mass flux boundary conditions. Combined diffusive and advective thermal surface fluxes are specified as boundary conditions through separate specifications for the diffusive and advective terms.

$$\mathbf{D}_{e,W} = \dot{Q}_{e,WB} \quad (4.85)$$

$$F_{e,w} = \sum_{j=\ell,g} [(\rho_{j,WB} h_{j,WB}) \max[u_{j,WB}, 0] - (\rho_{j,P} h_{j,P}) \max[-u_{j,WB}, 0]] \quad (4.86)$$

The discretized form of the species mass conservation equation uses a power-law scheme to combine the diffusive-dispersive terms with the advective terms. This approach increases the complexity of applying species flux boundary conditions. As an example, species flux across a *west* boundary surface can be expressed as shown in Equations (4.87) and (4.88) for both Cartesian and cylindrical coordinate systems. Substituting Equations (4.87) and (4.88) into the discretized form of the species mass conservation equation, Equation (4.54), yields the modified form of the discretized species mass conservation equation for a species flux boundary on a *west* boundary surface, as shown in Equation (4.89) for both Cartesian and cylindrical coordinate systems.

$$F_{c,w} = a_w C_w - a_w^* C_P = \dot{Q}_{c,WB} \quad (4.87)$$

$$a_w^* = a_{\ell,w}^* + a_{g,w}^*$$

$$a_{j,w}^* = D_{j,w} \max \left[ 0, \left( 1 - \frac{0.1 |u_{j,w}|}{D_{j,w}} \right)^5 \right] + \max[0, -u_{j,w}]$$

for  $j = \ell, g$

(4.88)

$$(a_P + a_w^*) C_P - a_E C_E - a_S C_S - a_N C_N - a_B C_B - a_T C_T = (b_P + \dot{Q}_{c,WB}) \quad (4.89)$$

#### 4.5 Newton-Raphson Linearization Scheme

The discretized forms of the governing equations for conservation of water mass, air mass, and energy, Equations (4.23) and (4.43), are highly nonlinear and coupled. The discretized form of the governing equation for species conservation, Equation (4.54), may be treated as linear and decoupled from the thermal-hydrologic governing equations. Nonlinearities in the governing conservation equations for thermal-hydrologic fields arise because of the strong dependence of soil characteristics on phase pressures and thermal properties on temperature. Coupling between the governing equations for mass and energy conservation occurs because of the interdependence of the thermal and hydrologic fields (i.e., the subsurface temperatures depend on the subsurface saturations and Darcy velocities, and vice versa). Because of the coupled character of the thermal-hydrologic conservation equations, a simultaneous solution approach is applied. Conversely, because of the decoupled character of the species conservation equation with respect to the thermal-hydrologic equations, a sequential solution approach is applied. Nonlinearities in the thermal-hydrologic equations are accommodated with a Newton-Raphson linearization scheme, which involves iterating to converged solutions. The solution approach applied to the governing conservation equations, therefore, entails a simultaneous solution of the conservation equations for mass and energy through an iterative scheme, followed by a direct solution of the species transport equation.

The Newton-Raphson linearization scheme is an iterative method for solving equations of the form shown in Equation (4.90), where  $f$  is differentiable. The concept involves approximating the graph of  $f$  by suitable tangents. Each iteration generates a new estimate of  $x$  as the intersection of the tangent to the curve  $f$  at the previous estimate of  $x$  and the  $x$ -axis. The general formula for the Newton-Raphson technique is shown in Equation (4.91). The function  $f(x)$  may be thought

of as the iteration residual. For a convergent system, the residual decreases with iteration count. For multivariable systems, the scalar function  $f(x)$  may be replaced with the vector function  $\mathbf{R}(x)$ ; and the general formula is shown in Equation (4.92). The vector function  $\mathbf{R}(x)$  represents the system of nonlinear thermal-hydrologic conservation equations in discretized form, and the vector of unknowns  $x$  represents the primary variables. Because of the solution option and variable switching logic incorporated into MSTs, the vector function and vector of unknowns will vary between applications. Upon rewriting Equation (4.92) in terms of a vector of changes in unknowns, the Newton-Raphson general formula may be expressed as a system of linear equations, as shown in Equation (4.93). When expanded, the partial derivative terms in Equation (4.94) form the Jacobian matrix.

$$f(x) = 0 \tag{4.90}$$

$$x^{n+1} = x^n - \frac{f(x)}{f'(x)} \tag{4.91}$$

$$x^{n+1} = x^n - \frac{\mathbf{R}(x^n)}{\left[ \frac{\partial \mathbf{R}(x^n)}{\partial x} \right]} \tag{4.92}$$

$$\frac{\partial \mathbf{R}(x)}{\partial x} \Delta x = -\mathbf{R}(x) \tag{4.93}$$

Consider a one-dimensional system, where the conservation equations for water mass, air mass, and energy are solved, and the set of primary variables equals the aqueous pressure, gas pressure, and temperature. The system of linear equations for this system is shown in Equation (4.94) for an "n"-node computational domain. For this system with three conservation equations per node, each Jacobian matrix element represents a third-order square submatrix as shown in Equation (4.95). Each unknown vector element and solution vector element is a subvector that contains three elements as shown in Equations (4.96) and (4.97), respectively. The unknown vector elements represent changes in a particular primary variable or the amount a particular primary variable will be incremented between iterations. The solution vector elements are the conservation equation residuals, written in discretized form, corrected for boundary conditions, and evaluated at the most recent iterate values of the primary variables.

For a two-dimensional system, the Jacobian matrix would contain the elements shown in Equation (4.94) for the one-dimensional system, plus two diagonal bands of elements (one below and one above the main diagonal) located one half-band width from the main diagonal band. The half-band width for a two-dimensional system equals the lesser of the two domain ranges. For a three-dimensional system, the Jacobian matrix would contain the elements shown in Equation (4.94) for the one-dimensional system, plus four diagonal bands of elements, two below and two above the main diagonal. The off-diagonal bands are located at the minimum half-band widths of the Jacobian matrix for a particular computational domain geometry. Minimum half-band widths for a three-dimensional system equal the product of two least domain ranges. For example, a computational domain that contained 30 nodes along the x-axis, 20 nodes along the y-axis, and 40 nodes along the z-axis would have a minimum half-band width of 20 x 30, or 600.

$$\begin{vmatrix}
\frac{\partial R_1}{\partial x_1} & \frac{\partial R_1}{\partial x_2} & 0 & 0 & 0 & 0 & 0 \\
\frac{\partial R_2}{\partial x_1} & \frac{\partial R_2}{\partial x_2} & \frac{\partial R_2}{\partial x_3} & 0 & 0 & 0 & 0 \\
0 & \frac{\partial R_3}{\partial x_2} & \frac{\partial R_3}{\partial x_3} & \frac{\partial R_3}{\partial x_4} & 0 & 0 & 0 \\
\cdot & \cdot & \cdot & \cdot & \cdot & \cdot & \cdot \\
\cdot & \cdot & \cdot & \cdot & \cdot & \cdot & \cdot \\
0 & 0 & 0 & 0 & \frac{\partial R_{n-1}}{\partial x_{n-2}} & \frac{\partial R_{n-1}}{\partial x_{n-1}} & \frac{\partial R_{n-1}}{\partial x_n} \\
0 & 0 & 0 & 0 & 0 & \frac{\partial R_n}{\partial x_{n-1}} & \frac{\partial R_n}{\partial x_n}
\end{vmatrix}
\begin{vmatrix}
x_1 \\
x_2 \\
x_3 \\
\cdot \\
\cdot \\
x_{n-1} \\
x_n
\end{vmatrix}
=
\begin{vmatrix}
-R_1 \\
-R_2 \\
-R_3 \\
\cdot \\
\cdot \\
-R_{n-1} \\
-R_n
\end{vmatrix}
\tag{4.94}$$

$$\frac{\partial R_k}{\partial x_l} = \begin{vmatrix}
\frac{\partial R_k^w}{\partial P_{\ell,l}} & \frac{\partial R_k^w}{\partial P_{g,l}} & \frac{\partial R_k^w}{\partial T_l} \\
\frac{\partial R_k^a}{\partial P_{\ell,l}} & \frac{\partial R_k^a}{\partial P_{g,l}} & \frac{\partial R_k^a}{\partial T_l} \\
\frac{\partial R_k^e}{\partial P_{\ell,l}} & \frac{\partial R_k^e}{\partial P_{g,l}} & \frac{\partial R_k^e}{\partial T_l}
\end{vmatrix}
\tag{4.95}$$

$$x_l = \begin{vmatrix}
\Delta P_{\ell,l} \\
\Delta P_{g,l} \\
\Delta T_l
\end{vmatrix}
\tag{4.96}$$

$$-R_k = \begin{vmatrix}
-R_k^w \\
-R_k^a \\
-R_k^e
\end{vmatrix}
\tag{4.97}$$

The partial derivatives of the residuals of the discretized governing equations in the Jacobian matrix represent a majority of the computational effort. The Newton-Raphson scheme requires that these partial derivatives be computed during each iteration. Because of the complex dependencies of the governing equation residuals on the primary variables, the partial derivatives in the Jacobian matrix are not computed from analytical expressions, but rather computed numerically, as exemplified in Equation (4.98) for the water conservation equation and aqueous-pressure primary variable. The expression in Equation (4.98) is computed by evaluating the residual of the governing equation, first at the value of the primary variable, then at the value of the primary variable slightly incremented.

$$\frac{\partial R_k^w}{\partial P_{\ell,l}} \equiv \frac{R_k^w(P_{\ell,l} + \Delta P_{\ell,l}) - R_k^w(P_{\ell,l})}{\Delta P_{\ell,l}} \quad (4.98)$$

The Newton-Raphson linearization procedure begins at the start of a new time step or after a failed convergence. The first step of the procedure is to numerically evaluate all of the partial derivatives that make up the Jacobian matrix. The numerical evaluation begins by computing values of the governing equation residuals, corrected for boundary conditions and evaluated at the most recent iterate values of the primary variables. For a new time step or after a failed convergence, the most recent iterate of the primary variable equals its value from the previous time step. The governing equation residuals, corrected for boundary conditions, are reevaluated at incremented values of the primary variables. The governing equation residuals evaluated at incremented and nonincremented values of the primary variables are then used to compute the partial derivative functions that make up the Jacobian matrix and the elements of the solution vector.

The resulting system of linear equations is then solved with either a direct or an iterative solver. Solution of the system of equations yields changes to the primary variables. An iteration ends by updating the primary variables with the changes computed from the system of linear equations. If the ratio of residuals to accumulation terms falls below the convergence criterion for every equation and every node, then the procedure is determined to have converged and a new time step begins. Otherwise, another iteration commences. If the ratio of residuals to accumulation terms fails to decrease below the convergence criterion within a specified number of iterations, the system is considered nonconvergent. Nonconvergent systems are handled by reducing the simulation time step, resetting the primary variables to their previous time-step values, and reinitiating the time-step procedures.

#### 4.6 Linear Equation Solution

The system of linear equations that results from the discretization of the governing partial differential equations over a particular computational domain always has a banded structure, where the number of off-diagonal bands equals the dimensionality of the computational domain. Elements within the Jacobian coefficient are actually submatrices, where the submatrix order equals the number of solved coupled governing equations. For example, the solution of only the water conservation equation produces single-element submatrices, whereas the solution of the three mass conservation equations simultaneously with the energy equation yields four-by-four submatrices. These structured Jacobian coefficient matrices arise from the element sequencing scheme incorporated into MSTS and limitations on the computational domain structures. The matrix sequencing or numbering algorithms are designed to minimize the largest half-band width for a given computational domain and solution option combination. The sequencing algorithms are designed for orthogonal grid systems that have six surfaces in three dimensions or have four surfaces in two dimensions.

Two linear equation solvers are available within MSTS: a direct banded matrix algorithm and an iterative conjugate gradient algorithm. The banded matrix algorithm is generally more appropriate for small to moderately sized Jacobian matrices (order less than 15,000), whereas the conjugate gradient algorithm appears more appropriate for larger-order Jacobian matrices. In general, the banded matrix algorithm requires more memory than does the conjugate gradient algorithm, which utilizes an efficient sparse-matrix storage scheme. The banded matrix algorithm is computationally more efficient on small to moderately sized problems; for larger problems,

however, the conjugate gradient algorithm becomes the better performer. Both linear equation solution algorithms were obtained from publicly available software packages.

The banded matrix solution algorithm was extracted from the LINPACK subroutines (Dongarra et al. 1980) for general nonsymmetric band matrices. The algorithm operates on band matrices by decomposing the matrix into an upper triangular and a lower triangular matrix. The matrix product of the lower triangular matrix with the upper triangular matrix equals the original band matrix  $\mathbf{A} = \mathbf{LU}$ , where  $\mathbf{A}$  is the band matrix,  $\mathbf{L}$  is the lower triangular matrix, and  $\mathbf{U}$  is the upper triangular matrix. The system of linear equations  $\mathbf{A} \mathbf{x} = \mathbf{b}$  is solved with the above decomposition or factorization by solving successively  $\mathbf{L} (\mathbf{U} \mathbf{x}) = \mathbf{b}$ . This factorization procedure produces nonzero elements outside the bands of the original band matrix. If  $m_l$  equals the half-band width of the Jacobian coefficient matrix (MSTS produces band matrices with equal lower- and upper-band widths), then the two triangular factors have band widths  $m_l$  and  $2m_l$ . Storage must be provided for the extra  $m_l$  diagonals. This is illustrated for a one-dimensional problem of seven nodes and two solved mass conservation equations. The Jacobian coefficient matrix for this problem would appear as shown in Equation (4.99). The band storage requires  $3m_l + 1 = 10$  rows of storage arranged as shown in Equation (4.100). The \* indicates elements that are never referenced but for which storage space must be provided. The + indicates elements that may be occupied during the factorization process. The original Jacobian coefficient matrix is referred to as  $\mathbf{A}$  and its storage counterpart as  $\mathbf{a}$ ; then the columns of  $\mathbf{A}$  are stored in the columns of  $\mathbf{a}$ , and the diagonals of  $\mathbf{A}$  are stored in the rows of  $\mathbf{a}$ , such that the principal diagonal is stored in row  $2m_l + 1$  of  $\mathbf{a}$ .

$$\mathbf{A} = \begin{array}{c} \left| \begin{array}{cccccccccc} x_{1,1} & x_{1,2} & x_{1,3} & x_{1,4} & 0 & 0 & 0 & 0 & 0 & 0 \\ x_{2,1} & x_{2,2} & x_{2,3} & x_{2,4} & 0 & 0 & 0 & 0 & 0 & 0 \\ x_{3,1} & x_{3,2} & x_{3,3} & x_{3,4} & x_{3,5} & x_{3,6} & 0 & 0 & 0 & 0 \\ x_{4,1} & x_{4,2} & x_{4,3} & x_{4,4} & x_{4,5} & x_{4,6} & 0 & 0 & 0 & 0 \\ 0 & 0 & x_{5,3} & x_{5,4} & x_{5,5} & x_{5,6} & x_{5,7} & x_{5,8} & 0 & 0 \\ 0 & 0 & x_{6,3} & x_{6,4} & x_{6,5} & x_{6,6} & x_{6,7} & x_{6,8} & 0 & 0 \\ 0 & 0 & 0 & 0 & x_{7,5} & x_{7,6} & x_{7,7} & x_{7,8} & x_{7,9} & x_{7,10} \\ 0 & 0 & 0 & 0 & x_{8,5} & x_{8,6} & x_{8,7} & x_{8,8} & x_{8,9} & x_{8,10} \\ 0 & 0 & 0 & 0 & 0 & 0 & x_{9,7} & x_{9,8} & x_{9,9} & x_{9,10} \\ 0 & 0 & 0 & 0 & 0 & 0 & x_{10,7} & x_{10,8} & x_{10,9} & x_{10,10} \end{array} \right| \end{array} \quad (4.99)$$

$$\mathbf{a} = \begin{pmatrix} * & * & * & * & * & * & + & + & + & + \\ * & * & * & * & * & + & + & + & + & + \\ * & * & * & * & + & + & + & + & + & + \\ * & * & * & x_{1,4} & 0 & x_{3,6} & 0 & x_{5,8} & 0 & x_{7,10} \\ * & * & x_{1,3} & x_{2,4} & x_{3,5} & x_{4,6} & x_{5,7} & x_{6,8} & x_{7,9} & x_{8,10} \\ * & x_{1,2} & x_{2,3} & x_{3,4} & x_{4,5} & x_{5,6} & x_{6,7} & x_{7,8} & x_{8,9} & x_{9,10} \\ x_{1,1} & x_{2,2} & x_{3,3} & x_{4,4} & x_{5,5} & x_{6,6} & x_{7,7} & x_{8,8} & x_{9,9} & x_{10,10} \\ x_{2,1} & x_{3,2} & x_{4,3} & x_{5,4} & x_{6,5} & x_{7,6} & x_{8,7} & x_{9,8} & x_{10,9} & * \\ x_{3,1} & x_{4,2} & x_{5,3} & x_{6,4} & x_{7,5} & x_{8,6} & x_{9,7} & x_{10,8} & * & * \\ x_{4,1} & 0 & x_{6,3} & 0 & x_{8,5} & 0 & x_{10,7} & * & * & * \end{pmatrix} \quad (4.100)$$

The conjugate gradient solution algorithm was extracted from a package of subroutines intended for solving large sparse linear systems by iterative methods (Oppe et al. 1988). This package of subroutines is referred as NSPCG (for Nonsymmetric Preconditioned Conjugate Gradient) and has available various acceleration techniques and preconditioners for solving large sparse linear systems. The algorithms available from the NSPCG package are the "Incomplete Cholesky" (IC) preconditioner and the "Generalized Minimal Residual Method" (GMRES) accelerator. Preconditioners compute a splitting matrix  $\mathbf{Q}$  such that the preconditioned system of linear equations,  $\mathbf{Q}^{-1} \mathbf{A} \mathbf{x} = \mathbf{Q}^{-1} \mathbf{b}$ , is better conditioned than the original system,  $\mathbf{A} \mathbf{x} = \mathbf{b}$ . The splitting matrix for the IC preconditioner is an incomplete LU decomposition of the Jacobian matrix  $\mathbf{A}$ . The form of the splitting matrix  $\mathbf{Q}$  is  $\mathbf{Q} = (\mathbf{D} - \mathbf{S}) \mathbf{D}^{-1} (\mathbf{D} - \mathbf{T})$ , where  $\mathbf{D}$  is a diagonal matrix containing the factorization pivots,  $\mathbf{S}$  is a lower triangular matrix, and  $\mathbf{T}$  is an upper triangular matrix. It is necessary to store both  $\mathbf{S}$  and  $\mathbf{T}$  because the Jacobian coefficient matrix  $\mathbf{A}$  is not symmetric.

The NSPCG package allows several modes of storage for the Jacobian coefficient matrix. The storage mode selected for MSTS represents the Jacobian coefficient matrix with two rectangular arrays, one real and one integer. Both arrays are dimensioned  $n$  by  $m$ , where  $n$  equals the number of unknowns and  $m$  equals 7 times the number of solved coupled governing equations. Each row in the real coefficient matrix  $\mathbf{C}$  contains the nonzero values of the corresponding row in the Jacobian coefficient matrix  $\mathbf{A}$ ; the corresponding row in the integer coefficient matrix  $\mathbf{J}$  contains the column indices. The Jacobian matrix shown in Equation (4.99) would be expressed as the real and integer matrices shown in Equations (4.101) and (4.102), respectively. Although this storage format requires two coefficient matrices, the storage requirements for large sparse systems (such as those for large multidimensional problems) are greatly reduced from those for the banded matrix solution scheme.

$$\mathbf{C} = \begin{pmatrix}
 x_{1,1} & x_{1,2} & x_{1,3} & x_{1,4} & 0 & 0 \\
 x_{2,1} & x_{2,2} & x_{2,3} & x_{2,4} & 0 & 0 \\
 x_{3,1} & x_{3,2} & x_{3,3} & x_{3,4} & x_{3,5} & x_{3,6} \\
 x_{4,1} & x_{4,2} & x_{4,3} & x_{4,4} & x_{4,5} & x_{4,6} \\
 x_{5,3} & x_{5,4} & x_{5,5} & x_{5,6} & x_{5,7} & x_{5,8} \\
 x_{6,3} & x_{6,4} & x_{6,5} & x_{6,6} & x_{6,7} & x_{6,8} \\
 x_{7,5} & x_{7,6} & x_{7,7} & x_{7,8} & x_{7,9} & x_{7,10} \\
 x_{8,5} & x_{8,6} & x_{8,7} & x_{8,8} & x_{8,9} & x_{8,10} \\
 x_{9,7} & x_{9,8} & x_{9,9} & x_{9,10} & 0 & 0 \\
 x_{10,7} & x_{10,8} & x_{10,9} & x_{10,10} & 0 & 0
 \end{pmatrix} \tag{4.101}$$

$$\mathbf{J} = \begin{pmatrix}
 1 & 2 & 3 & 4 & 0 & 0 \\
 1 & 2 & 3 & 4 & 0 & 0 \\
 1 & 2 & 3 & 4 & 5 & 6 \\
 1 & 2 & 3 & 4 & 5 & 6 \\
 3 & 4 & 5 & 6 & 7 & 8 \\
 3 & 4 & 5 & 6 & 7 & 8 \\
 5 & 6 & 7 & 8 & 9 & 10 \\
 5 & 6 & 7 & 8 & 9 & 10 \\
 7 & 8 & 9 & 10 & 0 & 0 \\
 7 & 8 & 9 & 10 & 0 & 0
 \end{pmatrix} \tag{4.102}$$

## 5.0 Code Architecture

The source code for MSTS is written in the FORTRAN 77 following the American National Standards Institute (ANSI) standards. To obtain execution time and date information, the code requires machine- and operating-system-dependent calls to nonstandard ANSI FORTRAN 77 library functions. Algorithms that call for time and date information have been provided in the MSTS source code for several different computing platforms, from workstations to supercomputers, for a number of manufacturers. The source code is written with minimal memory sharing (i.e., overwriting of variables). Memory requirements for the executable version of MSTS are controlled through a limited number of "PARAMETER" statements. The executable must be properly dimensioned through parameterization of the source code. The required dimensions for each parameter in the source code are dependent on the input file specifications (see Nichols and White 1992 for parameterization rules). The executable version of MSTS will execute properly with an overly dimensioned source code; however, failure to properly dimension a single parameter to the required minimum dimension may result in erroneous results or an execution failure.

The code was designed as a scientific tool for investigating multiphase subsurface transport phenomena. A minimal number of error-checking routines exist in MSTS. Within the limits of the input structure, few restrictions exist on the types of problems that can be created, including ill-posed problems, problems with conflicting boundary conditions, simulation steps that violate the Courant limit, and/or problems with missing or erroneous data. Moreover, execution of a problem to completion does not guarantee the user of correct or even sensible results.

As with most FORTRAN computer codes, MSTS is composed of a single main program and numerous subroutines and functions. The main program in MSTS serves as primary logic controller, which directs the execution through the various subroutines. The program was designed with very few computations occurring within the main program, but rather restricts the function of the main program to a control capacity. The main program contains three principal components: initialization, iteration, and termination. The initialization and termination components are executed once per simulation. The primary purpose of the initialization component of the code is to initialize variables, and includes those initializations that occur from user inputs, external file reads, data statements, and equivalence statements. The iteration component of the main program contains the time advance logic and directs the iterative solution of the governing conservation equations and constitutive theory. The termination component concludes the iteration component and serves primarily to complete post-simulation calculations and close files. Output from the executable is generated during all three components of an execution. Output generated during the initialization component generally reflects input data, whereas output generated during the iteration and termination components is related to specific results from the simulation. Output files are generated with several formats, including those intended for restart purposes, records, graphics, error analysis, and debugging. A logic flow chart that depicts the main program, subroutine groups, and iteration loops appears in Figure 5.1.

The main program begins with variable initializations. Variables are initialized from external file data (e.g., input files, restart files, property data files) and internal data with data statements and simple equivalences. All code variables are initialized explicitly, eliminating the problems of FORTRAN compiler-dependent implicit variable initializations. Variables initialized from input files include simulation reference information, simulation and numerical control parameters, computational domain data, soil zonation data, primary and secondary variable data, boundary condition specifications, and output control parameters. Initial values for primary variables may also be read from restart files. Restart files contain "snapshots" of the primary variables at a

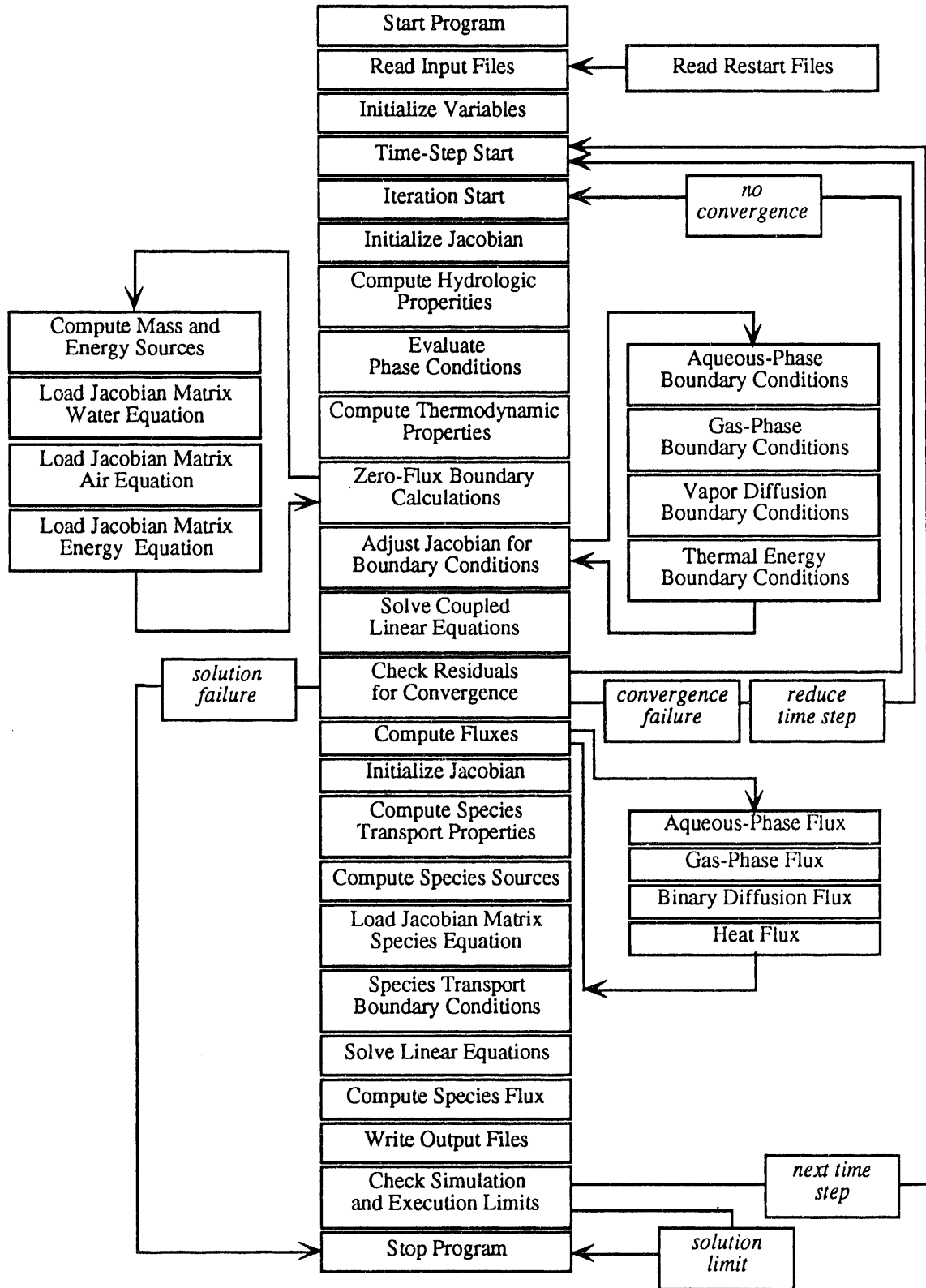


Figure 5.1. MSTS-Logic Flow Chart

particular point in simulation time. Restart files are designed to work in conjunction with input files, not as complete specifications.

The iteration component of the main program contains two principal loops, one nested within the other. The outer loop tracks advances in time step, whereas the inner loop tracks Newton-Raphson iterations. Each time-step advance involves the iterative solution of the coupled governing equations for conservation of component mass and energy, followed by an optional solution of the species mass conservation equation. A time-step loop begins with variable initializations, which primarily involve updating previous time-step variables to the values of their respective variables at the current time step and incrementing the simulation time by current time-step length. The variable initialization stage is followed by the iterative solution stage, where the discretized forms of the governing equations for water mass, air mass, and energy are solved simultaneously with a Newton-Raphson scheme. The next stage of the time-step loop involves computing Darcy velocities, mass fluxes, and heat fluxes from the converged fields of pressure and temperature. If the simulation includes species transport, then the next stage of the time-step loop is the direct solution of the species mass conservation equation. No time-step partitioning occurs with the species transport solution (i.e., the species transport solution uses the same time-step advance as the thermal-hydrologic solution). Auxiliary calculations (such as those for computing travel times, quantity balances, and surface flux integrations) follow the solution of the thermal-hydrologic and species transport equations. The final stage of the time-step loop involves writing results to output files, including restart files, and checking simulation and execution time limits. If none of the simulation limits are exceeded, then the simulation proceeds to the beginning of the next time-step loop. Otherwise, the simulation exits the time-step loop and proceeds to the termination component of the main program.

The inner loop of the iteration component will be referred to as the Newton-Raphson loop and involves a variable number of iterations depending on the nonlinearities associated with the thermal-hydrologic governing equations. Each Newton-Raphson loop begins with variable initializations, which include initializing the Jacobian coefficient matrix and solution vector. Variable initializations are followed by secondary variable calculations. Secondary variables are computed from the most current values of the primary variables, whether from the previous iteration or from the time-step loop. Secondary variable calculations begin with the hydrologic parameters (phase saturations, phase relative permeabilities, and phase tortuosities). Hydrologic parameters are computed first because phase saturations define the phase conditions for the evaluation of the thermodynamic properties. After the hydrologic parameters are computed, a short subroutine is executed that determines the phase condition for every active computational node. The phase-condition logic subroutine is followed by a series of subroutines that compute the remaining secondary variables necessary for the solution of the coupled thermal-hydrologic conservation equations. These secondary variables include physical parameters (e.g., viscosity and density), thermodynamic parameters (e.g., vapor mass fraction and component partial pressure), and thermal properties (e.g., effective thermal conductivity and phase enthalpy). Execution performance is enhanced by computing only those physical, thermodynamic, and thermal secondary variables necessary for the specified solution option.

The numerical derivative approach used by MST5 to compute the Jacobian matrix coefficients requires that values of the thermal and hydrologic parameters be computed for both primary variables and incremented primary variables. Each secondary variable is parameterized as a two-dimensional array; one dimension marks the node, and the other marks the incremented primary variable. Five secondary variable values are defined for each node: 1) previous time-step value, 2) current value, 3) current value with the temperature incremented, 4) current value with the aqueous pressure or water-vapor mass fraction incremented, and 5) current value with the gas

pressure incremented. "Current value" refers to the most recent iterate values of the primary variables.

After the thermal and hydrologic parameters have been computed, the next portion of the Newton-Raphson loop entails computing the Jacobian matrix and solution vector coefficients. The Jacobian matrix and solution vector coefficients are computed in two steps. First, the computations are completed by assuming zero-flux boundary conditions for all external boundaries and internal boundaries adjacent to inactive nodes. Second, the Jacobian matrix and solution vector coefficients are modified according to the user-imposed boundary conditions. The zero-flux boundary and imposed boundary condition steps are each divided into three sections, which correspond with the three governing thermal-hydrologic equations: water mass, air mass, and energy. Only those sections required for the particular solution option are executed. The order of the Jacobian matrix depends on the number of active nodes times the number of coupled governing equations solved, exclusive of the species concentration conservation equation.

The Jacobian matrix and solution vector element computations are followed by the solution of the governing thermal and hydrologic equations in linearized form. In terms of computational effort, this portion of the execution frequently dominates. Simulations that are characterized as two-phase nonisothermal require the solution of the water mass, air mass, and energy conservation equations, which yield Jacobian matrices of order  $3N$ , where  $N$  equals the number of active computational nodes. Solution times for linear systems of equations are dependent on the matrix order, where dependencies vary between  $(3N)$  and  $(3N)^3$ . First-order dependencies between solution times and matrix order are typical of multigrid techniques (Fogwell and Brakhagen 1989). Second-order dependencies are typical of banded matrix solvers and conjugate gradient iterative solvers. Third-order dependencies are typical of direct LU decomposition or Gaussian-type solvers. Because of the large linear systems that evolve from nonisothermal, three-phase simulations, an efficient linear equation solver is critical to the applicability of the engineering simulator. The spatial discretization scheme used on the governing partial differential equations, of a seven-point finite-difference stencil applied to a three-dimensional physical domain, yields block-banded Jacobian matrices, where the block order equals the number of solved mass and energy conservation equations. The Newton-Raphson method yields matrices that are positive-definite but nonsymmetric.

The Newton-Raphson linearization method results in a solution scheme for increments to the primary variables. Following a solution iteration, if every residual function falls below a specified fraction of the accumulation term, then the solution is considered converged and the simulation advances to the species transport equation solution. Otherwise, another solution iteration is attempted. Occasionally, the increments to the primary variables either diverge or converge too slowly with each solution iteration. In these situations, the time step is restarted with the original primary variables, but with a reduced time-step advance. Solution failures are also possible, where convergence failures occur even after numerous time-step reductions. Solution failures result in an aborted simulation.

The species transport solution is a direct solution procedure. The species transport solution begins with an initialization of the Jacobian coefficient matrix and solution vector. Because the species transport solution and thermal-hydrologic solution are sequential, the Jacobian matrix and solution vector memory space is shared between solution schemes. The species transport solution proceeds by computing the species transport parameters (e.g., diffusivities, partition coefficients, and dispersivities) and species source terms. The Jacobian coefficient matrix and solution vector are computed next for zero-flux boundary conditions, and subsequently modified for the specified species boundary conditions. All of the thermal-hydrologic parameters used in conjunction with

the species transport solution are those values computed from the most recent converged thermal-hydrologic solution. The final step of the species solution procedure involves the solution of the system of linear equations with one of the linear system solvers.

## 6.0 References

- 10 CFR 60. 1987. U.S. Nuclear Regulatory Commission, "Disposal of High-Level Radioactive Nuclear Wastes in Geologic Repositories." *U.S. Code of Federal Regulations*.
- 40 CFR 191. 1985. U.S. Environmental Protection Agency, "Environmental Standards for the Management and Disposal of Spent Nuclear Fuel, High-Level and Transuranic Radioactive Wastes; Final Rule." *U.S. Code of Federal Regulations*.
- ASHRAE. 1977. *ASHRAE Handbook and Product Directory, 1977 Fundamentals*. American Society of Heating, Refrigerating, and Air-Conditioning Engineers, Inc., New York.
- ASME. 1967. *Thermodynamic and Transport Properties of Steam*. The American Society of Mechanical Engineers, United Engineering Center, New York.
- Bear, J. 1972. *Dynamics of Fluids in Porous Media*. Elsevier, New York.
- Bird, R. B., W. E. Stewart, and E. N. Lightfoot. 1960. *Transport Phenomena*. John Wiley & Sons, Inc., New York.
- Brooks, R. H., and A. T. Corey. 1966. "Properties of Porous Media Affecting Fluid Flow." *Journal of Irrigation and Drainage Division* 93(3):61-88.
- Burdine, N. T. 1953. "Relative Permeability Calculations from Pore-Size Distribution Data." *Petroleum Trans.* 198:71-77.
- DOE. 1988. *Site Characterization Plan, Yucca Mountain Site, Nevada Research and Development Area, Nevada*. DOE/RW-0199, Volume II, Part A, Office of Civilian Radioactive Waste Management, U.S. Department of Energy, Washington, D.C.
- Dongarra, J. J., C. B. Moler, J. R. Bunch, and G. W. Stewart. 1980. *LINPACK User's Guide*. Society for Industrial and Applied Mathematics, Philadelphia.
- Falta, R. W., K. Pruess, I. Javandel, and P. A. Witherspoon. 1990. *Numerical Modeling of Steam Injection for the Removal of Nonaqueous Phase Liquids from the Subsurface: 1. Numerical Formulation*. LBL-29615, Lawrence Berkeley Laboratory, Berkeley, California.
- Fatt, I., and W. A. Klikoff. 1959. "Effect of Fractional Wettability on Multiphase Flow Through Porous Media." *AIME Transactions* 216:246.
- Fogwell, T. W., and F. Brakhagen. 1989. "Multigrid Methods in Modelling Porous Media Flow." In *Proceedings of the Joint IMA/SPE European Conference on the Mathematics of Oil Recovery Held at Cambridge University 25-27 July, 1989*. Oxford Press, Oxford.
- Jury, W. A., W. R. Gardner, and W. H. Gardner. 1991. *Soil Physics*. John Wiley & Sons, Inc., New York. pp. 180-184.
- Klavetter, E. A., and R. R. Peters. 1986. *Estimation of Hydrologic Properties of Unsaturated, Fractured Rock Mass*. SAND84-2642, Sandia National Laboratories, Albuquerque, New Mexico.

- Kreyszig, E. 1979. *Advanced Engineering Mathematics*. 4th ed. John Wiley & Sons, Inc., New York. p. 765.
- Leverett, M. C. 1941. "Capillary Behavior in Porous Solids." *ASME Trans.* 124:152.
- Millington, R. J., and J. P. Quirk. 1959. "Permeability of Porous Media." *Nature* 183:387-388.
- Montazer, P., and W. E. Wilson. 1984. *Conceptual Hydrologic Model of Flow in the Unsaturated Zone, Yucca Mountain, Nevada*. U.S. Geological Survey Water Resources Investigation Report 84-4345, U.S. Geological Survey, Denver.
- Mualem, Y. 1976. "A New Model for Predicting the Hydraulic Conductivity of Unsaturated Porous Media." *Water Resour. Res.* 12:513-522.
- Nichols, W. E., and M.D. White. 1992. *MSTS, Multiphase Subsurface Transport Simulator: User's Guide and Reference*. PNL-8637, Pacific Northwest Laboratory, Richland, Washington.
- Nitao, J. J. 1988. *Numerical Modeling of the Thermal and Hydrological Environment Around a Nuclear Waste Package Using the Equivalent Continuum Approximation: Horizontal Emplacement*. UCID-2144, Lawrence Livermore National Laboratory, Livermore, California.
- Oppe, T. C., W. D. Joubert, and D. R. Kincaid. 1988. *NSPCG User's Guide Version 1.0*. Center for Numerical Analysis, University of Texas, Austin, Texas.
- Patankar, S. V. 1980. *Numerical Heat Transfer and Fluid Flow*. Hemisphere Publishing Corporation, Washington, D.C.
- Peters, R. R., and E. A. Klavetter. 1988. "A Continuum Model for Water Movement in an Unsaturated Fractured Rock Mass." *Water Resour. Res.* 24(3): 416-430.
- Pruess, K. 1987. *TOUGH User's Guide*. LBL-20700, Lawrence Berkeley Laboratory, Berkeley, California.
- Public Law 97-425. 1983. *Reprints from Public Laws; P.L. 97-425, January 7, 1983; Title V of P.L. 100-203, December 22, 1987; P.L. 100-507, October 18, 1988*. U.S. Department of Energy, Office of Civilian Radioactive Waste Management, Washington, D.C.
- Public Law 100-203. 1987. *Reprints from Public Laws; P.L. 97-425, January 7, 1983; Title V of P.L. 100-203, December 22, 1987; P.L. 100-507, October 18, 1988*. U.S. Department of Energy, Office of Civilian Radioactive Waste Management, Washington, D.C.
- Reid, R. C., J. M. Prausnitz, and B. E. Poling. 1987. *The Properties of Gases and Liquids*. McGraw-Hill, Inc., New York.
- Sandler, S. I. 1989. *Chemical and Engineering Thermodynamics*. John Wiley & Sons, Inc., New York.
- Slattery, J. C., and R. B. Bird. 1958. "Calculation of the Diffusion Coefficient of Dilute Gases and of the Self-Diffusion Coefficient of Dense Gases." *Am. Inst. Chem. Engr. J.* 4(2):137-142.

Somerton, W. H., A. H. El-Shaarani, and S. M. Mobarak. 1974. "High Temperature Behavior of Rocks Associated with Geothermal Type Reservoirs." Paper SPE-4897, presented at 44th Annual California Regional Meeting of the Society of Petroleum Engineers, San Francisco.

Somerton, W. H., J. A. Keese, and S. L. Chu. 1973. "Thermal Behavior of Unconsolidated Oil Sands." Paper SPE-4506, presented at 48th Annual Fall Meeting of the Society of Petroleum Engineers, Las Vegas, Nevada.

Udell, K. S., and J. S. Fitch. 1985. "Heat and Mass Transfer in Capillary Porous Media Considering Evaporation, Condensation, and Non-Condensable Gas Effects." Presented at 23rd ASME/AIChE National Heat Transfer Conference, Denver.

van Genuchten, M. T. 1980. "A Closed-Form Equation for Predicting the Hydraulic Conductivity of Unsaturated Soils." *Soil Sci. Soc. Am. J.* 44: 892-898.

van Wylen, G. J., and R. E. Sonntag. 1978. *Fundamentals of Classical Thermodynamics*. 2nd ed., Revised Printing. John Wiley & Sons, Inc., New York.

Weeks, E. P., E. E. Douglas, and G. M. Thompson. 1982. "Use of Atmospheric Fluorocarbons F-11 and F-12 to Determine the Diffusion Parameters of the Unsaturated Zone in the Southern High Plains of Texas." *Water Resour. Res.* 18(5):1365-1378.

## **Appendix**

### **Numerical Values of Liquid Water, Water-Vapor, and Saturation Line Constants**

## Appendix

### Numerical Values of Liquid Water, Water-Vapor, and Saturation Line Constants

The following tables contain the numerical values of the constants for the liquid water, water vapor, and the saturation line. The values shown in Table A.1 are used to compute the density, enthalpy, and internal energy of liquid water. The values shown in Tables A.2, A.4, and A.5 are used to compute the density, enthalpy, and internal energy of water vapor. The values shown in Table A.3 are used to compute the saturation pressure function. The values shown in Table A.6 are used to compute the thermal conductivity of liquid water.

Table A.1. Liquid Water Primary Constants

<u>Symbol</u>	<u>Numerical Value</u>
A <sub>0</sub>	6.824 687 741 x 10 <sup>3</sup>
A <sub>1</sub>	-5.422 063 673 x 10 <sup>2</sup>
A <sub>2</sub>	-2.096 666 205 x 10 <sup>4</sup>
A <sub>3</sub>	3.941 286 787 x 10 <sup>4</sup>
A <sub>4</sub>	-6.733 277 739 x 10 <sup>4</sup>
A <sub>5</sub>	9.902 381 028 x 10 <sup>4</sup>
A <sub>6</sub>	-1.093 911 774 x 10 <sup>5</sup>
A <sub>7</sub>	8.590 841 667 x 10 <sup>4</sup>
A <sub>8</sub>	-4.511 168 742 x 10 <sup>4</sup>
A <sub>9</sub>	1.418 138 926 x 10 <sup>4</sup>
A <sub>10</sub>	-2.017 271 113 x 10 <sup>3</sup>
A <sub>11</sub>	7.982 692 717 x 10 <sup>0</sup>
A <sub>12</sub>	-2.616 571 843 x 10 <sup>-2</sup>
A <sub>13</sub>	1.522 411 790 x 10 <sup>-3</sup>
A <sub>14</sub>	2.284 279 054 x 10 <sup>-2</sup>
A <sub>15</sub>	2.421 647 003 x 10 <sup>2</sup>
A <sub>16</sub>	1.269 716 088 x 10 <sup>-10</sup>
A <sub>17</sub>	2.074 838 328 x 10 <sup>-7</sup>
A <sub>18</sub>	2.174 020 350 x 10 <sup>-8</sup>
A <sub>19</sub>	1.105 710 498 x 10 <sup>-9</sup>
A <sub>20</sub>	1.293 441 934 x 10 <sup>1</sup>
A <sub>21</sub>	1.308 119 072 x 10 <sup>-5</sup>
A <sub>22</sub>	6.047 626 338 x 10 <sup>-14</sup>
a <sub>1</sub>	8.438 375 405 x 10 <sup>-1</sup>
a <sub>2</sub>	5.362 162 162 x 10 <sup>-4</sup>
a <sub>3</sub>	1.720 000 000 x 10 <sup>0</sup>
a <sub>4</sub>	7.342 278 489 x 10 <sup>-2</sup>
a <sub>5</sub>	4.975 858 870 x 10 <sup>-2</sup>
a <sub>6</sub>	6.537 154 300 x 10 <sup>-1</sup>
a <sub>7</sub>	1.150 000 000 x 10 <sup>-6</sup>
a <sub>8</sub>	1.510 800 000 x 10 <sup>-5</sup>
a <sub>9</sub>	1.418 800 000 x 10 <sup>-1</sup>

**Table A.1. (contd)**

<u>Symbol</u>	<u>Numerical Value</u>
a <sub>10</sub>	7.002 753 165 x 10 <sup>0</sup>
a <sub>11</sub>	2.995 284 926 x 10 <sup>-4</sup>
a <sub>12</sub>	2.040 000 000 x 10 <sup>-1</sup>

**Table A.2. Water-Vapor Primary Constants**

<u>Symbol</u>	<u>Numerical Value</u>
B <sub>0</sub>	1.683 599 274 x 10 <sup>1</sup>
B <sub>01</sub>	2.856 067 796 x 10 <sup>1</sup>
B <sub>02</sub>	-5.438 923 329 x 10 <sup>1</sup>
B <sub>03</sub>	4.330 662 834 x 10 <sup>-1</sup>
B <sub>04</sub>	-6.547 711 697 x 10 <sup>-1</sup>
B <sub>05</sub>	8.565 182 058 x 10 <sup>-2</sup>
B <sub>11</sub>	6.670 375 918 x 10 <sup>-2</sup>
B <sub>12</sub>	1.388 983 801 x 10 <sup>0</sup>
B <sub>21</sub>	8.390 104 328 x 10 <sup>-2</sup>
B <sub>22</sub>	2.614 670 893 x 10 <sup>-2</sup>
B <sub>23</sub>	-3.373 439 453 x 10 <sup>-2</sup>
B <sub>31</sub>	4.520 918 904 x 10 <sup>-1</sup>
B <sub>32</sub>	1.069 036 614 x 10 <sup>-1</sup>
B <sub>41</sub>	-5.975 336 707 x 10 <sup>-1</sup>
B <sub>42</sub>	-8.847 535 804 x 10 <sup>-2</sup>
B <sub>51</sub>	5.958 051 609 x 10 <sup>-1</sup>
B <sub>52</sub>	-5.159 303 373 x 10 <sup>-1</sup>
B <sub>53</sub>	2.075 021 122 x 10 <sup>-1</sup>
B <sub>61</sub>	1.190 610 271 x 10 <sup>-1</sup>
B <sub>62</sub>	-9.867 174 132 x 10 <sup>-2</sup>
B <sub>71</sub>	1.683 998 803 x 10 <sup>-1</sup>
B <sub>72</sub>	-5.809 438 001 x 10 <sup>-2</sup>
B <sub>81</sub>	6.552 390 126 x 10 <sup>-3</sup>
B <sub>82</sub>	5.710 218 649 x 10 <sup>-4</sup>
B <sub>90</sub>	1.936 587 558 x 10 <sup>2</sup>
B <sub>91</sub>	-1.388 522 425 x 10 <sup>3</sup>
B <sub>92</sub>	4.126 607 219 x 10 <sup>3</sup>
B <sub>93</sub>	-6.508 211 677 x 10 <sup>3</sup>
B <sub>94</sub>	5.745 984 054 x 10 <sup>3</sup>
B <sub>95</sub>	-2.695 088 365 x 10 <sup>3</sup>
B <sub>96</sub>	5.035 718 623 x 10 <sup>2</sup>
b	7.633 333 333 x 10 <sup>-1</sup>
b <sub>61</sub>	4.006 073 948 x 10 <sup>-1</sup>
b <sub>71</sub>	8.636 081 627 x 10 <sup>-2</sup>
b <sub>81</sub>	-8.532 322 921 x 10 <sup>-1</sup>
b <sub>82</sub>	3.460 208 861 x 10 <sup>-1</sup>

**Table A.3. Saturation Line Constants**

<u>Symbol</u>	<u>Numerical Value</u>
k <sub>1</sub>	-7.691 234 564 x 10 <sup>0</sup>
k <sub>2</sub>	-2.608 023 696 x 10 <sup>1</sup>
k <sub>3</sub>	-1.681 706 546 x 10 <sup>2</sup>
k <sub>4</sub>	6.423 285 504 x 10 <sup>1</sup>
k <sub>5</sub>	-1.189 646 225 x 10 <sup>2</sup>
k <sub>6</sub>	4.167 117 320 x 10 <sup>0</sup>
k <sub>7</sub>	2.097 506 760 x 10 <sup>1</sup>
k <sub>8</sub>	1.0 x 10 <sup>9</sup>
k <sub>9</sub>	6.0

**Table A.4. Derived Constants**

<u>Symbol</u>	<u>Numerical Value</u>
L <sub>0</sub>	1.574 373 327 x 10 <sup>1</sup>
L <sub>1</sub>	-3.417 061 978 x 10 <sup>1</sup>
L <sub>2</sub>	1.931 380 707 x 10 <sup>1</sup>

**Table A.5. Numerical Indices**

<u>j</u>	<u>n(j)</u>	<u>z(j, 1)</u>	<u>z(j, 2)</u>	<u>z(j, 3)</u>	<u>l(j)</u>	<u>x(j, 1)</u>	<u>x(j, 2)</u>	<u>j</u>
1	2	13	3	-	-	-	-	1
2	3	18	2	1	-	-	-	2
3	2	18	10	-	-	-	-	3
4	2	25	14	-	-	-	-	4
5	3	32	28	24	-	-	-	5
6	2	12	11	-	1	14	-	6
7	2	24	18	-	1	19	-	7
8	2	24	14	-	2	54	27	8

**Table A.6.** Liquid Thermal Conductivity Constants

<u>Symbol</u>	<u>Numerical Value</u>
a <sub>0</sub>	-922.47
a <sub>1</sub>	2839.5
a <sub>2</sub>	-1800.7
a <sub>3</sub>	525.77
a <sub>4</sub>	73.44
b <sub>0</sub>	0.94730
b <sub>1</sub>	2.5186
b <sub>2</sub>	-2.0012
b <sub>3</sub>	0.51536
c <sub>0</sub>	1.6563 x 10 <sup>-3</sup>
c <sub>1</sub>	-3.8929 x 10 <sup>-3</sup>
c <sub>2</sub>	2.9323 x 10 <sup>-3</sup>
c <sub>3</sub>	-7.1693 x 10 <sup>-4</sup>
T <sub>0</sub>	273.15

DISTRIBUTION

No. of  
Copies

No. of  
Copies

OFFSITE

12 DOE Office of Scientific and Technical  
Information  
Technical Information Center  
P.O. Box 62  
Oak Ridge, TN 37830

8 Yucca Mountain Site Characterization  
Project Office  
U.S. Department of Energy  
P.O. Box 98608  
Las Vegas, NV 89193-8608  
ATTN: J. M. Boak  
J. R. Dyer  
C. P. Gertz (5)  
J. J. Lorenz

15 DOE Nevada Field Office  
U.S. Department of Energy  
P.O. Box 98518  
Las Vegas, NV 89193-8518  
ATTN: D. R. Elle  
P. K. Fitzsimmons  
Tech Information Officer (12)  
C. L. West

Science and Technology Division  
Office of Scientific & Technical  
Information  
U.S. Department of Energy  
P.O. Box 62  
Oak Ridge, TN 37831  
ATTN: A. T. Tamura

8 U.S. Department of Energy  
1000 Independence Avenue, S.W.  
Washington, DC 20585  
ATTN: S. J. Brocoum RW-22  
P. Bunton RW-331  
L. Desell RW-331  
R. A. Milner RW-332  
G. J. Parker RW-322  
J. Roberts RW-30  
S. Rousso RW-50  
T. Wood RW-52

C. Anderson  
National Academy of Sciences  
2101 Constitution Ave. NW  
Harris Bldg, Rm 456  
Washington, DC 20418

2 Agency for Nuclear Projects  
State of Nevada  
Evergreen Center, Suite 252  
1802 N. Carson St.  
Carson City, NV 89710  
ATTN: C. H. Johnson  
R. R. Loux

C. R. Allen  
Nuclear Waste Technical Review Board  
1000 E. California Boulevard  
Pasadena, CA 91106

E. Anderson  
Mountain West Research  
Southwest, Inc.  
2901 N. Central Ave., #1000  
Phoenix, AZ 85012-2730

Argonne National Laboratory  
9700 S. Cass Avenue  
Argonne, IL 60439  
ATTN: A. Anderson Bldg 362

No. of  
Copies

No. of  
Copies

M. L. Baughman  
35 Clark Road  
Fiskdale, MA 01518

C. G. Bell, Jr.  
Professor of Civil Engineering  
Civil and Mechanical Engineering  
University of Nevada, Las Vegas  
4505 S. Maryland Parkway  
Las Vegas, NV 89154

J. A. Blink  
Deputy Project Leader  
Lawrence Livermore Natl Laboratory  
101 Convention Center Drive  
Suite 280, MS 527  
Las Vegas, NV 89109

S. Bradhurst  
P.O. Box 1510  
Reno, NV 89505

L. Bradshaw  
Nye County District Attorney  
P.O. Box 593  
Tonopah, NV 89049

G. D. Brewer  
Nuclear Waste Technical Review Board  
The Dana Building, Room 3516  
University of Michigan  
Ann Arbor, MI 48109-1115

R. J. Budnitz  
President, Future Resource Associates  
2000 Center Street, Suite 418  
Berkeley, CA 94704

R. L. Bullock  
Raytheon Services Nevada  
Suite P-250 (MS-403)  
101 Convention Center Dr.  
Las Vegas, NV 89109

J. E. Cantlon, Chairman  
Nuclear Waste Technical Review Board  
1795 Bramble Drive  
East Lansing, MI 48823

2 City of Caliente  
P.O. Box 158  
Caliente, NV 89008  
ATTN: J. Foremaster  
G. Van Roekel

City of Boulder City  
Community Development & Planning  
P.O. Box 61350  
Boulder City, NV 89006

City of North Las Vegas  
Community Planning & Development  
P.O. Box 4086  
North Las Vegas, NV 89030

City of Las Vegas  
Economic Development Department  
400 E. Stewart Avenue  
Las Vegas, NV 89101

Clark County  
Department of Comprehensive Planning  
225 Bridger Ave., 7th Floor  
Las Vegas, NV 89155

B. W. Colston  
Las Vegas Branch  
Raytheon Services Nevada  
P.O. Box 95487, MS 416  
Las Vegas, NV 89193-5487

T. A. Cotton  
JK Research Associates, Inc.  
4429 Butterworth Place, N.W.  
Washington, DC 20016

No. of  
Copies

No. of  
Copies

	R. H. Cuenca Oregon State University Department of Bioresource Engineering Gilmore Hall 106 Corvallis, OR 97331		T. Hay, Executive Assistant Office of the Governor State of Nevada Capitol Complex Carson City, NV 89710
2	Desert Research Institute P.O. Box 60220 Reno, NV 89506 ATTN: J. Fordham D. Rhode		J. Hayes P.O. Box 490 Goldfield, NV 89013
	P. A. Domenico Nuclear Waste Technical Review Board Geology Department Texas A & M University College Station, TX 77843		D. Hedges Roy F. Weston, Inc. 4425 Spring Mountain Road, Suite 300 Las Vegas, NV 89102
	C. E. Ezra YMP Support Office Manager EG7G Energy Measurements, Inc. P.O. Box 1912, MS V-02 Las Vegas, NV 89125		D. Hillel Department of Plant and Soil Science 12A Stockbridge Hall University of Massachusetts Amherst, MA 01003
	Exploratory Shaft Test Manager Los Alamos National Laboratory 101 Convention Center Drive Suite 820, Mail Stop 527 Las Vegas, NV 89101		R. G. Hills Department of Mechanical Engineering Box 30001, Department 3450 New Mexico State University Las Cruces, NM 88003
	L. J. Fiorenzi P.O. Box 257 Eureka, NV 89316		R. Horton Department of Agronomy Iowa State University Ames, IA 50011
	L. D. Foust Nevada Site Manager TRW Environmental Safety Systems 101 Convention Center Dr. Suite 540, MS 423 Las Vegas, NV 89109	5	INTERA, Inc. 101 Convention Center Drive Phase II, Suite 540 Las Vegas, NV 89193 ATTN: R. W. Nelson (2) S. Pawah A. E. Van Luik H. N. Kalia
	B. Hastings TRW Environmental Safety Systems 2650 Park Tower Drive, Suite 800 Vienna, VA 22180		G. G. Katul Department of Hydrologic Science Vehmeyer Hall University of California Davis, CA 95616

No. of  
Copies

No. of  
Copies

	D. Langmuir Nuclear Waste Technical Review Board 109 S. Lookout Mountain Creek Golden, CO 80401	A. Makhijani Institute for Energy and Environmental Research 6935 Laurel Avenue Takoma Park, MD 20912
7	Lawrence Berkley Laboratory Berkeley, CA 94720 ATTN: E. P. Binnall W. W.-L. Lee T. N. Narasimhan W. J. O'Connell K. Pruess C. F. Tsang J. Wang	C. John Mann Department of Geology 245 Natural History Bldg. 1301 West Green Street Urbana, IL 61801  M. Marshall c/o LATIR Energy Consultants Route 7, Box 126 B Old Santa Fe Trail Santa Fe, NM 87505
5	Lawrence Livermore National Laboratory P.O. Box 808 Livermore, CA 94551 ATTN: T. A. Buscheck D. Chesnut W. L. Clarke W. Halsey W. J. O'Connell  Lincoln County Commission Lincoln County P.O. Box 90 Pioche, NV 89043  H. Loo Weston House Idaho Nuclear Co. P.O. Box 4000, M/S 5219 Idaho Falls, ID 83415	J. E. Martin Asst Professor of Radiological Health University of Michigan School of Public Health Ann Arbor, MI 48109  J. Massmann Department of Civil Engineering 306 More Hall, FX-10 University of Washington Seattle, WA 98195  J. J. McKetta, Jr. Nuclear Waste Technical Review Board Department of Chemical Engineering CPE Building 1.450 Austin, TX 78712
2	Los Alamos National Laboratory P.O. Box 1663 Los Alamos, NM 87545 ATTN: J. A. Canepa R. Rundberg      J-514	H. R. Meyer C.N.S.I. 750 East Park Drive, Suite 200 Harrisburg, PA 17111  I. Miller Golder Associates 4104 184th Avenue N.E. Redmond, WA 98052

No. of  
Copies

No. of  
Copies

	R. H. Neill Director, New Mexico Environmental Evaluation Group 7007 Wyoming Boulevard, N.E. Suite F-2 Albuquerque, NM 87109		T. Pigford Department of Nuclear Engineering 4153 Etcheverry Hall University of California Berkeley, CA 94720
	D. W. North Nuclear Waste Technical Review Board Decision Focus, Inc. 4984 El Camino Real Los Altos, CA 94062		J. Pitts Lincoln County Courthouse Pioche, NV 89043
2	North Carolina Agricultural and Technical University Department of Civil Engineering Greensboro, NC 27411 ATTN: E. U. Nzewi L. E. Peele		V. Poe P.O. Box 1026 Hawthorne, NV 89415
	NRC Document Control Desk Division of Waste Management Nuclear Regulatory Commission Washington, DC 20555		P. T. Prestholt NRC Site Representative 301 E. Stewart Avenue, Room 203 Las Vegas, NV 89101
	Nye County Planning Department P.O. Box 153 Tonopah, NV 89049		D. L. Price Nuclear Waste Technical Review Board 1011 Evergreen Way Blacksburg, VA 24060
2	Oak Ridge National Laboratory P.O. Box 2008 Oak Ridge, TN 37831 ATTN: A. G. Croff MS-6235 F. O. Hoffman		M. Reeves INTERA, Inc. 6850 Austin Ctr. Blvd, Suite 300 Austin, TX 78731
	ONWI Library Battelle Columbus Laboratory Office of Nuclear Waste Isolation 505 King Ave. Columbus, OH 43201	3	Reynolds Electrical & Engineering Co. P.O. Box 98521 Las Vegas, NV 89193-8521 ATTN: M. J. Dorsey MS-407 D. L. Fraser MS-555 R. F. Pritchett MS-408
			J. Riley Heinman Research Laboratories Charlotte, NC 28207
			B. Ross Disposal Safety, Inc. 1660 L. Street, N.W., Suite 314 Washington, DC 20036

No. of  
Copies

No. of  
Copies

	G. Ross Heath, Chairman College of Ocean & Fishery Sciences 583 Henderson hall University of Washington Seattle, WA 98185		L. Shepard Ogden Environmental & Energy Services 7301A Indian School Rd., NE Albuquerque, NM 87110
5	Roy F. Weston, Inc. 955 L'Enfant Plaza, S.W. Washington, D.C. 20024 ATTN: L. Rickertsen E. L. Snow Chris Charles Janet Docka Technical Info. Center	4	Southwest Research Institute 6220 Culebra Road San Antonio, TX 78228 ATTN: B. Sagar (3) J. Walton
8	Sandia National Laboratory Albuquerque, NM 87185 ATTN: R. W. Barnard 6312 G. E. Barr 6312 F. W. Bingham 6312 T. E. Blejwas 6302 R. R. Eaton 1513 P. G. Kaplan 6312 M. J. Martinez 6312 M. A. Wilson 6312		C. Thistlethwaite, AICP Associate Planner Inyo County Planning Dept. Drawer L Independence, CA 93526
	F. W. Schwartz Dept of Geology and Mineralogy The Ohio State University 1090 Carmack Road Columbus, OH 43210-1398	2	University of California at Riverside Department of Soils Riverside, CA 92502 ATTN: W. A. Jury M. Th. van Genuchten
3	Science Applications International Corporation (SAIC) 101 Convention Center Blvd, Suite 450 Las Vegas, NV 89109 ATTN: A. Brandstetter P. L. Cloke M. D. Voegele		U.S. Bureau of Reclamation Code D-3790 P.O. Box 25007 Denver, CO 80225
	B. Selinder 190 W. First St. Fallon, NV 89406	3	U.S. Environmental Protection Agency 401 "M" Street, S.W. Washington, DC 20460 ATTN: D. M. Clark A-101F K. W. Conway A-101F W. Russo ANR 460
		2	U.S. Geological Survey 2255 N. Gemini Drive Flagstaff AZ 86001 ATTN: J. H. Sass S. C. Wu
			U.S. Geological Survey 345 Middlefield Road Menlo Park, CA 94025 ATTN: E. J. Helley

No. of  
Copies

No. of  
Copies

- 6 U.S. Geological Survey  
P.O. Box 25046  
Denver CO 80225  
ATTN: D. H. Appel  
G. L. Ducret  
L. R. Hayes  
W. R. Keefer  
J. M. LaMonaca  
J. S. Stuckless
- U.S. Geological Survey  
Federal Building, Room 224  
Carson City, NV 89701  
ATTN: P. A. Glancy
- 3 U.S. Geological Survey  
101 Convention Center Drive  
Suite 860 MS 509  
Las Vegas, NV 89109  
ATTN: R. W. Craig  
D. Hoxie  
D. Zesiger
- U.S. Geological Survey  
Water Resources Division  
6770 S. Paradise Road  
Las Vegas, NV 89119  
ATTN: D. A. Beck
- U.S. Geological Survey  
P.O. Box 327, MS 721  
Mercury, NV 89023  
ATTN: A. L. Flint
- 2 U.S. Geological Survey  
106 National Center  
12201 Sunrise Valley Drive  
Reston, VA 22092  
ATTN: J. F. Devine  
V. R. Schneider
- 4 U.S. Nuclear Regulatory Commission  
Division of Engineering Safety  
Washington, D.C. 20555  
ATTN: D. Code'l  
S. Coplan NLS-260  
N. Eisenberg 4-H-3  
T. J. Nicholson NL-005
- U. S. Nuclear Regulatory Commission  
Division of Waste Management  
Repository Licensing & Quality  
Assurance-Project Directorate  
Washington, DC 20555
- U. S. Nuclear Regulatory Commission  
Senior Project Manager  
Repository Project Branch  
Washington, DC 20555
- Ellis D. Verink  
Nuclear Waste Technical Review Board  
4401 N.W. 18th Place  
Gainesville, FL 32605
- J. E. Watson, Jr.  
Department of Environmental Sciences  
and Engineering  
Campus Box 7400  
University of North Carolina at Chapel  
Hill  
Chapel Hill, NC 27599-7400
- P. J. Weeden  
U.S. Environmental Protection Agency  
Nuclear Radiation Assessment Division  
Environmental Monitoring Systems  
Laboratory  
P.O. Box 93478  
Las Vegas, NV 89193-3478
- C. Whipple  
Clement International  
160 Spear Street, Suite 1380  
San Francisco, CA 94105-1535

No. of  
Copies

No. of  
Copies

P. J. Wierenga  
New Mexico State University  
Department of Soil Science  
Las Cruces, NM 88004

R. Williams, Jr.  
P.O. Box 10  
Austin, NV 89310

J. L. Smoot K6-77  
G. P. Streile K6-77  
J. L. Stroh K6-77  
J. E. Szecsody K6-77  
L. V. Vail K6-77  
R. W. Wallace K6-77  
G. Whelan K6-77  
M. D. White (25) K6-77  
M. D. Williams K6-77  
B. D. Wood K6-77  
S. K. Wurstner K6-77  
S. B. Yabusaki K6-77  
Publishing Coordination  
Technical Report Files (5)

ONSITE

2 DOE Field Office, Richland

D. C. Langstaff A5-90  
J. J. Sutey A5-90

99 Pacific Northwest Laboratory

M. P. Bergeron K6-77  
J. W. Cary K6-77  
C. R. Cole K6-77  
J. L. DeVary K6-77  
L. A. Doremus K6-96  
D. W. Engel K7-34  
D. J. Epstein K6-77  
P. W. Eslinger (5) K6-96  
M. J. Fayer K6-77  
M. D. Freshley K6-77  
T. R. Ginn K6-77  
G. W. Gee K6-77  
C. T. Kincaid K6-77  
R. R. Kirkham K6-77  
M. R. Kreiter K7-90  
R. L. Lenhard K6-77  
M. I. McKinley K6-77  
P. D. Meyer K6-77  
W. E. Nichols (25) K6-77  
D. A. Perez K6-86  
W. A. Perkins K6-77  
J. C. Ritter K6-77  
K. R. Roberson K6-77  
J. S. Roberts K7-15  
M. L. Rockhold K6-77  
C. Sato K6-77  
T. D. Scheibe K6-77  
C. S. Simmons K6-77

Routing

R. M. Ecker SEQUIM  
M. J. Graham K6-78  
C. J. Hostetler K6-81  
P. M. Irving K6-98  
R. L. Skaggs K6-77  
C. S. Sloane K6-04  
P. C. Hays (last) K6-86

**END**

---

**DATE  
FILMED**

9 / 8 / 193

